Heavy Ion Collisions, Quasinormal Modes and Non-Linear Sigma Models

Georgios Michalogiorgakis

A Dissertation
Presented to the Faculty
of Princeton University
in Candidacy for the Degree
of Doctor of Philosophy

Recommended for Acceptance
by the Department of
Physics

September, 2007

ἐρεβοδιφῶσιν

Abstract

It has been known for a long time that certain supersymmetric gauge theories can be described by string theory. These gauge theories share common features with QCD when the temperature of the theory is above the confinement temperature. Recently there has been strong evidence, even though not conclusive, that a Quark Gluon Plasma (QGP) above the confinement temperature is formed from gold on gold collisions at the Relativistic Heavy Ion Collider. Furthermore the evidence suggests that the QGP is strongly coupled, making a string description of the plasma possible.

We use the dual string theory of the maximally supersymmetric gauge theory to find the profile of the gluonic fields sourced by a moving heavy quark through the plasma, suggesting that a picture of a wake is possible in string theory. Later on, inspired by the qualitative agreement between the measured thermalization time and the predicted time from a dual model we calculate some low-lying gravitational modes in an asymptotically AdS black hole. We find good agreement with the modes predicted by the boundary theory. Finally we calculate some of the higher order corrections to the supergravity description of heterotic non-linear sigma models.

Acknowledgements

I am grateful to my advisor, Steve Gubser, for his generous sharing of ideas and patience. I have learned many things from him, and this thesis would not have been completed without his help and advice. I would also like to thank Juan Maldacena, Igor Klebanov and Herman Verlinde for various discussions and Lyman Page for his help with my experimental project. I am indebted to Chiara Nappi for guidance during my graduate studies.

Josh Friess has been a great friend and collaborator in all my years in Princeton. We have discussed almost every problem either of us has worked on. Working with Silviu Pufu has been fun and he has contributed greatly for this thesis. Many thanks also go to Matt Buican, Tolya Dymarksy, Justin Kinney and Gasper Tkacik.

Many people have made my time in Princeton enjoyable, Alex, Barbara, Chrysanthos, Eleni, Evan, Giorgos, Giannis, Joanna, Katerina, Mpampis, Nikitas, Stratis, Spyros and Milena, and I owe them special thanks. Also special thanks go to Antonis, my house mate for two years, for his patience and for providing a different perspective to my political views. I am really happy that my sister Maria has shared with me almost all the good and bad moments of my life, including the ones in Princeton. I am sad to part from her. Eve, has filled my life with love and excitement, making me look at the bright side of things.

Finally, above all I thank my parents for their love and support.

Contents

List of Figures

List of Tables

Chapter 1

Introduction

1.1 Motivation

For almost four decades research has been done on the connection between string theory and gauge theories. In fact string theory was originally thought of as a theory of the strong interactions. This was due to the stringy nature of phenomena like confinement and Regge behavior which arise naturally in string theories. Another description of strong interactions, QCD was later developed that is in perfect agreement with all experimental data. The fact that QCD, as most gauge theories in four dimensions, is asymptotically free led to a good perturbative description of the high energy behavior of strong interactions. However, for phenomena related to low energy physics such as confinement and chiral symmetry breaking only numerical methods are available. In the last decade it has been realized that some gauge theories can have two different descriptions. When one description is weakly coupled the other one is strongly coupled and vice versa. One could hope that such a duality exists for QCD, making the low energy description of the theory more accessible to analytic methods. There are several arguments that QCD should have such a dual description. When one tries to separate a quark from an anti-quark, a flux tube forms between them, which in many respects behaves as a string. The most striking indication that such a duality exists comes from the large N 't Hooft limit which we describe in the following section.

This thesis addresses some of the aspects of this duality. It is organized as follows. In section 1.2 we review the 't Hooft large N limit and arguments suggesting that gauge theories may be dual to string theories. In section 1.3 a brief introduction to the AdS/CFT correspondence is presented. Section 1.4 contains some of the experimental results from RHIC, along with a basic introduction of the experimental setup. In chapter 2 the Fourier space profile of trF^2 is computed for a heavy quark moving through an $\mathcal{N}=4$ SYM quark-gluon plasma. Chapter 3 deals with gravitational modes in the case of a black hole in AdS_4. Finally in chapter 4 higher order corrections to the supergravity action are calculated for the heterotic string. Chapter 1 has drawn material from [7], chapter 2 is based on [8], chapter 3 on [9] and chapter 4 on [10].

1.2 String theory and large N gauge theories

Before describing the full four dimensional model let us focus on a two dimensional analog that exhibits similar behavior, such as asymptotic freedom and has a mass gap. Consider a theory that has N fields and is described by the action

$$S = \frac{1}{2g_0^2}\int d^2\sigma \left((\partial\vec{n})^2 + \lambda(\vec{n}^2 - 1)\right) \tag{1.1}$$

where λ is a Lagrange multiplier enforcing the constraint $\vec{n}^2 = 1$. We can integrate out the fields $\vec{n}$ since they only appear in quadratic terms and get

$$S = \frac{N}{2}\log\det(-\partial^2 + \lambda) - \frac{1}{g_0 N^2}\int d^2\lambda\sigma \ . \tag{1.2}$$

Taking the large N limit gives a classical theory for the field λ. Indeed computing $\frac{\partial S}{\partial\lambda} = 0$ we derive

$$1 = \frac{Ng_0^2}{4\pi}\log\frac{\Lambda^2}{\lambda} \tag{1.3}$$

which leads to an expectation value for the field λ

$$\lambda = \Lambda^2 e^{-\frac{4\pi}{g_0^2 N}} = \mu^2 e^{-\frac{-4\pi}{4g^2 N}} \ . \tag{1.4}$$

In the last equation we have defined the renormalized constant g^2. We note that the dependence of the interaction on the cutoff scale is that of an asymptotically free theory.

Moreover we see that the expectation value of λ introduces a mass gap for the theory as is evident from (1.1). In this small calculation we have obtained the mass by effectively calculating an one loop diagram and a tree level term. The large N limit the diagram set that had to be calculated. A more complete discussion of these issues is given in sections 4.1,4.2 and 4.2.1 We go on to consider four dimensional gauge theories, that in general exhibit similar phenomena as our two dimensional toy model, namely asymptotic freedom and the existence of a mass gap.

A first step is to understand how to scale the coupling g_{YM} in the large N limit [11]. A natural choice is to do so in a manner such that the QCD scale Λ is not affected. The one loop beta function for pure $SU(N)$ Yang-Mills theories is given by

$$\mu \frac{dg_{YM}}{d\mu} = -\frac{11}{3}\frac{g_{YM}^2 N}{16\pi^2} \ . \tag{1.5}$$

It is evident that the effective coupling of the theory is $g_{YM}^2 N$. Taking the limit $N \to \infty$ while keeping $g_{YM}^2 N$ fixed that QCD scale does not change. The effective coupling $\lambda = g_{YM}^2 N$ is known as the 't Hooft coupling and the corresponding limit as the 't Hooft limit. As long as the theory is asymptotically free the same conclusion is valid even if we include matter fields.

Instead of presenting arguments about a specific Yang-Mills theory, let us consider a general theory where the basic field is a hermitian matrix. An example of such a theory would be $U(N)$ Yang-Mills theory with matter in the adjoint. Heuristically the Lagrangian has the form

$$\mathcal{L} = \frac{1}{g^2} Tr[(\partial M)^2 + V(M)] \ . \tag{1.6}$$

A standard technique is to use a double line for a propagator of the M field, each line representing a matrix index. It is simple to derive the Feynman rules for this theory and we see that each propagator contributes a factor of g_{YM}^2 and each vertex contributes a factor of $\frac{1}{g_{YM}^2}$. Each loop, because of the trace over the matrix index will contribute a factor of N. Finally we can calculate how each diagram scales with both g_{YM}, N. A diagram with P propagators V vertices and L loops has a scaling factor of $g_{YM}^{2(P-V)} N^L$. This can be rearranged to

$$(g_{YM}^2 N)^{P-V} N^{L-P+V} \ . \tag{1.7}$$

Remembering our double line notation, propagators correspond to edges and loops to faces. The previous factor can be recast into the form

$$(g_{YM}^2 N)^{E-V} N^{2-2h} \tag{1.8}$$

where h is the genus of the two dimensional surface. We can now rearrange all Feynman diagrams according to their N scaling and write the partition function as

$$\log Z = \sum_{h=0}^{\infty} N^{2-2h} f_h(g_{YM}^2 N) \ . \tag{1.9}$$

We can now take the 't Hooft limit $N \to \infty$, $\lambda \quad fixed$. It is obvious that only planar diagrams survive. This looks suspiciously similar to the expansion of string perturbation theory. Indeed, now imagine making λ large. The planar diagrams become concentrated on the sphere and one can think of them as a discretized worldsheet of string theory. After this brief exposition of large N gauge theories we turn our attention to a specific theory. Instead of starting with gauge theory and carefully taking the 't Hooft limit we will focus on the opposite procedure. Firstly we examine string theory in the presence of D-branes and then briefly explain the emergence of the dual gauge theory.

1.3 Introduction to AdS/CFT

In this section a brief introduction to AdS/CFT is presented. AdS/CFT [12, 13, 14] is a duality relating string theory in a $d+1$-dimensional negatively curved background to field theory in d dimensions. Several review articles exist in the literature [15, 16, 17].

1.3.1 The physics of near-extremal D3-branes

D-branes are extended objects in string theory, that also have a dynamic nature. They have a tension and therefore can be a source for gravity. Moreover they can be charged under the fields present in ten dimensional supergravity. Similarly to black hole solutions in four dimensions there are black brane solutions in ten dimensions. It is instructive to consider the physics of a stack of N D-branes. Before doing that we take a small historical detour.

AdS/CFT originated in part from attempts to characterize black hole microstates in such a way that the famous Bekenstein-Hawking formula $S = A_H/4G$ can be reproduced using a partition function. The most successful examples of this program, starting with [18], are near-extremal charged black holes. The most familiar example is the near-extremal Reissner-Nordstrom solution in four dimensions:

$$ds^2 = -\left(1 - \frac{2M}{r} + \frac{Q^2}{r^2}\right) dt^2 + \frac{dr^2}{1 - 2M/r + Q^2/r^2} + r^2 d\Omega^2 \qquad A = \frac{Q}{r} dt\,, \tag{1.10}$$

where $d\Omega^2 = d\theta^2 + \sin^2\theta d\phi^2$ is the metric on the unit two-sphere S^2. The extremal solution has $M = Q$, and by introducing a new coordinate $\tilde{r} = r - Q$ one obtains

$$ds^2 = -\frac{\tilde{r}^2}{(\tilde{r}+Q)^2} dt^2 + \frac{(\tilde{r}+Q)^2}{\tilde{r}^2} d\tilde{r}^2 + (\tilde{r}+Q)^2 d\Omega^2\,. \tag{1.11}$$

The near-horizon geometry is the region where $0 < \tilde{r} \ll Q$. The line element in this region is

$$ds^2 = -\frac{\tilde{r}^2}{Q^2} dt^2 + \frac{Q^2}{\tilde{r}^2} d\tilde{r}^2 + Q^2 d\Omega^2\,. \tag{1.12}$$

It is notable that the geometry factorizes into an S^2 of radius Q and a two-dimensional geometry which turns out to be AdS_2. The metric on AdS_2 is a Wick rotation of the natural metric on the upper half-plane, with Euclidean time playing the role of the real part.

Embeddings of four-dimensional charged black holes in String/M-theory unfortunately involve non-trivial intersecting brane configurations. We will not delve into this direction here but mention some essential properties of these constructions. In one regime of parameters, they are well-described by line elements like (1.11), and the semi-classical formula $S = A/4G$ can be used. In another regime of parameters, they are well-described by a two-dimensional CFT with large central charge. Nearly unbroken supersymmetry, together with the special properties of CFT's in two dimensions, permit an extrapolation from one regime to the other, such that precise agreement is found for the entropy. While remarkable, these and other mathematically precise comparisons with two-dimensional CFT's do not appear to have immediate physical application. Fortunately, the story generalizes to four-dimensional CFT's, in particular $\mathcal{N} = 4$ super-Yang-Mills theory, which describes the low-energy excitations of D3-branes. The gluons of this theory, and their superpartners, are realized as strings with each end attached to a brane. This is easy to visualize if one things of a string that has one end on a D-brane and the other end on a different D-brane. The string inherits group theory indices from the indices of the D-branes. Similarly to QCD one can have a red-blue string if one associates color with D-branes. Gluons, being excitations of this open string also inherit these group theory factors.

Near-extremal D3-branes are 10-dimensional generalizations of the Reissner-Nordstrom solution for charged black holes. The relevant part of the type IIB string theory action is

$$S = \frac{1}{2\hat{\kappa}^2} \int d^{10}x \sqrt{\hat{G}} \left[\hat{R} - \frac{1}{4}\hat{F}_5^2 - \frac{1}{2}(\partial\hat{\phi})^2 \right] - \frac{1}{2\pi\alpha'} \int d^2\sigma \, e^{\hat{\phi}/2} \sqrt{\hat{g}} \tag{1.13}$$

where for later convenience we have included the dilaton and the Nambu-Goto action for a string worldsheet Σ. Here, $\hat{g}_{\alpha\beta} = \partial_\alpha X^M \partial_\beta X^N \hat{G}_{MN}$ is the induced metric on the worldsheet. The term $e^{\hat{\phi}/2}$ arises because $\hat{G}_{MN}$ is the Einstein metric. Hatted quantities like $d\hat{s}^2$ and $\hat{\kappa}^2$ are ten-dimensional, while five-dimensional quantities will be represented by unhatted variables like ds^2 and κ^2. Finally $\hat{F}_5 = *\hat{F}_5$ is imposed after other equations of motion are derived.

The non-extremal D3-brane solution has the following line element:

$$d\hat{s}^2 = \left(1 + \frac{L^4}{r^4}\right)^{-1/2} \left[-\left(1 - \frac{r_H^4}{r^4}\right) dt^2 + d\vec{x}^2 \right] + \left(1 + \frac{L^4}{r^4}\right)^{1/2} \left[\frac{dr^2}{1 - r_H^4/r^4} + r^2 d\Omega_5^2 \right] , \tag{1.14}$$

where $d\Omega_5^2$ is the metric on the unit five-sphere, S^5. Taking the limit $r \ll L$ and introducing a new radial coordinate $z = L^2/r$ leads to

$$d\hat{s}^2 = \frac{L^2}{z^2} \left(-h dt^2 + d\vec{x}^2 + \frac{dz^2}{h} \right) + L^2 d\Omega_5^2 \qquad h = 1 - (z/z_H)^4 \, . \tag{1.15}$$

Standard arguments lead to

$$L^4 = \frac{\hat{\kappa} N}{2\pi^{5/2}} = g_{YM}^2 N \alpha'^2 \qquad T = \frac{1}{\pi z_H} \, . \tag{1.16}$$

The horizon across a coordinate volume V_3 in the $\vec{x}$ directions is proportional to the entropy of the gauge theory in the same volume [19]:

$$\begin{aligned} A_H &= V_3 \frac{L^3}{z_H^3} \pi^3 L^5 = V_3 T^3 L^8 \pi^6 \\ s &= \frac{S}{V_3} = \frac{A_H}{V_3 \hat{\kappa}^2 / 2\pi} = \frac{\pi^2}{2} N^2 T^3 \,. \end{aligned} \tag{1.17}$$

This is 75% of the free field value

$$s = \frac{2\pi^2}{3} N^2 T^3 \,. \tag{1.18}$$

The mismatch is due to the fact that the semi-classical gravitational description leading to (1.17) relies on having $L \gg \sqrt[4]{\kappa}$ and $L \gg \sqrt{\alpha'}$—that is, $N \gg 1$ and $g_{YM}^2 N \gg 1$. It is hard to verify the factor of 3/4 in a way that does not involve AdS/CFT, but it is intriguing to see that this factor is comparable to the 20% deficit in energy observed in lattice calculations of QCD in the window $1.2T_c \lesssim T \lesssim 3.5T_c$. It is often supposed that $f(g_{YM}^2 N) \equiv -F/VT^4$ for $\mathcal{N} = 4$ super-Yang-Mills interpolates smoothly between 1 and 3/4 as $g_{YM}^2 N$ runs from 0 to ∞.

There is much more to AdS/CFT than the comparison of entropy. It relates the action on the string theory side,

$$\begin{aligned} I_{\text{string theory}} = &\frac{1}{2\kappa_5^2} \int_{AdS_5} d^5x \sqrt{-G} \left[R + \frac{12}{L^2} - \frac{1}{2} (\partial\phi)^2 + \ldots \right] \\ &- \frac{1}{2\pi\alpha'} \int_\Sigma d^2\sigma \sqrt{-g}\, e^{\phi/2} \,, \end{aligned} \tag{1.19}$$

to the generating functional of connected Green's functions for $\mathcal{N} = 4$ super-Yang-Mills,

$$W_{\mathcal{N}=4} \equiv \left\langle \int_{\mathbf{R}^{3,1}} d^4x \left[\phi\big|_{\text{bdy}} \operatorname{tr} F^2 + h_{mn}\big|_{\text{bdy}} T^{mn} \right] \right\rangle_{\text{connected}} \tag{1.20}$$

in the following manner:

$$W_{\mathcal{N}=4} \left[\phi\big|_{\text{bdy}} \,, \, h_{mn}\big|_{\text{bdy}} \right] = -I_{\text{string theory}} \left[\text{on shell} \right] \,, \tag{1.21}$$

where on the right hand side, the dilaton and metric are required to take on limiting values near the boundary of AdS_5 (at $z = 0$ in the coordinate system used in (1.15)). On shell means that once the boundary values are imposed, one extremizes $I_{\text{string theory}}$. The resulting value of $I_{\text{string theory}}$ is a connected correlator of the gauge theory. A more precise, but more abstract statement of the duality is that the partition functions of type IIB string theory on $AdS_5 \times S^5$ and $\mathcal{N} = 4$ gauge theory on the boundary of AdS_5 coincide. We will use this fact in chapter 2 to evaluate the profile of TrF^2 in a certain case.

In short, near-extremal D3-branes encode, via the AdS/CFT duality, the finite temperature dynamics of $\mathcal{N} = 4$ super-Yang-Mills theory in $3 + 1$ dimensions, and so provide us with an "analogous system" to the QGP over which we have good analytical control at large N and large $g_{YM}^2 N$. There are some elaborations to this statement that are worth noting. If there is a black hole horizon inside AdS_5 (as in the AdS_5-Schwarzschild solution), then infalling conditions must be imposed on classical fields at the horizon. Although many interesting quantities can be calculated starting from the five-dimensional action (1.19), obtained by making a Kaluza-Klein reduction on S^5, sometimes it is important to use the full ten-dimensional geometry, $AdS_5 \times S^5$. For the purposes of this thesis, we do not consider the complications of the complete ten dimensional space. Corrections to (1.21) arise in inverse powers of $g_{YM}^2 N = L^4/\alpha'^2$ and $N = 2\pi L^{3/2}/\kappa_5$ due to α' corrections and quantum effects in string theory. It is generally accepted that objects near the boundary of AdS_5 correspond to well-localized, hard field configurations in the boundary theory, whereas objects deep inside AdS_5 correspond to larger, more diffuse field configurations. A great number of variants of the duality exist in the literature, relating less supersymmetric and even non-conformal four-dimensional gauge theories to more complicated string theory geometries. Unfortunately, we do not yet know the "holographic dual" of pure QCD, or even if it has one. If it does, it cannot be described wholly within supergravity because the coupling gets weak in the UV.

1.3.2 Viscosity in strongly coupled plasmas

The relevance of strings to RHIC started to seem possible because of a computation [20, 21] of the ratio of shear viscosity to entropy density for near-extremal D3-branes:

$$\frac{\eta}{s} = \frac{\hbar}{4\pi} \,. \tag{1.22}$$

This dovetails better with the "experimentally observed" range $0 \leq \eta/s \ll 1$ than other first-principles calculations: for example, the leading log, weak coupling result [22, 23, 24] for QCD with $N_f = 3$ is

$$\frac{\eta}{s} \approx \frac{46.1}{g_{YM}^4 N^2 \log(4.17/g_{YM}\sqrt{N})} \,, \tag{1.23}$$

which attains a minimum of approximately 1.66 at $g_{YM}^2 N \approx 10.5$. Additional interest attaches to (1.22) because it saturates a conjectured viscosity bound $\eta/s \geq \hbar/4\pi$ [21] to which there are no known exceptions. The derivation of the experimental value $0 \leq \eta/s \ll 1$ will be explained in section 1.4.

The calculation leading to (1.22) hinges on graviton absorption by branes:

$$S_{\rm D3-brane} \supset \int d^4x \, h_{\mu\nu} T_{\mu\nu} \,. \tag{1.24}$$

The absorption cross-section a graviton h_{xy}, from the coupling (1.24), is

$$\sigma(\omega) = V_3 \frac{8\pi G_N}{\omega} \int d^4x \, e^{i\omega t} \langle [T_{xy}(t,\vec{x}), T_{xy}(0)] \rangle \,. \tag{1.25}$$

The factor of V_3 is because the D3-brane is extended: V_3 is its (infinite) 3-volume in the $\vec{x}$ directions.

In the gravitational picture where the D3-brane has a horizon, the graviton has some classical cross-section to fall into it. It turns out that

$$\sigma(\omega) \to A_{\rm horizon} = 4G_N S \qquad \text{as } \omega \to 0 \,. \tag{1.26}$$

Using Kubo's formula that is derived from statistical mechanics the viscosity is

$$\begin{aligned} \eta &= \lim_{\omega \to 0} \frac{1}{2\omega} \int d^4x \, e^{i\omega t} \langle [T_{xy}(t,\vec{x}), T_{xy}(0)] \rangle \\ &= \frac{\sigma(0)}{16\pi G_N V_3} = \frac{s}{4\pi} \,. \end{aligned} \tag{1.27}$$

So we've verified (1.22). The key step is (1.26). An old result [25], refreshed and extended in [26], says that (1.26) is always true for backgrounds of two-derivative supergravity. The main idea behind this claim of universality is that spin-two gravitons decouple from matter fields in backgrounds of interest and so satisfy Klein-Gordon equation in dimensions transverse to the brane. All the complications of the relevant supergravity geometries are in directions *orthogonal* to indices of $h_{\mu\nu}$. But higher-derivative terms (finite λ corrections) *do* affect η/s, and the first of these for D3-branes (from $\alpha'^3 R^4$) makes $\eta/s > 1/4\pi$ [21].

The smallness of η/s is now proposed by some RHIC physicists as a measure of strong coupling [5].

1.3.3 Comparison of $\mathcal{N} = 4$ SYM and QCD

The combination of the entropy deficit (1.17) and the viscosity calculation (1.22) has already drawn considerable attention from the RHIC and string theory communities. This attention is merited. However we should not forget the differences that exist between $\mathcal{N} = \triangle$ SYM theory and QCD. $\mathcal{N} = 4$ gauge theory exhibits neither confinement nor asymptotic freedom. The coupling doesn't run, instead it's a parameter that can be set at a prefered value. There is no chiral symmetry breaking in $\mathcal{N} = 4$ gauge theory. There is no suppersymmetry in QCD and all the fundamental matter fields in $\mathcal{N} = 4$ gauge theory are in adjoint representation. Moreover in addition to the gluons A_μ, there are four Majorana fermions λ_i and six real scalars X_I. These superpartners transform in representations of $SO(6)$, which (not accidentally) is also the symmetry group of the five sphere S^5.

While serious, these points may not be fatal to the proposed connection between AdS/CFT and heavy-ion collisions. Neither confinement nor (according to lattice calculations) chiral symmetry breaking are operative in the QGP. Conformal symmetry is clearly an imperfect guide to the QGP at RHIC (although it might perhaps be a better one in the higher energy lead-on-lead collisions planned at the LHC). More realistic equations of state can perhaps be incorporated in the future by considering holographic renormalization group flows. The absence of matter that transforms in the fundamental representation is perhaps the most troublesome. On one hand, the absence of fundamentally charged dynamical particles means that the QCD string cannot break. On the other, the presence of unwanted massless adjoint fields could plausibly imply $O(1)$ deviations from the behavior of QCD above the confinement scale.

In summary, we have to ask more of string theory before we can expect broad agreement with QCD. Still, the worst problems relate to the vacuum, so comparisons of AdS/CFT with RHIC are merited. It should also encourage us that lattice calculations of transport coefficients are difficult, while perturbative methods are difficult to apply, leaving string theory a window of opportunity. At the very least, AdS/CFT provides an analogous system to the QGP which is richly featured and under relatively precise theoretical control. We should not fail to ask what AdS/CFT calculations might tell us about physics in heavy ion collisions.

1.4 Synopsis of R.H.I.C.

This small chapter briefly presents some of the experimental results from RHIC and their interpretation. We focus on three aspects of the quark-gluon plasma. Firstly, there is good reason to believe that the QGP thermalizes at a temperature significantly above the deconfinement transition of QCD. Secondly, in non-central gold-gold collisions, the QGP undergoes a collective motion, elliptic flow. Measurements of these collisions indicates that the shear viscosity of the QGP is small. Finally, hard partons lose energy quickly when they pass through the QGP, a phenomenon known as jet-quenching. This account depends on the review by Muller and Nagle [5], and some parts on the authoritative account of results through 2005 can be found in [27, 3, 28, 29].

1.4.1 The experimental setup

The primary physical process investigated at RHIC is the collision of beams of gold nuclei in moving opposite directions. The main beam ring is roughly 3.8 km in circumference, and has four separate experiments (BRAHMS, PHENIX, PHOBOS, and STAR) with complementary capabilities situated at four of the six beam intersection points. The beam energy is 100 GeV per nucleon. In addition to gold, RHIC can handle other species, e.g. copper.

Gold nuclei have 79 protons and 118 neutrons, and are fairly spherical with a radius R of about 7 fm. With respect to the center of mass frame, each nucleus moves with a Lorentz contraction factor γ of about 100, and consequently the front-to-back length of $2R/\gamma \approx 0.14\,\mathrm{fm}$. The inelastic cross-section can be estimated *roughly* as $\sigma_{\mathrm{tot}} = 4\pi R^2$. This is just the geometric overlap of the nuclei.

RHIC's design luminosity is $2 \times 10^{26}\,\mathrm{cm}^{-2}\mathrm{s}^{-1}$. To date, they have achieved a total integrated luminosity in the ballpark of $4\,\mathrm{nb}^{-1}$. An idealized version of RHIC detectors is the ability to assign p_T, ϕ, η (pseudorapidity), and particle identity (e.g. π, K, p, $\bar{p}$, Λ, Σ, Ξ, Ω, ϕ, J/ψ, D, etc.) to all hadrons coming out of the collision region, as well as to electrons, photons, and in restricted circumstances (i.e. high rapidity) muons. In reality, acceptance in η and ϕ varies: e.g. STAR accepts $|\eta| < 1$, while PHENIX accepts $|\eta| < 0.35$ with incomplete ϕ coverage. Most particles come out with $p_T < 1\,\mathrm{GeV}$, but the high-momentum tails reach up to $p_T \sim 10\,\mathrm{GeV}$.

1.4.2 The quark-gluon plasma

When gold nuclei collide, about 400 nucleons go in, and about 7500 come out. A lot of entropy gets produced. A more interesting and non-trivial claim is that a thermalized quark-gluon plasma (QGP) is formed with a temperature as high as 300 MeV. After formation, the QGP cools approximately isentropically and then hadronizes.

Part of the evidence for a thermalized QGP is that hadron yields at mid-rapidity can be fit to a thermal model: even multi-strange hadrons fit. See figure 1.1. The temperature $T_{\mathrm{ch}} \approx 157\,\mathrm{MeV}$, which is determined by fitting hadron yields to thermal occupation numbers (i.e. Bose-Einstein or Fermi-Dirac statistics) is only slightly lower than the accepted temperature for the confinement transition, $T_c \approx 170\,\mathrm{MeV}$, as determined through lattice calculations: see for example [2]. In fact, deconfinement and chiral symmetry restoration are believed to occur not through a true phase transition but through a rapid cross-over,

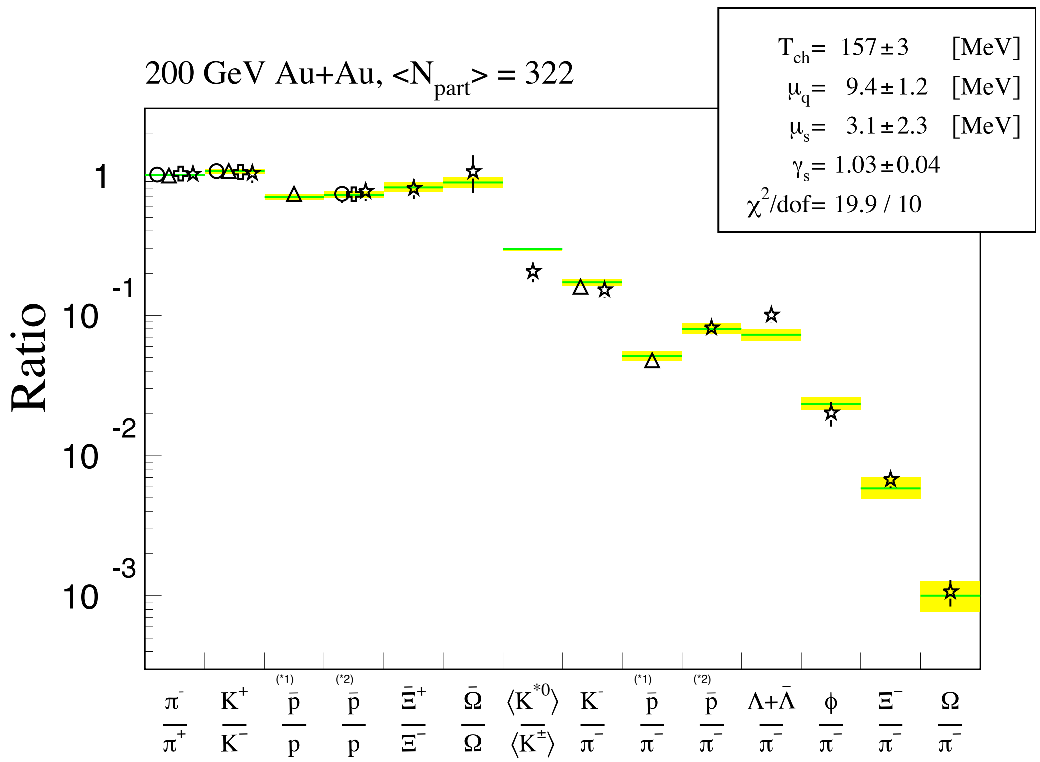

Figure 1.1: Ratios of hadron yields observed near mid-rapidity. The lines are the predictions of the thermal model. From [1]. Note that the chemical potentials for light quarks and strange quarks are *small* compared to the temperature.

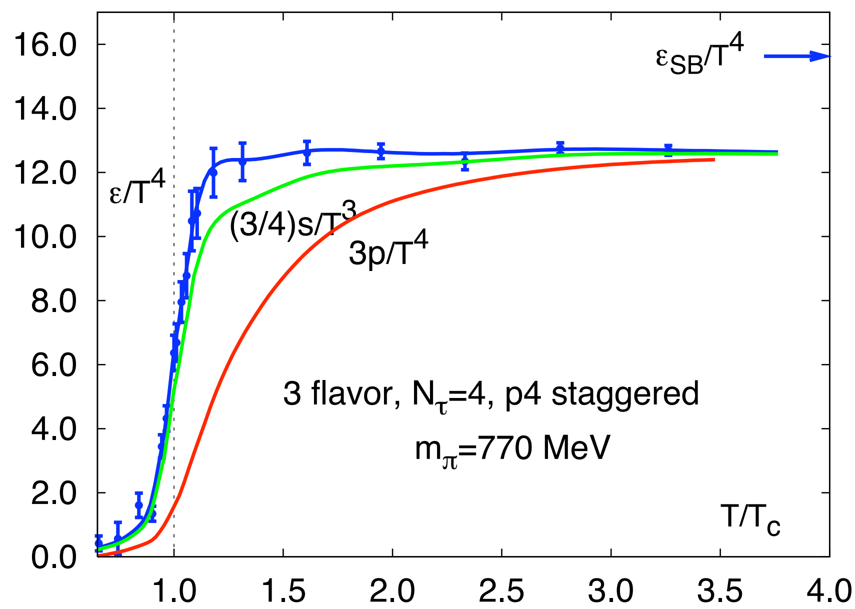

Figure 1.2: Lattice results for the equation of state of QCD. From [2].

above which the energy density is given approximately by

$$\epsilon \approx 6.3\,\mathrm{GeV/fm}^3 \left(\frac{T}{250\,\mathrm{MeV}}\right)^4 . \tag{1.28}$$

See figure 1.2. The validity of (1.28) seems to extend to several times T_c. It is notable that the value of ϵ/T^4 in (1.28) is about 80% of the free-field value.

Rapidity distributions of protons in central collisions indicate that 28 ± 3 TeV of the total 39 TeV of energy winds up in heating the newly created medium (putatively the QGP) and in its collective motion [30]. If 28 TeV were entirely concentrated in the Lorentz-contacted sphere of the gold nuclei at full overlap, the result would be an energy density of roughly $2000\,\mathrm{GeV/fm}^3$. This is almost certainly a substantial overestimate of the peak energy density: simple phenomenological models (with some support from experiment) indicate that energy densities in gold-gold collisions may reach $30\,\mathrm{GeV/fm}^3$ and thermalize by the time $\epsilon \sim$ 5-9 $\mathrm{GeV/fm}^3$ [3]—well above the QGP threshhold of $1\,\mathrm{GeV/fm}^3$. See figure 1.3.

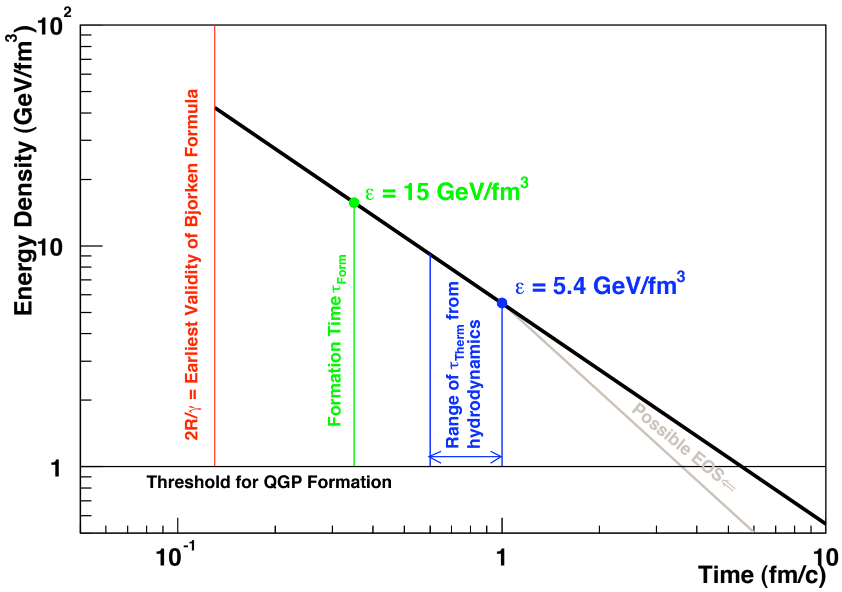

Figure 1.3: Energy density as a function of time in a central gold-gold collision, according to an elaboration of the phenomenological Bjorken model. From [3].

1.4.3 Centrality, elliptic flow, and jet-quenching

An important way to classify collisions of nuclei is the impact parameter of the collision. As described above, a crude approximation for collision rates comes from geometric overlap. *Centrality* refers to the extent of the overlap. A central collision is one where the gold nuclei hit head-on, whereas a peripheral collision is one where they almost missed.

Experiments at RHIC are capable of making an event-by-event determination of centrality, as well as the reaction plane defined by the beam line and the impact parameter. In other words, they can measure the impact parameter $\vec{b}$ as a vector. See figure 1.4. In order to avoid referring to a specific model of the cross-section, centrality is described in percentile terms. The 10% of all events that have the smallest values of b are described as having centrality of 0 to 10%. Note that this is somewhat reversed from what you might expect—head-on collisions have zero centrality. In the sphere-overlap model of the inelastic cross-section, the impact parameter corresponding to 10% centrality is evaluated like this

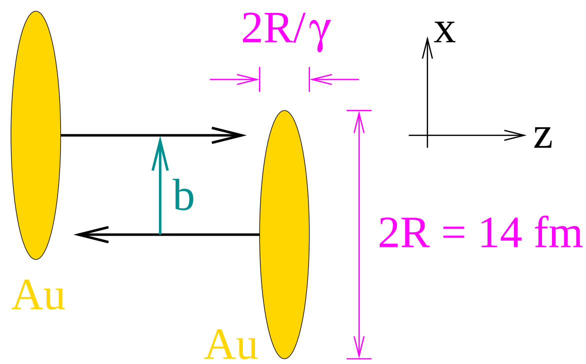

Figure 1.4: A gold-gold collision of intermediate centrality. The reaction plane is the plane of the page, in which the centers of mass of both gold nuclei are assumed to lie.

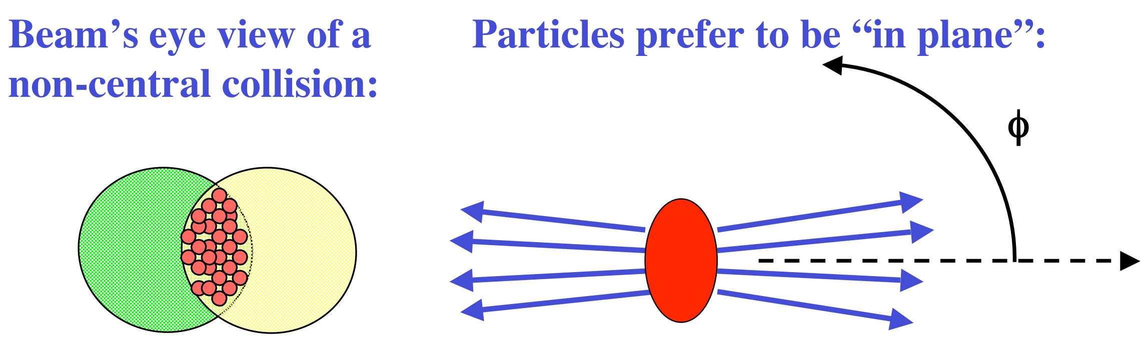

Figure 1.5: Cartoon of elliptic flow. From [4].

[31]:

$$0.1\ \sigma_{\mathrm{tot}} = \int_0^{b_{10}} dr\ 2\pi r \qquad \text{so} \qquad b_{10} = 2R\sqrt{0.1}\,. \tag{1.29}$$

In non-central collisions, an important process called *elliptic flow* occurs. The overlap region is roughly ellipsoidal with all axes unequal (biggest in y, smallest in z). The distribution of observed particles is parametrized as

$$\frac{dN}{p_T dp_T dy d\phi}(p_T, y, \phi; b) = \frac{dN}{p_T dp_T dy}\left[1 + 2v_2(p_T, y; b)\cos 2\phi + \ldots\right], \tag{1.30}$$

Here, v_2 is experimentally measured for different particle species, and $\phi = 0$ refers to emission in the reaction plane, so $v_2 > 0$ means this is preferred. The sizable observed values of v_2 are in line with non-viscous hydrodynamic models of collective flow:

$$\frac{D}{Dt}(\epsilon\vec{v}) = -\nabla P \tag{1.31}$$

with ∇P bigger at $\phi = 0$ than $\phi = \pi/2$ because the ellipsoid is shorter at $\phi = 0$ and longest at $\phi = \pi/2$.

Jet-quenching refers to the rapid loss of energy of a hard parton propagating through the hot dense matter created in a gold-gold collision. The prima facie evidence for jet quenching is the the suppression of high p_T jets (more precisely, high p_T hadrons) relative to expectations from "binary collision scaling." In binary scaling arguments, one replaces each gold atom by an equivalent flux of nucleons, each carrying 100 GeV of energy, which do not interact with one another, but which collide with nucleons going the other way. The number of collisions that would occur in this way is denoted $\langle N_{\text{binary}}\rangle$. Thus a single gold-gold collision is replaced by $\langle N_{\text{binary}}\rangle$ independent nucleon-nucleon collisions. To obtain an expected yield for a given particle species in a gold-gold collision, one scales up the yield measured in proton-proton collisions by the factor $\langle N_{\text{binary}}\rangle$. The ratio of this theoretical quantity to the observed outgoing particles is called R_{AA}:

$$R_{AA} \equiv \frac{dN(\text{gold-gold})/dp_T d\eta}{\langle N_{\text{binary}}\rangle dN(\text{proton-proton})/dp_T d\eta} \,. \tag{1.32}$$

Binary scaling is a successful predictor of the flux of outgoing photons with $p_T > 4\,\text{GeV}$: $R_{AA} \simeq 1$ for most p_T. This indicates that the QGP is fairly transparent to photons. For hadrons, however, the detected flux is considerably less than what is expected: $R_{AA} \approx 0.2$. The interpretation is that when an energetic scattering event occurs, the hard outgoing partons tend to lose a large fraction of their energy while plowing through the QGP.

1.4.4 Summary of experiment

The essential aspects of the experiment are summarized here. In central gold-gold collisions with 200 GeV per nucleon center-of-mass energy, a thermalized QGP forms as early as $t \sim 0.6\,\text{fm}/c$ with T as high as 300 MeV. It expands and cools isentropically with $\epsilon \propto 1/t$ (or maybe $1/t^{4/3}$) and hadronizes at about $t \sim 6\,\text{fm}/c$. Sizable anisotropy v_2 indicates elliptic flow of the QGP: a collective hydrodynamic motion which can be successfully modeled via inviscid hydro. Significant viscosity spoils the agreement: $\eta/s \ll \hbar$ seems to be a consensus from RHIC. Measurements of R_{AA} show that the QGP is approximately transparent to high-energy photons, but remarkably opaque to hadrons. Lattice simulations are quite good at predicting the equation of state, the transition temperature, etc., but transport properties, e.g. v_2 and R_{AA}, are hard. But, $N = 3$ and $g_{YM}^2 N \sim 6$ or higher, so maybe we can make some progress with AdS/CFT.

1.5 Jet quenching in the dual picture

In this section we present the picture of a heavy quark moving through the plasma as seen from the dual string theory. We start by considering a general background that is asymptotically AdS_{d+1} [32]

$$ds^2 = g_{tt}dt^2 + g_{zz}dz^2 + g_{xx}\delta_{ij}dx^i dx^j \ . \tag{1.33}$$

As $z \to 0$ the metric should approach the AdS metric, i.e.

$$g_{tt}, g_{zz}, g_{xx} \to \frac{L^2}{z^2} \ . \tag{1.34}$$

and we also assume the existence of a horizon at z_h. In addition we assume that all the metric components only depend on the radial coordinate z. The Hawking temperature in this background is given by

$$T = \frac{\sqrt{g_{tt}{}' g^{zz}{}'}}{4\pi} \tag{1.35}$$

and the entropy is given by the Bekenstein-Hawking formula

$$s = \frac{g_{xx}^{d-1}}{4\pi} \tag{1.36}$$

where both expressions are evaluated at $z = z_h$.

In this model a quark moving through the plasma is modeled by a string with one end attached to the boundary at $z = 0$. The action for the string is given by the area swept by the string worldsheet.

$$S = -\frac{1}{2\pi\alpha'}\int d\sigma s\tau\sqrt{-G} \quad G = \det G_{\alpha\beta} \tag{1.37}$$

and $G_{\alpha\beta}$ is the induced metric on the worldsheet. We are interested in finding the profile of a sting that has as a boundary condition $\frac{\partial X^1}{\partial t} = v$, i.e. a moving quark with velocity

v. A natural ansatz that repsects the symmetries of (1.33) and the symmetry around the direction of motion is

$$\tau = t \quad \sigma = z \quad X^1 = vt + \xi(z) \quad X^i = 0\,. \tag{1.38}$$

The worldsheet metric then becomes

$$G_{00} = g_{tt} + g_{xx}v^2 \quad G_{01} = g_{xx}v\xi' \quad G_{11} = g_{zz} + g_{xx}\xi'^2 \tag{1.39}$$

The Lagrangian density then becomes

$$\mathcal{L} = \frac{\sqrt{-G}}{2\pi\alpha'} = \frac{1}{2\pi\alpha'}\sqrt{-g_{tt}g_{zz} - g_{tt}g_{xx}\xi'^2 - g_{zz}g_{xx}v^2}\,. \tag{1.40}$$

Note that g_{tt} is negative in the region between the boundary and the horizon, so the Lagrangian density is real. We see that this Lagrangian does not depend on the variable ξ, so the conjugate momentum is a constant

$$\pi_\xi = \frac{\partial\mathcal{L}}{\partial\xi} = \frac{1}{2\pi\alpha'}\frac{g_{tt}g_{xx}\xi'}{\sqrt{-g_{tt}g_{zz} - g_{tt}g_{xx}\xi'^2 - g_{zz}g_{xx}v^2}} = \frac{C}{2\pi\alpha'}\,. \tag{1.41}$$

This equation can be solved to derive the profile of the string as

$$\xi' = \pm C\sqrt{\frac{-g_{tt}g_{zz} - g_{zz}g_{xx}v^2}{(g_{tt}g_{xx}(g_{tt}g_{xx} - C^2)}} \tag{1.42}$$

The plus solution corresponds to a string trailing the quark, while the minus one corresponds to a solution preceding the quark. The constant C is determined by the requirement that the solution is real for all values of z. That means that the numerator and denominator must have a zero at the same point, setting the value of C. This value depends on the specific geometry in case..

It is easy to derive the loss of energy and the force acting on the quark from the momentum flow along the string worldsheet.

$$\frac{dE}{dt} = \pi_t^1 = \frac{1}{2\pi\alpha'}Cv \quad \frac{dP}{dt} = \pi_x^1 = \frac{1}{2\pi\alpha'}C \tag{1.43}$$

For the specific case of AdS_5 [33, 34] where the dual theory is $\mathcal{N} = \triangle$ SYM we find as a solution

$$\xi(z) = -\frac{vz_h}{4i}\left(\log\frac{1 - iz/z_h}{1 + iz/z_h} + i\log\frac{1 + z/z_h}{1 - z/z_h}\right) \tag{1.44}$$

and the drag force is evaluated to be

$$\frac{dP}{dt} = -\frac{\pi\sqrt{g_{YM}^2 N}}{2} T^2 \frac{v}{\sqrt{1-v^2}} \ . \tag{1.45}$$

The scaling of the force with the specific power of temperature comes from the conformal symmetry of the CFT. We should also note that this result agrees with the calculation of the diffussion coefficient done in [35].

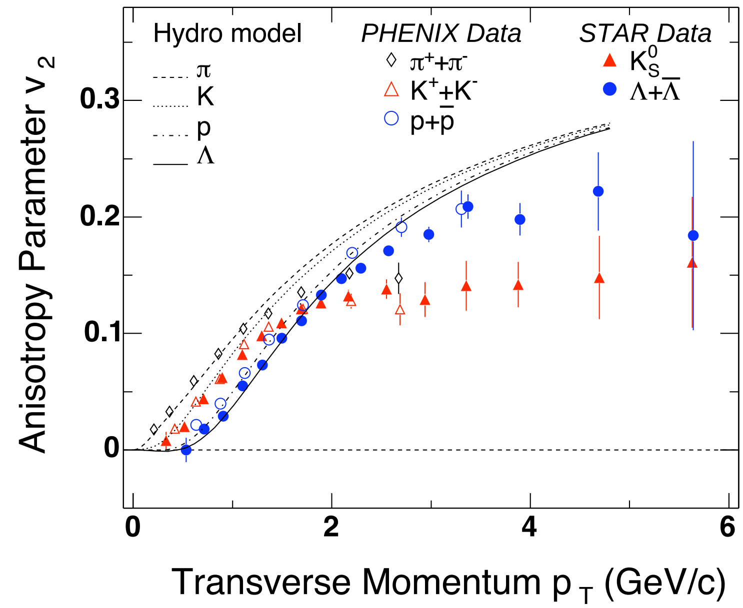

Figure 1.6: v_2 near mid-rapidity, with hydrodynamic calculations shown as dashed lines. From [5].

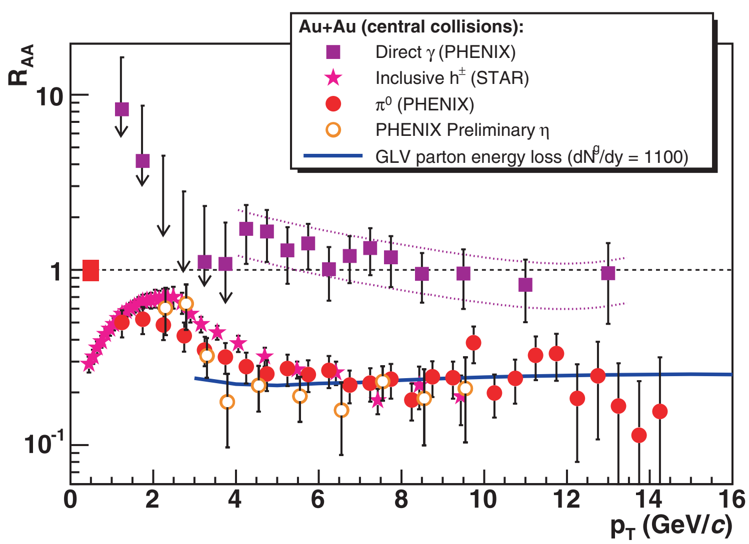

Figure 1.7: Nuclear modification factor R_{AA} for photons and hadrons in 0 to 10% central gold-gold collisions.

Chapter 2

Dissipation from a heavy quark

2.1 Introduction

In [33, 34], a classical solution of string theory is described that is dual in the sense of AdS/CFT [12, 13, 14] to an external quark passing through a thermal plasma of $\mathcal{N} = 4$ super-Yang-Mills theory at large N and strong 't Hooft coupling $g_{YM}^2 N$. The string is treated in the test string approximation: its back-reaction on the geometry is not considered. The string dangles into AdS_5-Schwarzschild from an external quark on the boundary which is constrained to move with constant velocity. The string trails out behind the quark and exerts a drag force

$$\frac{dp}{dt} = -\frac{\pi\sqrt{g_{YM}^2 N}}{2} T^2 \frac{v}{\sqrt{1-v^2}} \tag{2.1}$$

on the quark. Here v is the speed of the quark, and T is the temperature of the plasma, or equivalently the Hawking temperature of the horizon of AdS_5-Schwarzschild. The diffusion constant $D = 2/(\pi T \sqrt{g_{YM}^2 N})$ implied by (2.1) was derived independently in [35], also using AdS/CFT.

In the gauge theory, energy loss results from gluons (or superpartners of gluons) radiating off the heavy quark and interacting with the plasma. We should ask: How energetic are these radiated gluons? At what angle do they come off relative to the velocity of the heavy quark? To the extent that such questions can be posed in a gauge-invariant manner, AdS/CFT should be able to provide an answer. The aim of the present paper is to shed some light on these questions by computing the profile of $\langle \operatorname{tr} F^2 \rangle$ in the boundary gauge theory. To do this we compute the linear response of the dilaton field to the string, which is a first step in computing its back-reaction on the AdS_5-Schwarzschild background. Actually, what we will extract in the end is the vacuum expectation value (VEV) of the operator in $\mathcal{N} = 4$ super-Yang-Mills which couples to the dilaton. This is not quite $\operatorname{tr} F^2$, but rather the Lagrangian density plus a total derivative: in mostly plus signature,

$$\mathcal{O}_{F^2} = \frac{1}{2g_{YM}^2} \operatorname{tr} \left(-F_{mn}^2 + 2X^I D_m^2 X^I - 2i\bar{\lambda}^a \bar{\sigma}^m D_m \lambda_a + \text{more interactions} \right) , \tag{2.2}$$

where X^I are the six adjoint scalars, λ_a are the four Weyl adjoint fermions, D_m is the gauge-covariant derivative, and $\bar{\sigma}^m = (-\mathbf{1}, -\vec{\sigma})$ where $\vec{\sigma}$ are the Pauli matrices.

The near field of the heavy quark is just the Coulomb color-electric flux, appropriately Lorentz boosted. The contribution of this near field to $\langle \mathcal{O}_{F^2} \rangle$ can be computed analytically, following [36], and it has nothing to do with energy loss. When it is subtracted away from $\langle \mathcal{O}_{F^2} \rangle$, the remainder is peaked at momenta many times larger than the temperature. The information in $\langle \mathcal{O}_{F^2} \rangle$ is complementary to (2.1) in that it helps identify the energy scale at which dissipative phenomena occur but does not so clearly indicate the overall rate of dissipation. More complete information could be extracted from $\langle T_{\mu\nu} \rangle$, which could also be computed via AdS/CFT but requires a more technically involved treatment of metric perturbations.

Several related papers [37, 38, 32, 39] appeared recently, all aiming to describe at some level energy dissipation from a fundamental quark into a thermal plasma using AdS/CFT. The interest in this topic owes to a possible connection with relativistic heavy ion physics. A distinctive feature of RHIC experiments [27, 3, 28, 29] is jet-quenching, which is understood as strong energy loss as a high-energy parton passes through the quark-gluon plasma formed in a gold-on-gold collision.

The organization of the rest of this paper is as follows. In section 2.2 we explain the classical supergravity calculation that leads to $\langle \mathcal{O}_{F^2} \rangle$. Similar calculations were carried out in [40] for a string undergoing small oscillations around certain static configurations in

AdS_5. All the supergravity computations are done in five dimensions, but the final answer is the gauge theory quantity $\langle \mathcal{O}_{F^2} \rangle$ as a function of the coordinates (t, x^1, x^2, x^3) of Minkowski space. (Actually we will find it easier to pass to momentum space early in the computation.) One must solve a boundary value problem in order to extract $\langle \mathcal{O}_{F^2} \rangle$. Numerical techniques for doing so and results for several different choices of v are described in section 2.3. We conclude in section 2.4 with a discussion of the possible relevance of our work to recent experimental results. This chapter follows closely [8].

2.2 Dilaton perturbations

The background geometry is the well-known AdS_5-Schwarzschild solution,

$$ds^2 = G_{\mu\nu} dx^\mu dx^\nu = \frac{L^2}{z^2}(-h dt^2 + d\vec{x}^2 + dz^2/h) \qquad h = 1 - \frac{z^4}{z_H^4}\,, \tag{2.3}$$

and useful relations include

$$\frac{L^4}{\alpha'^2} = g_{YM}^2 N \qquad T = \frac{1}{\pi z_H}\,. \tag{2.4}$$

In static gauge, the string worldsheet is described as

$$\begin{gathered} X^\mu(t,z) \equiv \begin{pmatrix} t & X^1(t,z) & 0 & 0 & z \end{pmatrix} \\ X^1(t,z) = vt + \xi(z) \qquad \xi(z) = -\frac{z_H v}{4i}\left(\log\frac{1 - iz/z_H}{1 + iz/z_H} + i \log\frac{1 + z/z_H}{1 - z/z_H}\right)\,. \end{gathered} \tag{2.5}$$

To compute the dilaton response to this string, one starts with the following action:

$$S = \int d^5x\, \sqrt{-G}\left[-\frac{1}{4\kappa_5^2}(\partial\phi)^2\right] - \frac{1}{2\pi\alpha'}\int_M d^2\sigma\, e^{\phi/2}\sqrt{-g} \qquad g_{\alpha\beta} \equiv G_{\mu\nu}\partial_\alpha X^\mu \partial_\beta X^\nu\,. \tag{2.6}$$

Here α and β refer to worldsheet coordinates $\sigma^\alpha = (\tau, \sigma)$, and

$$\kappa_5^2 = \frac{4\pi^2 L^3}{N^2} = 8\pi G_5 \tag{2.7}$$

where G_5 is the five-dimensional gravitational constant. To derive the dilaton equation of motion, it helps first to rewrite the whole action as a single volume integral (we refrain briefly from choosing static gauge):

$$S = \int d^5x\, \sqrt{-G}\left[-\frac{1}{4\kappa_5^2}(\partial\phi)^2 - \frac{1}{2\pi\alpha'}\int d^2\sigma\, e^{\phi/2}\frac{\sqrt{-g}}{\sqrt{-G}}\delta^5(x^\mu - X^\mu(\sigma))\right]\,. \tag{2.8}$$

The five-dimensional delta function in (2.8) is a product of standard Dirac delta functions. So, for instance,

$$\delta^5(x^\mu) = \delta(t)\delta(x^1)\delta(x^2)\delta(x^3)\delta(z)\,. \tag{2.9}$$

The linearized equation of motion can now be straightforwardly derived as

$$\Box\,\phi = \frac{1}{\sqrt{-G}}\partial_\mu \sqrt{-G} G^{\mu\nu}\partial_\nu\phi = J \equiv \frac{\kappa_5^2}{2\pi\alpha'}\int d^2\sigma\, \frac{\sqrt{-g}}{\sqrt{-G}}\delta^5(x^\mu - X^\mu(\sigma))\,. \tag{2.10}$$

and by passing to static gauge one may explicitly perform then the remaining integral in (2.10):

$$J = \frac{\kappa_5^2}{2\pi\alpha'}\frac{\sqrt{-g}}{\sqrt{-G}}\delta(x^1 - X^1(t,z))\delta(x^2)\delta(x^3)\,. \tag{2.11}$$

In the spirit of finding the steady-state, late-time behavior, we assume that ϕ depends on x^1 and t only through the combination $x^1 - vt$. After computing

$$\frac{\sqrt{-g}}{\sqrt{-G}} = \frac{z^3}{L^3}\sqrt{1-v^2}\,, \tag{2.12}$$

one can easily show that $\Box\,\phi = J$ simplifies to

$$\left[z^3\partial_z\frac{h}{z^3}\partial_z + \left(1-\frac{v^2}{h}\right)\partial_1^2 + \partial_2^2 + \partial_3^2\right]\phi = \frac{\kappa_5^2\sqrt{1-v^2}}{2\pi\alpha'}\frac{z}{L}\delta(x^1 - vt - \xi(z))\delta(x^2)\delta(x^3)\,. \tag{2.13}$$

This partial differential equation can be attacked by Fourier transforming:

$$\phi(t,\vec{x},z) = \int \frac{d^3k}{(2\pi)^3}\, e^{ik_1(x^1-vt)+ik_2x^2+ik_3x^3}\phi_k(z)\,, \tag{2.14}$$

and similarly for J. Then one has

$$\left[z^3\partial_z\frac{h}{z^3}\partial_z - \left(1-\frac{v^2}{h}\right)k_1^2 - k_\perp^2\right]\phi_k = \frac{\kappa_5^2\sqrt{1-v^2}}{2\pi\alpha'}\frac{z}{L}e^{-ik_1\xi(z)}\,, \tag{2.15}$$

where $k_\perp^2 = k_2^2 + k_3^2$. All dimensionful factors drop out of the differential equation when we introduce rescaled variables

$$K_1 = z_H k_1 \qquad K_\perp = z_H k_\perp \qquad y = \frac{z}{z_H} \qquad \tilde{\phi}_K(y) = \frac{2\pi\alpha' L}{\kappa_5^2 z_H^3}\frac{1}{\sqrt{1-v^2}}\phi_k(z)\,. \tag{2.16}$$

Then $h = 1 - y^4$ and

$$\left[y^3\partial_y\frac{h}{y^3}\partial_y - \left(1-\frac{v^2}{h}\right)K_1^2 - K_\perp^2\right]\tilde{\phi}_K = ye^{-iK_1\xi/z_H} = y\left(\frac{1-iy}{1+iy}\right)^{vK_1/4}\left(\frac{1+y}{1-y}\right)^{ivK_1/4}\,. \tag{2.17}$$

There doesn't appear to be a solution to (2.17) in terms of known special functions. However it can be solved in two interesting limiting regimes:

- **Near the horizon,** y is slightly less than 1, a better choice of radial variable is $Y = \log(1-y)$. The leading terms in the differential equation near the horizon (that is, for large negative Y) are

$$\left[\partial_Y^2 + \left(\frac{vK_1}{4}\right)^2\right]\tilde{\phi}_K = \frac{1}{4}e^Y e^{-ivK_1(Y+\pi/2-\log 2)/4}\,, \tag{2.18}$$

  which is also the equation of motion for a simple harmonic oscillator with a complex driving force. The solutions are

$$\tilde{\phi}_{\text{near},K} = \frac{e^Y/4}{1-ivK_1/2}e^{-ivK_1(Y+\pi/2-\log 2)/4} + C_K^+ e^{ivK_1 Y/4} + C_K^- e^{-ivK_1 Y/4}\,, \tag{2.19}$$

  where $C_K^\pm$ are arbitrary constants. The standard boundary condition at a black hole horizon is to choose a purely infalling solution. This means that in the near-horizon limit, ϕ should depend on t and Y only through the combination $t + z_H Y/4$, not $t - z_H Y/4$: the quantity $z_H Y/4$ is essentially the tortoise coordinate. Thus $C_K^+ = 0$.

- **Near the boundary** of AdS_5-Schwarzschild, the leading terms in the differential equation are

$$y^3\partial_y \frac{1}{y^3}\partial_y \tilde{\phi}_K = y\,, \tag{2.20}$$

  and the solutions are

$$\tilde{\phi}_{\text{far},K} = -\frac{y^3}{3} + A_K + B_K y^4\,, \tag{2.21}$$

  where A_K and B_K are arbitrary constants. A_K should be set to zero because there is no deformation of the Lagrangian. B_K is proportional to $\langle \mathcal{O}_{F^2}\rangle$.

It is worth noting that the relation of B_K to $\langle \mathcal{O}_{F^2}\rangle$ involves a subtraction of contact terms. Conventionally, it is understood that

$$\langle \mathcal{O}_{F^2}(t,\vec{x})\rangle = -\frac{L^3}{2\kappa_5^2}\lim_{z\to 0}\frac{1}{z^3}\partial_z \phi(t,\vec{x},z)\,, \tag{2.22}$$

but in the present case, the limit doesn't exist because of the y^3 term in (2.21). Fortunately, this term has no $\vec{K}$ dependence. Thus when passing back to real space, it is proportional to a delta function supported at the location of the quark. This delta function has an infinite coefficient, but if it is subtracted, the remaining contribution to $\langle \mathcal{O}_{F^2}(t,\vec{x})\rangle$ indeed comes from B_K, and it is finite. The subtraction prescription has some arbitrariness: one could subtract off any finite multiple of the delta function at the same time, which corresponds to subtracting a K-independent quantity from every B_K.

Combining (2.4), (2.14), (2.16), (2.21), and (2.22), one finds

$$\langle \mathcal{O}_{F^2}(t,\vec{x})\rangle = -\pi^3 T^4 \sqrt{g_{YM}^2 N}\sqrt{1-v^2}\int \frac{d^3K}{(2\pi)^3} e^{\left[iK_1(x^1-vt)+iK_2x^2+iK_3x^3\right]/z_H} B_K\,. \tag{2.23}$$

In section 2.3, we will quote results in units where $z_H = 1$: this corresponds to $T = 1/\pi$.

For a wide range of K_1 and $K_\perp$, the dominant contribution to B_K comes from the near field of the quark, which in position space is proportional to $1/|\vec{x}|^4$ in the rest frame of the quark. Consider first the case $v = 0$. Following [36], consider a string dangling straight down in AdS_5. One obtains

$$\langle \mathcal{O}_{F^2}(t,\vec{x})\rangle = \frac{1}{16\pi^2}\frac{\sqrt{g_{YM}^2 N}}{|\vec{x}|^4}\,. \tag{2.24}$$

This calculation is done in the absence of a horizon, or equivalently at zero temperature. Fourier transforming (2.24) leads to

$$B_K^{\text{near field}} = \frac{\pi}{16}|\vec{K}| = \frac{\pi}{16}\sqrt{K_1^2 + K_\perp^2}\,. \tag{2.25}$$

We have expressed the result in terms of the dimensionless variables (2.16) with $z_H = 1/\pi T$ finite, even though $T = 0$ physically. This is a bookkeeping trick to obtain a form that can easily be compared with AdS_5-Schwarzschild results.

For $v \neq 0$, one may apply a Lorentz boost to the AdS_5 string configuration considered in the previous paragraph. This describes an external quark moving through the vacuum at speed v. The result for $B_K^{\text{near field}}$ in this case is

$$B_K^{\text{near field}} = \frac{\pi}{16}\sqrt{(1-v^2)K_1^2 + K_\perp^2}\,. \tag{2.26}$$

This is the analytic form that we will subtract from numerically evaluated B_K to excise the near field but leave behind all the dissipative dynamics.

2.3 Numerical algorithms and results

The boundary value problem described in and below (2.17) is reminiscent of both the glueball calculations initiated in [41, 42] and of quasi-normal modes in AdS_5-Schwarzschild [43]. But there is an additional simplifying feature: all the equations are affine in $\tilde{\phi}_K$—that is, they are linear combinations of $\tilde{\phi}_K(y)$, its derivatives, and functions of y that do not involve $\tilde{\phi}_K(y)$. To see this, consider the following formulation of the horizon boundary condition. One first expresses the asymptotic solutions $\tilde{\phi}_{\text{near},K}$ and $\tilde{\phi}_{\text{far},K}$ as a sum of the inhomogeneous solution and the permitted homogeneous solution. Explicitly, for the near-horizon solution,

$$\begin{aligned} \tilde{\phi}_{\text{near},K} &= \tilde{\phi}_{\text{near,P},K} + C_K^- \tilde{\phi}_{\text{near,H},K} \\ \tilde{\phi}_{\text{near,P},K} &\equiv \frac{e^Y/4}{1 - ivK_1/2} e^{-ivK_1(Y+\pi/2-\log 2)/4} \\ \tilde{\phi}_{\text{near,H},K} &\equiv e^{-ivK_1 Y/4} \,. \end{aligned} \tag{2.27}$$

The Wronskian

$$W_{\text{near}}(y) = (\tilde{\phi}_K(y) - \tilde{\phi}_{\text{near,P},K}(y))\tilde{\phi}'_{\text{near,H},K}(y) - (\tilde{\phi}'_K(y) - \tilde{\phi}'_{\text{near,P},K}(y))\tilde{\phi}_{\text{near,H},K}(y) \tag{2.28}$$

is a measure of how close the numerically computed function $\tilde{\phi}_K(y)$ is to the analytic approximation $\tilde{\phi}_{\text{near},K}$. Because the horizon is a singular point of the differential equation, one must impose the boundary condition $W_{\text{near}}(y_1) = 0$ at a point y_1 slightly less than 1, which is to say slightly outside the horizon. The quantity $W_{\text{near}}(y_1)$ is indeed a linear combination of $\tilde{\phi}_K(y)$, $\tilde{\phi}'_K(y)$, and a $\tilde{\phi}_K$-independent function known in terms of $\tilde{\phi}_{\text{near,H},K}(y)$ and $\tilde{\phi}_{\text{near,P},K}(y)$. One may similarly formulate a boundary condition $W_{\text{far}}(y_0) = 0$ which is also affine in $\tilde{\phi}_K$. The point y_0 should be chosen slightly greater than 0, which is to say close to the boundary of AdS_5-Schwarzschild.

There are special methods to solve boundary value problems of the type just described, where both the differential equation and the boundary conditions are affine, which are more efficient than standard shooting algorithms. Mathematica's `NDSolve` incorporates such methods internally. But we have found that we achieve greater numerical accuracy using a home-grown shooting method where B_K is guessed and then adjusted to make $C_K^+ = 0$. Accuracy was further improved by finding power series corrections to the asymptotic forms (2.19) and (2.21). A satisfactory choice of cutoff points was $y_0 = 0.01$ and $y_1 = 0.99$. The numerical challenge increases as K_1 and $K_\perp$ increase, requiring more CPU time. As we will see in figure 2.2, B_K is significantly weighted toward K larger than 10 when an appropriate phase space factor is included. So it would be worthwhile to have some alternative method adapted to this regime, perhaps based on a WKB approximation.

We take advantage of the axial symmetry of the problem to express $B_K = B(K_1, K_\perp)$ where $K_\perp = \sqrt{K_2^2 + K_3^2}$. Because $\phi(t, \vec{x}, z)$ and $\langle \mathcal{O}_{F^2}(t, \vec{x}) \rangle$ are real, it must be that $B(-K_1, K_\perp) = B(K_1, K_\perp)^*$. It is easy to see that this condition is enforced by the differential equation. Our results for $B(K_1, K_\perp)$, with the near field (2.26) subtracted, are shown in figures 2.1 and 2.2. A good match to the near field form (2.26) was obtained: for $K_\perp > 10$ the deviations are at the level of tenths of a percent. These deviations are interesting and can be seen in magnified form in panes b, d, f, and h of figure 2.2. Much of our discussion in section 2.4 will hinge on these high-momentum tails.

2.4 Discussion

Before attempting a comparison of our results with recent RHIC results, we will give a brief summary of how the measurements of interest are done. The reader is warned that we are non-experts and is referred to the experimental literature—for example [44, 45]—for an authoritative account.

Consider the following scenario:

1. Two highly energetic partons collide near the surface of the hot dense matter produced in a relativistic heavy ion collision. After the collision, the partons have large transverse momentum.

2. One parton escapes without interacting significantly with the quark-gluon plasma (QGP) and fragments in vacuum into what is termed the near side jet.

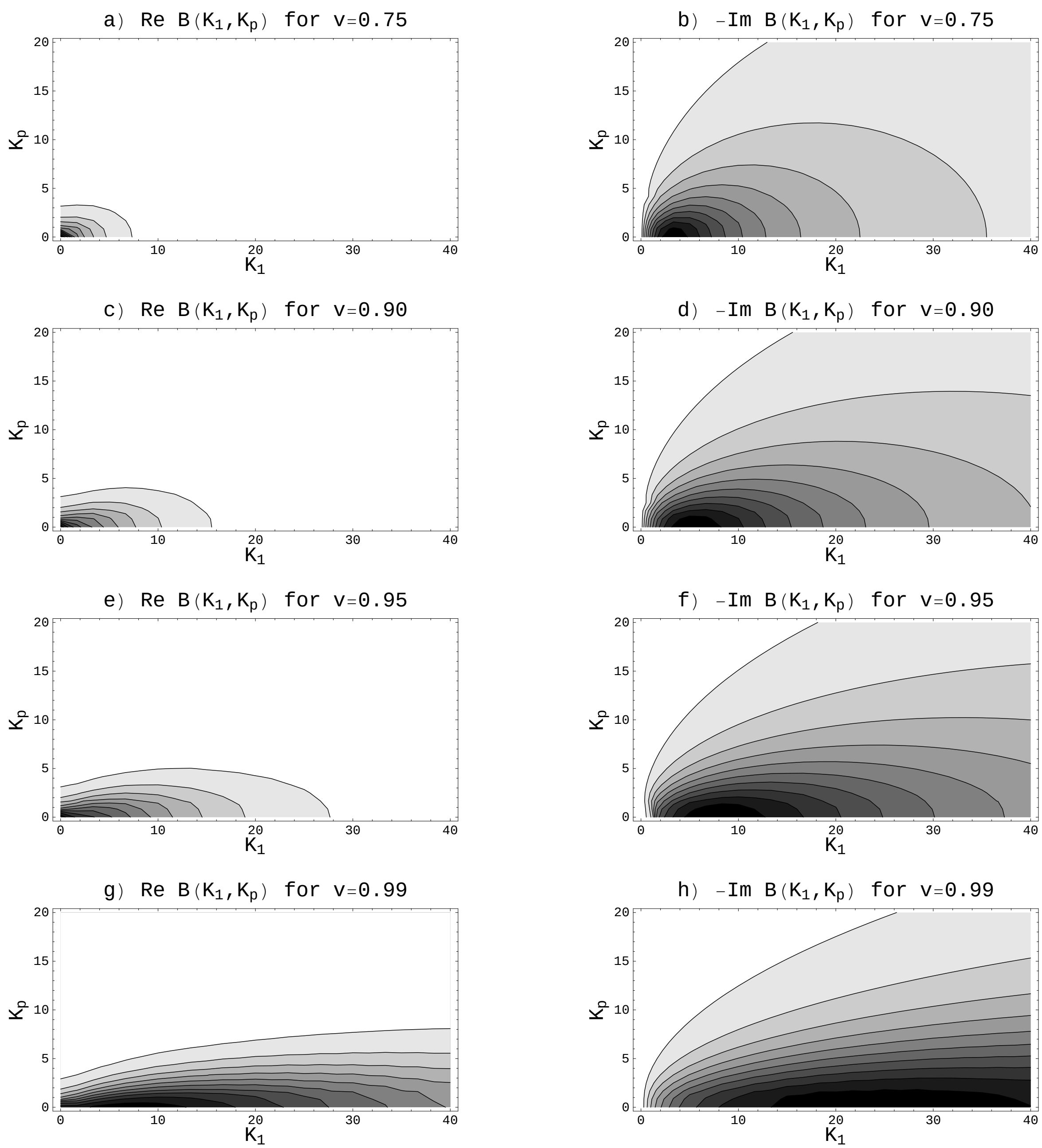

Figure 2.1: Contour plots of the real part and minus the imaginary part of $B(K_1, K_\perp)$ for several values of v. The near field contribution (2.26) has been subtracted. $B(K_1, K_\perp)$ is proportional to the K-th Fourier mode of $\langle \mathcal{O}_{F^2} \rangle$: see (2.23). In each plot, the white region is closest to zero, and the black region is the most positive.

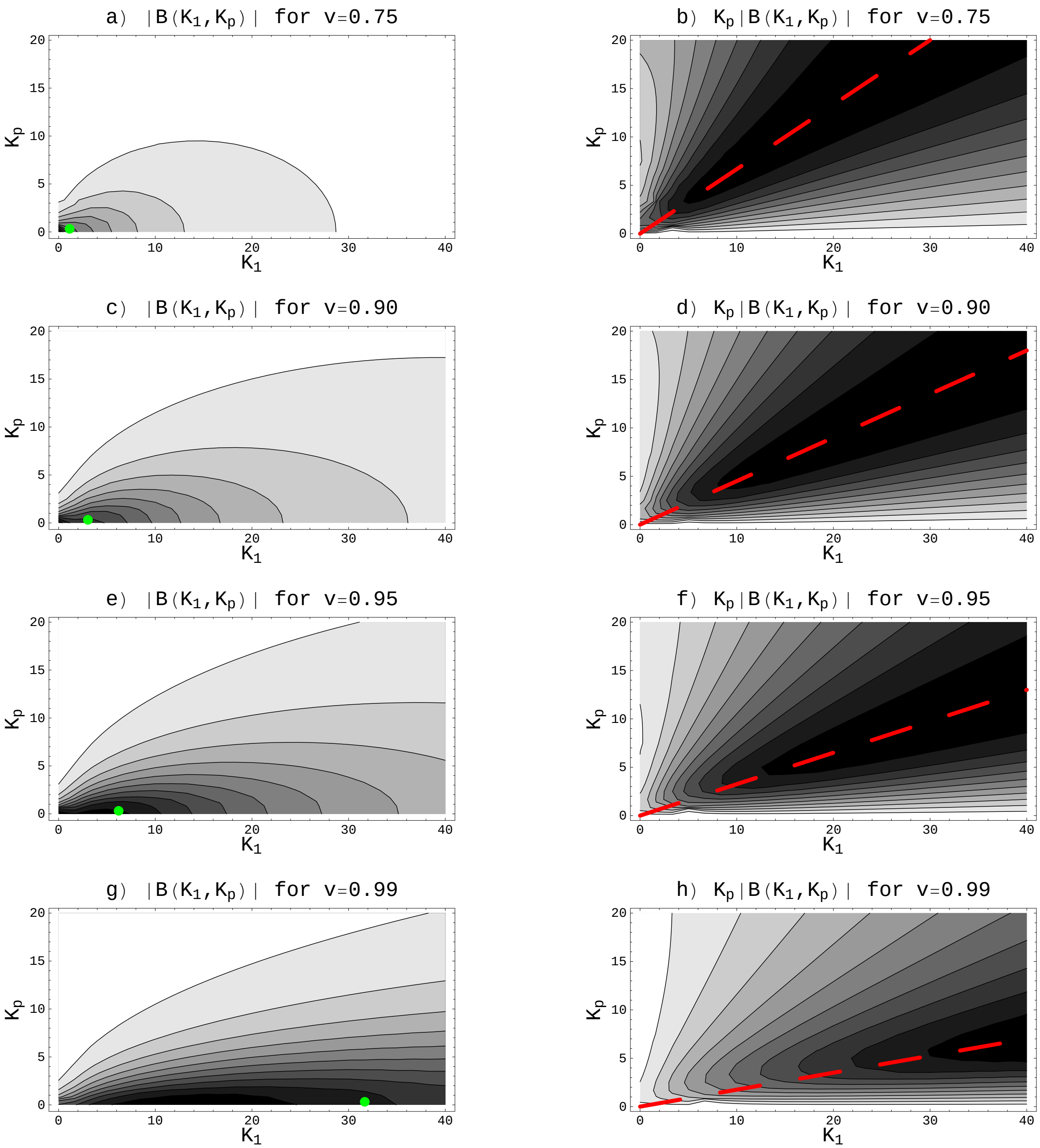

Figure 2.2: The absolute value of $B(K_1, K_\perp)$ with and without the phase space factor $K_\perp$. The near field contribution (2.26) has been subtracted. The green dot is the recoil energy of a thermal gluon: see (2.30). The dashed red lines indicate the direction in which $K_\perp |B(K_1, K_\perp)|$ is largest: see the discussion around (2.4). In each plot, the white region is closest to zero, and the black region is the most positive.

3. The other parton travels through the QGP. Its evolution into observed particles is strongly affected by its interaction with the QGP. If it weren't for these interactions, this parton would simply fragment into an away side jet, approximately back-to-back with the near side jet.

Because of difficulties in unambiguously identifying jets, a standard strategy is to look for angular correlations between two energetic charged particles: the trigger particle, which is presumed to be part of the near-side jet, and the partner particle, which is the putative probe of jet-quenching. Histograms of the azimuthal angle $\Delta\phi$ between these two particles invariably show a peak at small angles, which means that the partner particle is often part of the near-side jet. A peak at $\Delta\phi = \pi$ is evidence for an away side jet. In central collisions, the peak at $\Delta\phi = \pi$ disappears [44] or even splits [45]. In [45], the trigger particle is required to have $2.5\,\mathrm{GeV}/c < p_T < 4.0\,\mathrm{GeV}/c$ while the partner particles has $1.0\,\mathrm{GeV}/c < p_T < 2.5\,\mathrm{GeV}/c$, and for central collisions a broad peak is observed roughly between $\Delta\phi = 1.6$ and $\Delta\phi = 2.6$. (All angles will be quoted in radians.) There is actually a minimum at $\Delta\phi = \pi$.

The recent theoretical literature on jet-quenching, with which we have less familiarity than we would like, offers several possibilities. Among them are scenarios [46, 47] where the QGP affects fragmentation by recombination of thermal quarks with the parton shower; extensions of traditional QCD methods such as the twist expansion [48]; predictions of a coherent high momentum ridge of color flux emanating from the quark [49, 50]; and related discussions of a QCD "sonic boom" giving rise to conical collective flow [51, 52].

In the backdrop of these experimental and theoretical investigations, it is interesting to say what we can about the energy flow and spectrum of particles radiated from the heavy quark described in the previous sections. The hazards of comparing strongly coupled $\mathcal{N} = 4$ super-Yang-Mills with real-world QCD are well known: for a brief summary, see [34]. To these difficulties we must add that we have treated the quark as infinitely massive, whereas the experimental results we have referred to do not include heavy-quark tagging. Also, it would be better to know $\langle T_{\mu\nu} \rangle$ in addition to $\langle \mathcal{O}_{F^2} \rangle$: energy flow is most crisply captured in the Poynting vector $S_i = T_{0i}$. Finally, it would be desirable to go to larger K_1 and $K_\perp$, which requires either CPU-intensive numerics or an improved calculational method, as discussed near the end of section 2.3.

Objects deep inside AdS_5 are understood to correspond to soft field configurations in the dual CFT, while objects near the boundary correspond to more localized configurations. So a reasonable expectation based on [33, 34] is that the profile of $\langle \mathcal{O}_{F^2} \rangle$ would have the form of a wake, consistent with the ideas of [49, 50, 51, 52]. The Fourier space profiles shown in figures 2.1 and 2.2 suggest a slightly different, possibly complementary picture. It helps our intuition to use explicit numbers. Let's set

$$T = \frac{1}{\pi}\,\mathrm{GeV} = 318\,\mathrm{MeV}\,. \tag{2.29}$$

This is in the upper range of temperatures for the QGP, and it is a convenient choice for us because the K_1 and $K_\perp$ axes in figure 2.1 and 2.2 can then be read in units of GeV/c. Another interesting number is the typical final energy of a free massless particle that collides elastically with the heavy quark. To compute this we take the initial momentum of the massless particle to be of magnitude T and directed perpendicular to the heavy quark's velocity. If the perpendicular component of the massless particle's momentum doesn't change during the collision, then its final energy is

$$E_f = \frac{1+v^2}{1-v^2} T = 6.2\,\mathrm{GeV} \qquad \text{for } v = 0.95. \tag{2.30}$$

We have indicated E_f for the various velocities with the green dots in panes a, c, e, and g of figure 2.2. If the gauge theory were almost free instead of strongly coupled, we would expect the energy loss to be dominated by collisions of the type that led to (2.30).

For $v = 0.95$, $|B(K_1, K_\perp)|$ is peaked in a range of momenta between 2 and 7 GeV/c (the black region in figure 2.2). Because $\mathcal{O}_{F^2} \sim \mathrm{tr}\, F^2$ starts with bilinears in the fundamental fields, this would correspond to radiated particles with momenta between 1 and 3.5 GeV/c: less than the E_f of (2.30) by a factor of a few. For $v = 0.99$, half the momentum at which $|B(K_1, K_\perp)|$ is peaked is less than E_f by a similar factor. These considerations encourage the view that dissipative events involve several quanta interacting with each other as they

v	0.75	0.90	0.95	0.99
θ	0.58	0.41	0.30	0.17

Table 2.1: The angle between the heavy quark's velocity and the directional peak of $K_\perp|B(K_1,K_\perp)|$ for various values of the velocity.

recoil from the heavy quark. This is broadly consistent with the picture of a coherent co-moving high momentum ridge dissipating energy from the heavy quark. But as we will see below, the peak regions of $|B(K_1,K_\perp)|$ may not dominate the dissipative physics.

Panes b, d, f, and h of figure 2.2 show that if one multiplies $|B(K_1,K_\perp)|$ by the factor $K_\perp$ that would arise in an integration over momentum space, the result is directionally peaked. This again brings to mind the picture of dissipation through radiation carried mostly in the high momentum ridge. The opening angle θ between the heavy quark's velocity and the directional peak of $K_\perp|B(K_1,K_\perp)|$ depends strongly on the speed as shown in Table 2.4

The values of θ in Table 2.4 were determined by setting the $K_\perp$ derivative of $K_\perp|B(K_1,K_\perp)|$ to zero at fixed and large K_1, then taking the appropriate arctangent function to find θ.

The phase space factor $K_\perp$ makes an enormous difference to the dominant momentum scale. In $K_\perp|B(K_1,K_\perp)|$, momenta many times E_f dominate. Indeed, along the preferred direction, $K_\perp|B(K_1,K_\perp)|$ seems to level off at a finite value as K increases. Evidently we have not explored sufficiently high momenta to discern whether the region where $K_\perp|B(K_1,K_\perp)|$ is above a finite threshhold has finite volume.[1]

To recap: the plots of $K_\perp|B(K_1,K_\perp)|$ not only indicate directionality, but also suggest that highly energetic fields are an important part of the description of the radiation process. To appreciate just how energetic, note that a charm quark moving in vacuum with $v = 0.95$ has energy 4.5 GeV, while a b quark with this speed has energy 15 GeV. If $K_\perp|B(K_1,K_\perp)|$ can be used as an approximate guide to the spectrum of radiated particles, the single particle energy could easily be in the 10 GeV ballpark. Recoil would obviously become an important

[1]Note that in the large momentum region of the plots shown, we are subtracting a quantity, $B_K^{\text{near field}}$, which scales linearly with momenta. The remainder, $B(K_1,K_\perp)$, scales roughly as $1/K$ in the region in question. This evidently requires substantial numerical precision. All internal checks of our numerical results suggest they are robust, but the importance of large K tails to our discussion is the reason we say it would be value to have WKB methods in hand.

consideration if a real-world c or b quark emitted a particle even approaching this range. This would substantially increase the opening angle θ. And it would encourage the idea that the QGP enhances fragmentation processes at energies close to the kinematic limit.

There are two main reasons to treat with particular caution a "prediction" from AdS/CFT that heavy quarks should undergo fragmentation near the kinematic limit:

1. We have not made a quantitatively precise connection between $\langle \mathcal{O}_{F^2} \rangle$ in Fourier space and the spectrum of radiated particles. Indeed, the peak region of $B(K_1, K_\perp)$ and its high-momentum tails send conflicting messages about the spectrum. We believe the tails are important, but it may be that they have to do mostly with fields near the quark rather than radiative dynamics. The question of the spectrum of radiated particles should be revisited purely within the context of AdS/CFT with the VEV of the stress-energy tensor in hand, and preferably with semi-analytic methods to buttress numerical analysis of the high-momentum tails.[2]

2. Relating hard processes in strongly coupled $\mathcal{N} = 4$ super-Yang-Mills and QCD is especially perilous. Elementary scattering processes with large momentum transfer can be treated perturbatively in QCD. In strongly coupled $\mathcal{N} = 4$ super-Yang-Mills the general expectation is that they cannot. But one should bear in mind that many amplitudes of $\mathcal{N} = 4$ are protected against all loop corrections. It would be interesting to inquire whether amplitudes for gluons scattering off an external quark have non-renormalization properties. This discussion recalls the basic conundrum of the connection between AdS/CFT and RHIC: are near-extremal D3-branes merely an analogous system to the QGP, or can they capture the dynamics of real-world QCD above the confinement transition sufficiently precisely to be a useful guide to RHIC physics?

Fragmentation near the kinematic limit seems to us consistent with the broad peak in $\Delta\phi$ observed in [45]. But the energy ranges for the hadrons in [45] are substantially lower,

[2]Indeed, a computation of the stress tensor gives clear-cut evidence at smaller wave-numbers for a wake in sense usually meant by phenomenologists [53].

relative to the temperature, than the energies we have discussed in relation to AdS/CFT. Recall that the upper limit on p_T of the partner particle is $2.5\,\mathrm{GeV}/c$. If the typical energy of the partner particles is sufficiently low, it would be a blow to the picture of enhanced high-energy fragmentation. Of course, without tagging most of the partons studied in [45] may be presumed to be light quarks or gluons.

In summary, the calculations we perform are based on the trailing string picture of [33, 34], which naively supports the notion of a coherent wake of color fields with the heavy quark at its tip. We do find evidence for a directional "prow," which becomes more and more forward as the speed increases. It seems that a full description of this prow involves high-momentum gauge fields. This may be a hint that, with a realistic cutoff on the quark mass imposed by hand, the quark could be deflected significantly by a single radiative event.

The drag force (2.1) computed in [33, 34] is a time-averaged quantity which provides no direct information about the energy scale of radiated particles. Calculating color-singlet VEV's in the boundary theory gives considerably more detailed information. Despite the hurdles string theory faces in connecting to relativistic heavy ion collisions, we hope that the trailing string picture can be further exploited to understand energy loss in the QGP.

Chapter 3

Low-lying gravitational modes

3.1 Introduction

Recently, a lot of attention has been devoted to the study of quasinormal perturbations in asymptotically anti-de Sitter (AdS) backgrounds. The first quasinormal mode (QNM) computation in AdS space was done in [54] for a conformally invariant scalar field, and then the problem was solved in [43] for any minimally-coupled scalar field in dimensions $d = 4$, 5, and 7. The gravitational perturbations of global AdS_4-Schwarzschild, which is what we are interested in, have been computed for the first time in [55]. Since then, various properties and generalizations of these QNM's have been considered, such as asymptotic relations [56, 57], different anti-de Sitter backgrounds [58, 59], or other boundary conditions [60].

We will phrase the problem in terms of the master field formalism that was developed by Kodama and Ishibashi in [61]. Based on previous ideas developed by Regge, Wheeler and Zerilli [62, 63] that were further extended in [55, 58, 64], Kodama and Ishibashi developed this formalism to decouple the linearized Einstein equations for the gravitational perturbations of the global AdS-Schwarzschild in a gauge-invariant way and in any number of dimensions. In general, the perturbations in AdS_d can be divided into tensor, vector, and scalar perturbations, depending on whether they correspond to expansions in tensor, vector, or scalar spherical harmonics on the S^{d-2} section of AdS_d. The basic idea then is that we can express each of these perturbations in terms of a master field Φ and the appropriate spherical harmonics, and all we have to do is solve a certain differential equation satisfied by Φ. This equation will in general depend on both the perturbation type we are considering and on the number of dimensions.

We will restrict our attention to the scalar sector of the perturbations in $d = 4$, where most QNM-related computations in the literature use a Dirichlet boundary condition on the master field Φ near the boundary of AdS. The purpose of this paper is to comment on the choice of this boundary condition, and to suggest that a Robin boundary condition[1] would be more appropriate, especially from the point of view of the AdS/CFT duality ([12, 13, 14]; for a review, see [65]). It follows from the AdS/CFT dictionary that a natural expectation is to demand that the perturbations do not deform the metric on the boundary of AdS, and this condition in turn determines the asymptotic behavior of the master field at the boundary. While having no boundary deformations amounts in other similar situations to imposing a Dirichlet boundary condition on Φ at the boundary, this is *not* the case for the scalar sector of gravitational perturbations in AdS_4, where a Robin boundary condition is required (see section 3.3).[2] Using the Robin boundary condition proposed in section 3.3, we find a family of low-lying modes that were not seen when a Dirichlet boundary condition was used instead (see for example [55]). In addition to the low-lying modes, we also find a tower of modes that is similar to the tower of modes found in [55]. For details on what makes the low-lying modes different, or for what other differences we find between our QNM's and the ones computed in [55], see section 3.4. It is important to note that our Robin boundary condition doesn't affect the vector gravitational perturbations in AdS_4, because in this case the Dirichlet boundary condition is still appropriate.

[1] A Robin boundary condition specifies a linear combination of a function and its derivative at the boundary.

[2] We can anticipate some trouble in the scalar sector of AdS_4 perturbations just by looking at the general large ρ dependence of the master field Φ for any kind of perturbations and in any number of dimensions. In general, Φ satisfies a second order differential equation whose linearly independent solutions behave like $\rho^{(d-6)/2+j}$ and $\rho^{(4-d)/2-j}$, where $j = 0$, 1, or 2 for scalar, vector, or tensor perturbations, respectively. The scalar perturbations in $d = 4$ are the first ones for which the behavior of the first family is subleading to the behavior of the second family.

A good check on the values of the low-lying quasinormal frequencies comes from a linearized hydrodynamics approximation on $S^2 \times \mathbf{R}$. The rationale of this approach lies in the observation that since M-theory on AdS_4-Schwarzschild$\times S^7$ is dual to a thermal CFT on the boundary, some QNM's should correspond to hydrodynamic modes of the thermal CFT. This idea has been developed in several interesting papers: in [66, 67, 68] it was shown that the quasinormal frequencies should correspond to poles of the correlation functions on the field theory side, and in [68, 59, 69] this result was checked by explicit numerical computations. We follow the approach in [70], where it was noted that the low-lying scalar and vector modes in *five*-dimensional AdS-Schwarzschild can be computed through a linearized hydrodynamics approximation. Extending the argument given in [70] to any dimension, we derive an approximate formula for the low-lying scalar and vector modes in AdS_d. We find excellent agreement between the numerically found low-lying modes (using our Robin boundary condition) and the linearized hydrodynamics prediction in $d = 4$.

The chapter is organized as follows: in section 3.2 we present an overview of the general setup of our calculation, in section 3.3 we comment on the choice of boundary conditions and derive the boundary asymptotics for the master field Φ, in section 3.4 we show the results of our numerical computation of the quasinormal frequencies of the global AdS_4-Schwarzschild solution, and finally, in section 3.5 we compare our results to what one would expect from the analysis of linearized hydrodynamics of a conformal plasma on $S^2 \times \mathbf{R}$. This chapter follows closely [9].

3.2 Setup of the calculation

In this section we briefly review the setup of our calculation. The global AdS_4-Schwarzschild black hole solution is given by

$$ds^2 = -\left(1 - \frac{\rho_0}{\rho} + \frac{\rho^2}{L^2}\right) d\tau^2 + \frac{d\rho^2}{1 - \frac{\rho_0}{\rho} + \frac{\rho^2}{L^2}} + \rho^2 d\Omega_2^2\,, \tag{3.1}$$

where $d\Omega_2^2$ is the standard metric on the unit S^2,

$$d\Omega_2^2 = \gamma_{ij} dy^i dy^j = d\theta^2 + \sin^2\theta d\phi^2 \,. \tag{3.2}$$

This metric is a solution to the Einstein equations that follow from the action

$$S = \frac{1}{2\kappa^2} \int d^4x \sqrt{g} \left(R + \frac{6}{L^2} \right) \,. \tag{3.3}$$

The horizon radius of the black hole solution (3.1) is then the positive root of the equation

$$\rho_0 = \rho_H \left(1 + \frac{\rho_H^2}{L^2} \right) \,. \tag{3.4}$$

For future reference, the mass, entropy, and Hawking temperature of this black hole solution are:

$$M = \frac{4\pi\rho_0}{\kappa^2} \qquad S = \frac{8\pi^2\rho_H^2}{\kappa^2} \qquad T = \frac{1 + 3\rho_H^2/L^2}{4\pi\rho_H} \,. \tag{3.5}$$

We are interested in linear perturbations of the background metric (3.1), of the form $g_{ab} + \delta g_{ab}$, that satisfy the linearized Einstein equations following from (3.3). The boundary conditions satisfied by these perturbations will be discussed in section 3.3.

The linearized equations satisfied by the perturbations can be solved by separation of variables. We assume $\delta g_{ab} \sim e^{-i\omega\tau}\Phi(\rho) S_{ab}(\theta, \phi)$, where the functions S_{ab} depend only on the angular variables on S^2, and can be written in terms of the spherical harmonics $Y_{lm}(\theta, \phi)$ and generalizations thereof. The exact equations describing the scalar, vector, and tensor perturbations of the d-dimensional AdS-Schwarzschild background can be found in [61]. As discussed previously, we will only focus on the scalar perturbations in the case $d = 4$. Using the notation in [70], we split the coordinates $y^a = (\tau, \rho, \theta, \phi)$ into $y^\alpha = (\tau, \rho)$ and $y^i = (\theta, \phi)$. We denote by ∇_i the covariant derivative with respect to the metric (3.2) on S^2, and by D_α the covariant derivatives with respect to the two-dimensional metric

$$ds_2^2 = -f d\tau^2 + \frac{1}{f} d\rho^2 \qquad f = 1 - \frac{\rho_0}{\rho} + \frac{\rho^2}{L^2} \,. \tag{3.6}$$

The equations describing the scalar perturbations then read:

$$\begin{gathered} \delta g_{\alpha\beta} = f_{\alpha\beta}\, \mathbb{S}(\theta, \phi) \qquad \delta g_{\alpha i} = \rho f_\alpha\, \mathbb{S}_i(\theta, \phi) \\ \delta g_{ij} = 2\rho^2 \left[H_L(\tau, \rho)\, \gamma_{ij}\, \mathbb{S}(\theta, \phi) + H_T(\tau, \rho)\, \mathbb{S}_{ij}(\theta, \phi) \right] \end{gathered} \tag{3.7}$$

$$\mathbb{S}_i = -\frac{1}{k_S}\partial_i\mathbb{S} \qquad \mathbb{S}_{ij} = \frac{1}{k_S^2}\nabla_i\partial_j\mathbb{S} + \frac{1}{2}\gamma_{ij}\mathbb{S} \tag{3.8}$$

$$H = m + 3w \qquad w = \frac{\rho_0}{\rho} \qquad m = k_S^2 - 2 \tag{3.9}$$

$$\begin{aligned} X_\alpha &= \frac{\rho}{k_S}\left(f_\alpha + \frac{\rho}{k_S}\partial_\alpha H_T\right) \\ F_{\alpha\beta} &= f_{\alpha\beta} + D_\alpha X_\beta + D_\beta X_\alpha \\ F &= H_L + \frac{1}{2}H_T + \frac{1}{\rho}\left(\partial^\alpha\rho\right)X_\alpha \end{aligned} \tag{3.10}$$

$$F^\alpha{}_\alpha = 0 \qquad D^\alpha F_{\alpha\beta} = 2\partial_\beta F \tag{3.11}$$

$$F_{\alpha\beta} = \frac{1}{H}\left(D_\alpha\partial_\beta\left(\rho H\Phi\right) - \frac{1}{2}g_{\alpha\beta}D_\gamma\partial^\gamma\left(\rho_H\Phi\right)\right) \tag{3.12}$$

$$\left(D_\alpha\partial^\alpha - \frac{V_S(\rho)}{f}\right)\Phi = 0 \tag{3.13}$$

$$V_S(\rho) = \frac{f}{\rho^2H^2}\left[m^3 + m^2\left(2+3w\right) + 9mw^2 + 9w^2\left(2f + 3w - 2\right)\right]\,. \tag{3.14}$$

where $\mathbb{S}$ denotes any of the spherical harmonics Y_{lm} on S^2, and k_S^2 is the corresponding eigenvalue of the laplacian:

$$\left(\nabla_i\partial^i + k_S^2\right)\mathbb{S} = 0 \qquad \mathbb{S}(\theta,\phi) = Y_{lm}(\theta,\phi) \qquad k_S^2 = l(l+1)\,. \tag{3.15}$$

It is worth noting that the above master field formulation is gauge invariant. So equations (3.7)–(3.14) don't determine the perturbations δg_{ab} uniquely: there is an implicit freedom of choosing four of these functions through a gauge transformation of the form $\delta g_{ab} \to \delta g_{ab} + \nabla_a v_b + \nabla_b v_a$, where this time ∇_a denotes the covariant derivative with respect to the full four-dimensional metric (3.1), and v_a are arbitrary functions. A small discussion of our gauge choice and the residual gauge freedom is included in the Appendix.

3.3 Boundary conditions

3.3.1 Boundary conditions at $\rho = \infty$

The question of what boundary conditions one should impose on the master field Φ at the boundary of AdS does not have a well-established answer: most of the previous authors have set $\Phi(\infty) = 0$ (see, for example, [71, 72, 56, 57]), but other boundary conditions have also been used (see, for example, [60]).[3] As we shall see below, the AdS/CFT dictionary relating perturbations and expectation values of operators in the dual field theory might help clarify this point.

From the AdS/CFT perspective, there are two independent behaviors of the metric perturbations δg_{ab} at large ρ: $\delta g_{ab} \sim \rho^2$, which corresponds to a deformation of the boundary metric, and $\delta g_{ab} \sim 1/\rho$, which corresponds to a non-zero VEV of the stress-energy tensor in the boundary theory. In defining the quasinormal frequencies it is sensible to require that the metric perturbations *do not* change the boundary metric, so they only produce a non-zero VEV of the stress-energy tensor $\langle T_{ab} \rangle$ of the thermal plasma on the boundary. This prescription is equivalent to requiring the quasinormal frequencies to correspond exactly to the poles of the correlation functions in the strongly coupled dual CFT in the planar limit (see for example [66]). With this in mind, the significant challenge is to find the relation between the asymptotic behaviors of δg_{ab} and Φ, which is what we'll now turn to.

At large ρ, the master equation (3.13) takes the form

$$\left[\frac{\Omega^2}{L^2} + \frac{\rho^2}{L^4}\partial_\rho \rho^2 \partial_\rho - \frac{k_S^2}{L^2} - \frac{18\rho_0^2}{L^4}\frac{1}{(k_S^2 - 2)^2}\right]\Phi_{\text{far}} = 0\,, \tag{3.16}$$

where we have assumed $e^{-i\omega\tau}$ behavior and denoted $\omega = \Omega/L$. Being a second order differential equation, equation (3.16) has two linearly independent solutions. Their asymptotic behaviors at large ρ are given by:

$$\begin{aligned} \Phi_{\text{far}}(\rho) &= e^{-i\Omega\tau/L}\left[\varphi^{(0)} + \mathcal{O}\left(\frac{L^2}{\rho^2}\right)\right] \qquad \text{and} \\ \Phi_{\text{far}}(\rho) &= e^{-i\Omega\tau/L}\left[\varphi^{(1)}\frac{L}{\rho} + \mathcal{O}\left(\frac{L^3}{\rho^3}\right)\right]\,. \end{aligned} \tag{3.17}$$

As noted earlier, the boundary condition that has been mostly used in the literature is $\varphi^{(0)} = 0$. As we shall see shortly, this condition is not consistent with the idea that $\delta g_{ab} \sim 1/\rho$ is the only behavior allowed. To argue this, we choose to work in axial gauge ($\delta g_{\rho a} = 0$), and we derive the boundary condition on Φ required by $\delta g_{ab} \sim 1/\rho$. While

[3] It is not clear to us how the boundary condition that we find is related to the one proposed in [60].

we include a detailed and more complete derivation in the Appendix, we now present the simplest way of arriving at the proposed boundary condition.

Setting $L = 1$, we can plug (3.17) into equation (3.12) and obtain, for the $F_{\tau\rho}$ component

$$F_{\tau\rho} = ie^{-i\Omega\tau}\left(\varphi^{(1)} + \frac{3\rho_0\varphi^{(0)}}{k_S^2 - 2}\right)\frac{1}{\rho} + \mathcal{O}\left(\frac{1}{\rho^2}\right) . \tag{3.18}$$

Using axial gauge and, as discussed above, assuming $\delta g_{ab} \sim 1/\rho$, we have:

$$\begin{aligned} & f_{\tau\rho} = 0 \qquad f_{\rho\rho} = 0 \qquad f_{\rho} = 0 \\ H_L &= \frac{A_L^{(3)}e^{-i\Omega\tau}}{\rho^3} + \mathcal{O}\left(\frac{1}{\rho^4}\right) \qquad H_T = \frac{A_T^{(3)}e^{-i\Omega\tau}}{\rho^3} + \mathcal{O}\left(\frac{1}{\rho^4}\right) \\ f_{\tau\tau} &= \frac{B^{(1)}e^{-i\Omega\tau}}{\rho} + \mathcal{O}\left(\frac{1}{\rho^2}\right) \qquad f_{\tau} = \frac{C^{(2)}e^{-i\Omega\tau}}{\rho^2} + \mathcal{O}\left(\frac{1}{\rho^3}\right) . \end{aligned} \tag{3.19}$$

By using (3.10) we can compute

$$F_{\tau\rho} = e^{-i\Omega\tau}\frac{-3C^{(2)}k_S + 6iA_T^{(3)}\Omega}{k_S^2}\frac{1}{\rho^2} + \mathcal{O}\left(\frac{1}{\rho^3}\right) . \tag{3.20}$$

This means that axial gauge and $\delta g_{ab} \sim 1/\rho$ force $F_{\tau\rho}$ to behave as $1/\rho^2$. By comparing this behavior to the general expectation (3.18), we conclude that the $1/\rho$ term in (3.18) must vanish:

$$\varphi^{(1)} + \frac{3\rho_0\varphi^{(0)}}{k_S^2 - 2} = 0 . \tag{3.21}$$

Thus we obtain a Robin boundary condition, involving the master field and its derivative.

3.3.2 Boundary conditions at the horizon

In contrast to the large ρ boundary conditions whose derivation was somewhat subtle and tedious, the horizon boundary conditions are straightforward, being based on the requirement that classical horizons don't radiate. So in appropriate coordinates, the perturbations near the horizon should take the form of an infalling wave. To make this explicit, we define the standard "tortoise" coordinate by

$$r_* = \int \frac{d\rho}{f(\rho)} , \tag{3.22}$$

which puts the master equation (3.13) into the form

$$\left[-\partial_\tau^2 + \partial_{r_*}^2 - V_S(\rho)\right]\Phi = 0\,. \tag{3.23}$$

Here, $\rho \to \rho_H$ corresponds to $r_* \to -\infty$. Noticing that $V_S(\rho_H) = 0$, we can immediately see that the near horizon behavior of the two linearly independent solutions to the master equation are $e^{-i\Omega(\tau \pm r_*)/L}$:

$$\Phi_{\text{near}}(\rho) = U e^{-i\Omega(\tau + r_*)/L} + V e^{-i\Omega(\tau - r_*)/L}\,. \tag{3.24}$$

The infalling boundary condition then means setting $V = 0$.

3.4 Numerical solutions

3.4.1 Change of variables

In order to solve the master equation (3.13) numerically, it is convenient to recast it in terms of a different field $\psi(y)$, defined by factoring out the near horizon behavior of the master field $\Phi(\rho)$:

$$\Phi = e^{-i\Omega(\tau + r_*)/L}\psi(y) \qquad y = 1 - \frac{\rho_H}{\rho}\,. \tag{3.25}$$

Setting $L = 1$, we can plug this ansatz into the master equation (3.13) to obtain the differential equation satisfied by ψ. We obtain

$$\left[s(y)\partial_y^2 + t(y)\partial_y + u(y)\right]\psi(y) = 0\,, \tag{3.26}$$

where

$$\begin{aligned} s(y) &= K(y)(1-y)^4 f^2 \\ t(y) &= K(y)\left[(1-y)^2 f \frac{\partial}{\partial y}\left[(1-y)^2 f\right] - 2i\Omega\rho_H (1-y)^2 f\right] \\ u(y) &= -K(y)\rho_H^2 V_S \\ K(y) &= \frac{1}{y}\left[1 + k_S^2 + 3\rho_H^2 - 3y(1+\rho_H^2)\right]^2\,. \end{aligned} \tag{3.27}$$

Here, $K(y)$ has been chosen so that $s(y)$, $t(y)$, and $u(y)$ are polynomial expressions in y that don't have any common factor and that don't vanish for any y between 0 and 1.

The remaining challenge before we proceed to solve the differential equation (3.26) is to translate the Robin boundary condition for Φ (3.21) into a boundary condition for ψ. This can be done by writing the first two terms in the series expansion of (3.25) at large ρ:

$$\Phi(\rho) \sim e^{-i\Omega(\tau+\rho_*)}\left[\psi(1) + \frac{i\Omega\psi(1)}{\rho} - \frac{\rho_H\psi'(1)}{\rho} + \mathcal{O}\left(\frac{1}{\rho^2}\right)\right]. \tag{3.28}$$

We get:

$$\psi'(1) = \frac{1}{\rho_H}\left[\frac{3\rho_0}{k_S^2-2} + i\Omega\right]\psi(1)\,. \tag{3.29}$$

Of course, the near horizon boundary condition $V=0$ translates into

$$\psi(0) = 1\,, \tag{3.30}$$

and we can now turn to describing the numerical techniques that we use to solve the differential equation (3.26) with the boundary conditions (3.29) and (3.30).

3.4.2 Numerical method and results

Following the method used in [70] for the computation of quasinormal frequencies of the scalar modes, we integrate the differential equation (3.26) in three steps: 1) we develop a series expansion around $y=0$ and evaluate it at $y=y_i=\frac{1}{4}$; 2) we integrate the differential equation numerically by using Mathematica's `NDSolve` from $y=y_i$ to $y=y_f$ (to be given below); and 3) we match our numerical solution onto a series expansion around $y=1$, which is computed using the boundary condition (3.29). In doing the matching, we compute the Wronskian between the numerical solution and the analytical approximation near $y=1$. The Wronskian vanishes only when the two functions are linearly dependent, i.e. when ψ satisfies the boundary condition (3.29) at $y=1$.

In developing the series expansions, we should keep in mind that the series solutions are guaranteed to converge only when $s(y)$, seen as a function of the complex variable y, doesn't vanish. It is easy to obtain the zeroes of $s(y)$ by writing

$$s(y) = y(y-y_1)^2(y-y_2)^2(y-\bar{y}_2)^2\,, \tag{3.31}$$

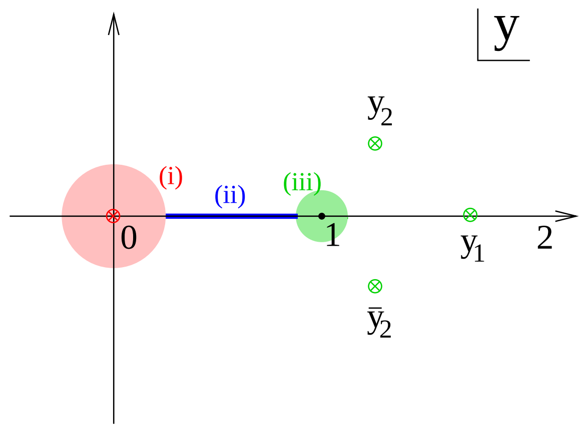

Figure 3.1: The zeroes of $s(y)$ represented as crosses in the complex plane. The red cross at $y=0$ denotes a simple zero, while the green crosses denote double zeroes. We use a series expansion in region (i), numerical integration in region (ii), and another series expansion in region (iii).

where

$$\begin{aligned} y_1 &= 1 + \frac{k_S^2 - 2}{3(1+\rho_H^2)} \\ y_2 &= 1 + \frac{\rho_H^2}{2(1+\rho_H^2)} + \frac{i\rho_H\sqrt{4+3\rho_H^2}}{2(1+\rho_H^2)} \,. \end{aligned} \tag{3.32}$$

It follows that the series expansion around $y=0$ converges on the whole interval between 0 and 1 (though the convergence close to $y=1$ might be slow, because of the nearby zero of $s(y)$). Similarly, the series expansion around $y=1$ has a radius of convergence r equal to the minimum of $|y_1 - 1| = \frac{k_S^2-2}{3(1+\rho_H^2)}$ and $|y_2 - 1| = \frac{\rho_H}{\sqrt{1+\rho_H^2}}$ (see figure 3.1). Experience has shown that a good value for y_f was $y_f = 1 - r/4$.

Using the method described above, we computed the lowest nine quasinormal frequencies for $\rho_H = 1$ and $l = 2$, 3, 4, 5, and 6 (see table 3.1), and for $\rho_H = 0.2$, 1, 10, and 100 at fixed $l = 2$ (see table 3.2). In these tables we have included only the quasinormal modes with $\mathcal{R}\rceil\Omega > 0$; equation (3.26) implies that if Ω is a quasinormal frequency, then so is $-\Omega^*$, so the QNM's with negative real parts can be trivially obtained from the ones with positive $\mathcal{R}\rceil\Omega$.

The most prominent feature of the quasinormal modes included in tables 3.1 and 3.2 is the separation of the quasinormal frequencies Ω_n into two groups: a main series of fast

freq\\l	2	3	4	5	6
Ω_0	$2.156 - 0.285\,i$	$3.361 - 0.354\,i$	$4.487 - 0.333\,i$	$5.561 - 0.298\,i$	$6.608 - 0.266\,i$
Ω_1	$3.463 - 2.573\,i$	$4.461 - 2.443\,i$	$5.528 - 2.271\,i$	$6.577 - 2.106\,i$	$7.610 - 1.963\,i$
Ω_2	$5.230 - 4.942\,i$	$6.023 - 4.791\,i$	$6.964 - 4.571\,i$	$7.935 - 4.340\,i$	$8.910 - 4.126\,i$
Ω_3	$7.096 - 7.308\,i$	$7.757 - 7.165\,i$	$8.592 - 6.942\,i$	$9.484 - 6.685\,i$	$10.40 - 6.432\,i$
Ω_4	$9.002 - 9.670\,i$	$9.572 - 9.540\,i$	$10.32 - 9.327\,i$	$11.15 - 9.064\,i$	$12.00 - 8.794\,i$
Ω_5	$10.93 - 12.03\,i$	$11.43 - 11.91\,i$	$12.12 - 11.71\,i$	$12.89 - 11.45\,i$	$13.69 - 11.18\,i$
Ω_6	$12.86 - 14.39\,i$	$13.32 - 14.28\,i$	$13.95 - 14.09\,i$	$14.68 - 13.84\,i$	$15.44 - 13.56\,i$
Ω_7	$14.81 - 16.74\,i$	$15.23 - 16.64\,i$	$15.82 - 16.47\,i$	$16.50 - 16.23\,i$	$17.23 - 15.95\,i$
Ω_8	$16.76 - 19.10\,i$	$17.14 - 19.00\,i$	$17.70 - 18.84\,i$	$18.35 - 18.61\,i$	$19.04 - 18.34\,i$

Table 3.1: Frequencies of scalar quasinormal modes for $\rho_H = 1$ in units where $L = 1$.

freq\\ρ_H	0.2	1	10	100
Ω_0	$2.793 - 0.0008\,i$	$2.156 - 0.285\,i$	$1.739 - 0.066\,i$	$1.732 - 0.007\,i$
Ω_1	$4.201 - 0.084\,i$	$3.463 - 2.573\,i$	$18.66 - 26.63\,i$	$185.0 - 266.4\,i$
Ω_2	$5.468 - 0.523\,i$	$5.230 - 4.942\,i$	$31.84 - 49.17\,i$	$316.1 - 491.6\,i$
Ω_3	$6.896 - 1.121\,i$	$7.096 - 7.308\,i$	$44.95 - 71.70\,i$	$446.5 - 716.8\,i$
Ω_4	$8.416 - 1.735\,i$	$9.002 - 9.670\,i$	$58.03 - 94.22\,i$	$576.6 - 941.8\,i$
Ω_5	$9.984 - 2.348\,i$	$10.93 - 12.03\,i$	$71.10 - 116.7\,i$	$706.6 - 1167\,i$
Ω_6	$11.58 - 2.956\,i$	$12.86 - 14.39\,i$	$84.18 - 139.2\,i$	$836.6 - 1392\,i$
Ω_7	$13.20 - 3.559\,i$	$14.81 - 16.74\,i$	$97.25 - 161.8\,i$	$966.5 - 1617\,i$
Ω_8	$14.83 - 4.158\,i$	$16.76 - 19.10\,i$	$110.3 - 184.3\,i$	$1096 - 1842\,i$

Table 3.2: Frequencies of scalar quasinormal modes for $l = 2$ in units where $L = 1$.

l\\ρ_H	5	10	20	50	100
2	$1.761 - 0.129\,i$	$1.739 - 0.066\,i$	$1.734 - 0.033\,i$	$1.732 - 0.013\,i$	$1.732 - 0.007\,i$
3	$2.547 - 0.312\,i$	$2.474 - 0.164\,i$	$2.456 - 0.083\,i$	$2.450 - 0.033\,i$	$2.450 - 0.017\,i$
4	$3.380 - 0.537\,i$	$3.219 - 0.292\,i$	$3.177 - 0.149\,i$	$3.165 - 0.060\,i$	$3.163 - 0.030\,i$
5	$4.273 - 0.787\,i$	$3.979 - 0.449\,i$	$3.900 - 0.231\,i$	$3.877 - 0.093\,i$	$3.874 - 0.047\,i$
6	$5.230 - 1.043\,i$	$4.761 - 0.631\,i$	$4.628 - 0.329\,i$	$4.590 - 0.133\,i$	$4.584 - 0.067\,i$
7	$6.246 - 1.286\,i$	$5.566 - 0.836\,i$	$5.362 - 0.442\,i$	$5.303 - 0.180\,i$	$5.294 - 0.090\,i$
8	$7.311 - 1.499\,i$	$6.399 - 1.059\,i$	$6.103 - 0.570\,i$	$6.017 - 0.233\,i$	$6.004 - 0.117\,i$
9	$8.410 - 1.675\,i$	$7.262 - 1.297\,i$	$6.852 - 0.713\,i$	$6.731 - 0.292\,i$	$6.714 - 0.147\,i$

Table 3.3: Frequencies of some of the low-lying modes in units where $L = 1$.

modes given by Ω_n with $n \geq 1$, and low-lying slow modes given by Ω_0 (for a similar feature of the quasinormal frequencies in AdS_5-Schwarzschild see [70]). The low-lying modes differ significantly from the fast ones in a number of ways:

- While the fast modes form a tower of modes at each value of ρ_H and l, the low-lying modes stand out as not being part of this tower (see figure 3.2).

- The low-lying modes have a different ρ_H-scaling from the main-series ones (see figure 3.2). This feature is most clearly seen at large ρ_H, where the low-lying modes approach $\Omega = \sqrt{l(l+1)}/\sqrt{2}$ as $\rho_H \to \infty$ (see next point), while the main series modes grow proportional to ρ_H: compare, for example, the columns corresponding to $\rho_H = 10$ and $\rho_H = 100$ in table 3.2.

- The low-lying modes can be interpreted as the linearized hydrodynamic modes of a conformal plasma on $S^2 \times \mathbf{R}$. While we will explain this correspondence in more detail in section 3.5, for now it is worth mentioning that a linearized hydrodynamics approximation on $S^2 \times \mathbf{R}$ gives, up to first order in $1/\rho_H$, that

$$\Omega = \pm \frac{k_S}{\sqrt{2}} - i\frac{k_S^2 - 2}{6\rho_H} + \mathcal{O}\left(\frac{1}{\rho_H^2}\right) , \tag{3.33}$$

  with $k_S = \sqrt{l(l+1)}$. A plot of low-lying modes for various values of l and ρ_H, together with the hydrodynamics prediction (3.33) can be seen in figure 3.3, which is based on the numerical values in table 3.3.

It is worth noting that while the tower-like feature of the scalar QNM's can be observed even if one imposes a Dirichlet boundary condition, the low-lying modes have *not* been seen in either numerical computations or analytical approximations that use the Dirichlet boundary condition (see, for example, [71, 57]).

Leaving the low-lying modes aside, we can compare the structure of the main series modes to the structure of the modes described in [71] that come from imposing the Dirichlet boundary condition on the master field. We find that the spacing between the main series modes at large Ω asymptotically approaches the spacing between the modes computed in

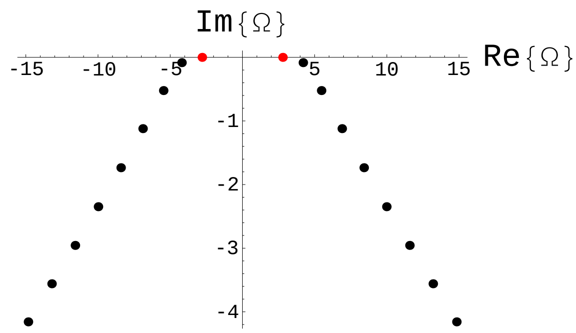

(a) $\rho_H = 0.2$

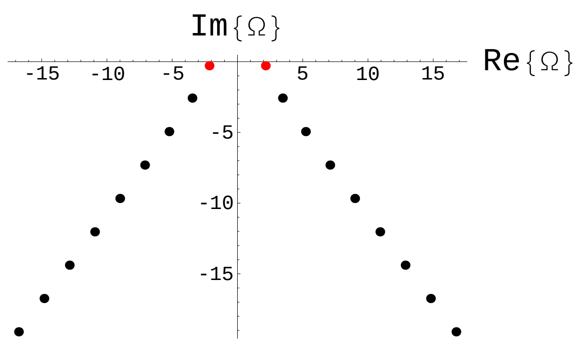

(b) $\rho_H = 1$

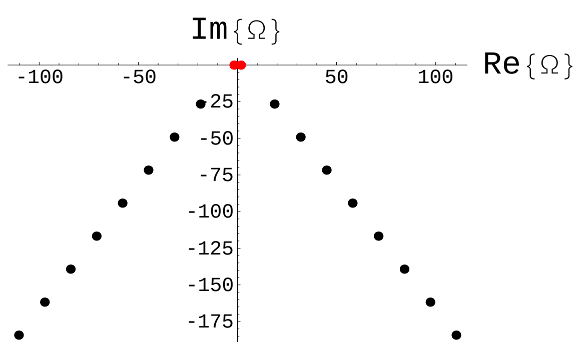

(c) $\rho_H = 10$

Figure 3.2: Quasinormal frequencies for $\rho_H = 0.2$, $\rho_H = 1$, and $\rho_H = 10$, in units where $L = 1$. The black dots represent the main-series modes, while the red ones represent the low-lying modes. It is fairly clear that for $\rho_H = 0.2$ and 1 the low-lying modes are not part of main series tower. This is not obvious in the $\rho_H = 10$ case, because of the plot scale.

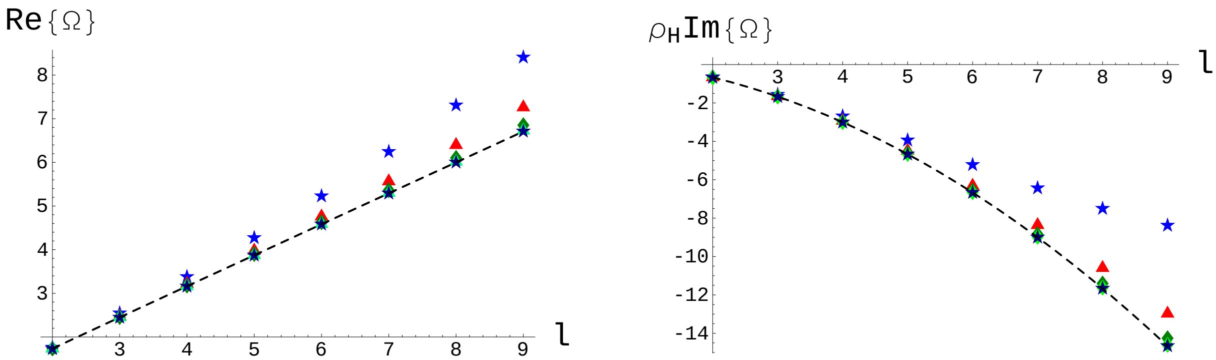

Figure 3.3: Quasinormal frequencies for different values of ρ_H plotted against l, in units where $L = 1$. The blue stars correspond to $\rho_H = 5$, the red triangles to $\rho_H = 10$, the dark green diamonds to $\rho_H = 20$, the light green triangles (barely visible) to $\rho_H = 50$, and the dark blue stars to $\rho_H = 100$. The dotted line represents the linearized hydrodynamics prediction (3.33), which matches almost perfectly the numerical results for large ρ_H.

[55]. However, the initial offset of the tower is different, our modes being in between the ones found in [55].

3.5 Linearized hydrodynamics

In [70] it was noticed that in the case of the global AdS_5 black hole there was a separation in the imaginary parts of low-lying scalar modes and the "main series" modes. The former were interpreted as hydrodynamic modes and the latter as microscopic. So a simple treatment of linearized hydrodynamics should be able to reproduce these low-lying modes in other dimensions as well. The goal of this section is to develop such a treatment.

In thinking about hydrodynamics, the general setup on $S^{d-2}\times\mathbf{R}$ is given by the following relations:

$$\begin{gathered} T_{ab} = (\epsilon + p)u_a u_b + p\tilde{g}_{ab} + \tau_{ab} \\ \tau_{ab} \equiv -\eta\left(\Delta_{ac}\tilde{\nabla}^c u_b + \Delta_{bc}\tilde{\nabla}^c u_a - \frac{2}{d-2}\Delta_{ab}\tilde{\nabla}^c u_c\right) - \xi\Delta_{ab}\tilde{\nabla}^c u_c \\ \Delta_{ab} = \tilde{g}_{ab} + u_a u_b \\ \tilde{\nabla}^a T_{ab} = 0\ . \end{gathered} \tag{3.34}$$

where $\tilde{g}_{ab}$ is the metric on $S^{d-2}\times\mathbf{R}$ and $\tilde{\nabla}_a$ is the covariant derivative with respect to this metric. Since the theory on the boundary of AdS is conformal we expect $T^a{}_a = 0$, which implies both $\epsilon = (d-2)p$ and $\xi = 0$. Following the same approach as in [70], we ignore the temperature-independent contribution from the Casimir energy to T^{ab}. The Casimir energy comes from considering the quantum field theory on the compact space S^{d-2}. For our purposes we can think of it as a temperature-independent shift of the zero point energy, which can be safely ignored.

The vector u^a describes the velocity at each point in the fluid, and we choose to normalize it by imposing $u^a u_a = -1$. Let us denote $u^a = (1, u^i)$ where i runs over the S^{d-2} directions. In the linearized approximation we consider u^i to be small. Perturbing at the same time the pressure $p = p_0 + \delta p$, one can derive from (3.34) the linearized equations

$$\begin{aligned} (d-2)\frac{\partial \delta p}{\partial \tau} + (d-1)p_0 \tilde{\nabla}_i u^i + \eta \frac{\partial}{\partial \tau}\tilde{\nabla}_i u^i = 0 \\ (d-1)p_0 \frac{\partial u^i}{\partial \tau} + \tilde{\nabla}^i \delta p + \eta(\partial_\tau^2 u^i - \tilde{\nabla}^2 u^i) - \eta \frac{d-4}{d-2}\tilde{\nabla}^i \tilde{\nabla}_j u^j = 0\,. \end{aligned} \tag{3.35}$$

Note that for $d = 5$ equation (3.35) reduces to the linearized Navier-Stokes equation on S^3, which was analyzed in section 5.3 of [70]. We wish to examine scalar perturbations next, which are described by the ansatz

$$\delta p = K_1 e^{-i\Omega\tau}\mathbb{S} \qquad u^i = K_2 e^{-i\Omega\tau}\tilde{\nabla}^i \mathbb{S}\,, \tag{3.36}$$

where $\mathbb{S}$ satisfies $\left(\tilde{\nabla}^2 + k_S^2\right)\mathbb{S} = 0$, as explained in section 3.2, and $L = 1$. Plugging (3.36) into (3.35), we obtain the following system of equations for K_1 and K_2:

$$\begin{aligned} -i\Omega(d-2)K_1 - K_2 k_S^2\left((d-1)p_0 - i\eta\Omega\right) = 0 \\ K_1 + K_2\left(-i\Omega(d-1)p_0 - \eta\Omega^2 + 2\eta\frac{d-3}{d-2}k_S^2 - (d-3)\eta\right) = 0\,. \end{aligned} \tag{3.37}$$

In order to have non-trivial solutions, this system must have zero determinant. This gives a cubic equation for Ω, whose solutions can be given in terms of a series expansion in η/p_0:

$$\Omega = \pm\frac{k_S}{\sqrt{d-2}} - i\frac{\eta}{p_0}\frac{k_S^2(d-3) - (d-2)(d-3)}{(d-1)(d-2)} + \mathcal{O}\left(\frac{\eta^2}{p_0^2}\right) \tag{3.38}$$

We can connect this result to the AdS_4 quasinormal mode problem by noting that

$$\frac{\eta}{p_0} = \frac{4\pi\eta}{s}\frac{\rho_H}{1+\rho_H^2}\,, \tag{3.39}$$

which can be easily derived from (3.5) in the case $d = 4$, but it is actually true in any number of dimensions. Using the conjectured lower bound on the viscosity $\frac{\eta}{s} = \frac{1}{4\pi}$ [21, 20], that has been checked in the AdS_4 case in [73], we find

$$\Omega = \pm \frac{k_S}{\sqrt{d-2}} - i\frac{1}{\rho_H}\frac{k_S^2(d-3)-(d-2)(d-3)}{(d-1)(d-2)} + \mathcal{O}\left(\frac{1}{\rho_H^2}\right) . \tag{3.40}$$

It is easily seen that this reproduces the hydrodynamical modes previously discussed in the global AdS_5 black hole case in [70]. For $d = 4$, equation (3.40) reduces to (3.33).

Similarly, we can describe the low-lying vector modes by the ansatz:

$$\delta p = 0 \qquad u^i = K_3 e^{-i\Omega\tau} V^i . \tag{3.41}$$

We find that the corresponding frequencies Ω are given by

$$\begin{aligned} \Omega = -i(d-1)\frac{1-\sqrt{1-4k_V^2\frac{\eta^2}{(d-1)^2p_0^2}}}{2\eta/p_0} &= -i\frac{k_V^2\eta}{(d-1)p_0} + \mathcal{O}\left(\frac{\eta^2}{p_0^2}\right) \\ \Omega = -i\frac{k_V^2}{d-1}\frac{1}{\rho_H} + \mathcal{O}\left(\frac{1}{\rho_H^2}\right) . \end{aligned} \tag{3.42}$$

It is interesting to note that the numerical value given by this formula when $d = 4$, $l = 2$ and $\rho_H = 100$ agrees within 10% with the low-lying vector mode of Table 9 in [71].

3.6 Conclusions

In this note we examine the relation between the asymptotic behavior of the master field and the behavior of the scalar sector of metric perturbations in the global AdS_4 black hole. We argue that the boundary condition that corresponds to a non-deformation of the metric on the boundary translates into a Robin boundary condition for the master field. With this boundary condition, we compute the scalar quasinormal modes. We find some low-lying modes that have not been previously observed, and compare them with the linearized hydrodynamical modes of the boundary CFT.

Chapter 4

Heterotic non linear sigma models and AdS target spaces

4.1 Introduction

Particular interest attaches to backgrounds of string theory involving AdS_{D+1} because of their relation to conformal field theories in D dimensions [74, 75, 76] (for a review see [15]). But because these geometries (with some exceptions) arise from the near-horizon geometry of D-branes, formulating a closed string description is complicated by the presence of Ramond-Ramond fields.

It was recently proposed [77] that AdS_{D+1} vacua might exist without any matter fields at all. Instead of relying upon the stress-energy of matter fields to curve space, the proposal is that higher powers of the curvature compete with the Einstein-Hilbert term to produce string-scale AdS_{D+1} backgrounds. The main support for this proposal comes from large D computations of the beta function for the quantum field theory on the string worldsheet. Before discussing these computations, let us review the lowest-order corrections to the beta function in an α' expansion:

$$\begin{aligned}
&\text{bosonic:} && \beta_{ij} = \alpha' R_{ij} + \frac{\alpha'^2}{2} R_{iklm} R_j{}^{klm} + O(\alpha'^3) \\
&\text{heterotic:} && \beta_{ij} = \alpha' R_{ij} + \frac{\alpha'^2}{4} R_{iklm} R_j{}^{klm} + O(\alpha'^3) \\
&\text{type II:} && \beta_{ij} = \alpha' R_{ij} + \frac{\zeta(3)\alpha'^4}{2} R_{mhki} R_{jrt}{}^m (R^k{}_{qs}{}^r R^{tqsh} + R^k{}_{qs}{}^t R^{hrsq}) + O(\alpha'^5)\,.
\end{aligned} \tag{4.1}$$

These expressions are obtained using dimensional regularization with minimal subtraction, and all derivatives of curvature are assumed to vanish as well as all matter fields. Derivatives of curvature indeed vanish for symmetric spaces: for example,

$$R_{ijkl} = -\frac{1}{L^2}(g_{ik}g_{jl} - g_{il}g_{jk}) \tag{4.2}$$

in the case of AdS_{D+1}. One indeed finds non-trivial zeroes for AdS_{D+1} from all three beta functions in (4.1). An examination of higher order corrections in the bosonic and type II cases shows that the zero persists in the most accurate expressions for the beta function that are available at present; however its location changes significantly, converging to $\alpha' D/L^2 = 1$ as D becomes large. One aim of the present paper is to pursue similar large D computations in the heterotic case.

It should be clear from the outset that the question of the existence of AdS_{D+1} vacua with $\alpha' D/L^2$ close to unity is a difficult one to settle perturbatively. Fixed order computations are not reliable guides because the scale of curvature is close to the string scale. Large D computations with finite $\alpha' D/L^2$ seem to be a better guide, but they too could be misleading, mainly because higher order effects in $1/D$ than we are able to compute could change the behavior of the beta function significantly. These difficulties were discussed at some length in [77]. Also, the vanishing of a beta function such as the ones in (4.1) is only a necessary condition for constructing a string theory: one must also cancel the Weyl anomaly and formulate a GSO projection that ensures modular invariance and the stability of the vacuum.

There is a more general reason to be interested in high-order computations of the beta function on symmetric spaces: from them we can extract information about the structure of high powers of the curvature that is quite different from what is available from expansions of the Virasoro amplitude. While the latter tells us about terms involving many derivatives but only four powers of the curvature (because only four gravitons are involved in the collision), the former tells us about many powers of the curvature with no extra derivatives.

The organization of the rest of this chapter is as follows. In section 4.2, some general properties of the heterotic NLσM are discussed. In section 4.3, the formalism and the results at $1/D$ order are presented. In section 4.4, the critical exponents at $1/D^2$, the beta function, and the central charge of the CFT are computed. The appendices include a brief explanation of the method of the calculation for the diagrams needed and the values of these diagrams. This chapter follows closely [10].

4.2 The heterotic non-linear sigma model

As in [77], much will be made of a connection through analytic continuation of the NLσM on AdS_{D+1} and the NLσM on S^{D+1}. If L is the radius of S^{D+1} and $g = \alpha'/L^2$, then continuing to negative g leads to the AdS_{D+1} NLσM. The argument in [77] is slightly formal because it relies on an order-by-order perturbative evaluation of the partition function.

The action for the S^{D+1} heterotic NLσM is

$$S = \frac{1}{4\pi g}\int d^2x d\bar{\theta}\left[D_+\Phi\partial_-\Phi + \Lambda(\Phi^2-1)\right] + \frac{1}{4\pi g}\int d^2x \lambda_A \partial_+ \lambda_A \tag{4.3}$$

where

$$\Phi = S + \bar{\theta}\Psi \qquad \Lambda = u + \bar{\theta}\sigma \qquad D_+ = \frac{\partial}{\partial\bar{\theta}} + \bar{\theta}\frac{\partial}{\partial x_+} \qquad \partial_\pm = \frac{\partial}{\partial x_\mp}\,. \tag{4.4}$$

Λ is a spinorial superfield, and u and Ψ have opposite chirality. This leads to the action

$$S = \frac{1}{4\pi g}\int d^2x\left[(\partial S)^2 + \bar{\Psi} i\partial\Psi + \sigma(S^2-1) + 2\bar{u}\Psi S\right]\,. \tag{4.5}$$

We have omitted the fermions λ_A from (4.5) because they decouple from the gravitational action when the gauge field is set to zero [78, 79] as in our case. The Feynman rules for the theory (4.5) can be seen in figure 4.1. There is also a tadpole for σ, but we omit it

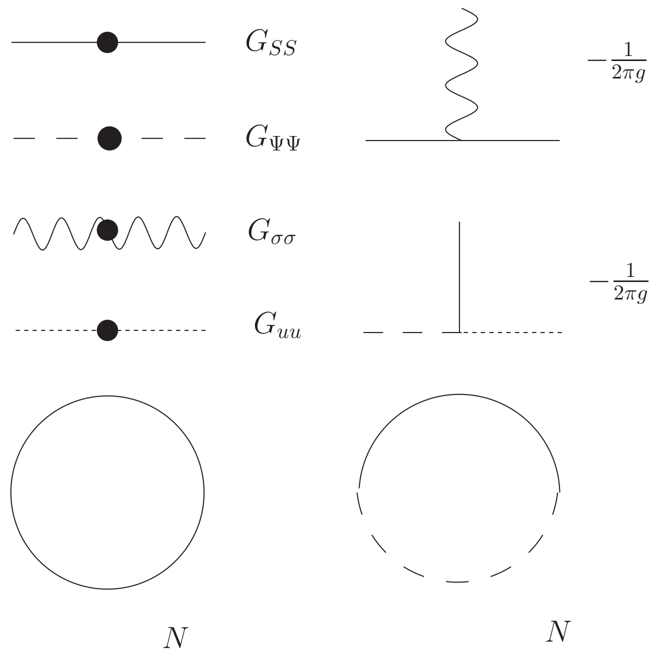

Figure 4.1: The Feynman rules for the heterotic sigma model. The shaded circles indicate a dressed propagator. The circles indicate that a loop involving only the components of the Φ superfield receives a factor of N. We have suppressed the tensor structure of the rules since only $\delta_{\mu\nu}$ appears.

because it does not contribute to the Dyson equations for the scaling parts of the dressed propagators, as in [80].

After a change of variables that renders the kinetic terms canonical, we can continue to negative values of g as in [77] to obtain an AdS_{D+1} heterotic NLσM. Quantities that are computed locally and perturbatively, such as n-point functions, cannot distinguish between a space of positive or negative curvature. As the beta function is derived from such quantities, it too can be continued to negative g, at least order by order in perturbation theory.

The heterotic NLσM on S^{D+1} is a generalization of the $O(D+2)$ model, and much of the relevant literature concentrates on an expansion in $1/(D+2)$ rather than $1/D$. We will therefore set

$$N = D + 2 \tag{4.6}$$

and work with N or D, according to convenience, in the rest of this paper.

4.2.1 Some properties of the heterotic NLσM for large D

It is known that in the bosonic sigma model a mass appears [81] in the 1/N expansion. The same phenomenon appears in the supersymmetric extension of the sigma model [82, 83] where also the fermions acquire the same mass, signaling chiral symmetry breaking. In the heterotic case the bosons S also acquire the same mass, showing that the interaction term does not destroy this effect. To understand this, let's start from our action (4.5), and in the partition function integrate first the fermionic fields and then the bosons, since the action is quadratic in these. We have omitted normalization factors of the partition function in the following.

$$\begin{aligned} Z &= \int \mathcal{D}S\mathcal{D}\Psi\mathcal{D}\sigma\mathcal{D}u \, \exp\left(-\frac{i}{4\pi g}\int d^2x[(\partial S)^2 + i\bar{\Psi}\partial\!\!\!/\Psi + \sigma(S^2-1) + 2\bar{u}(S\cdot\Psi)]\right) \\ &= \int \mathcal{D}S\mathcal{D}\sigma\mathcal{D}u \left[\det(i\partial\!\!\!/)\right]^{N/4} \exp\left[\frac{i}{4\pi g}\int d^2x\left(S(\partial^2-\sigma)S - S^i\bar{u}\frac{1}{i\partial\!\!\!/}uS^i\right)\right] \\ &= \int \mathcal{D}\sigma\mathcal{D}u \left[\det(i\partial\!\!\!/)\right]^{N/4}\left[\det\left(-\partial^2-\sigma\bar{u}\frac{1}{i\partial\!\!\!/}\bar{u}\right)\right]^{-N/2} \exp\left(\frac{i}{4\pi g}\int d^2x\,\sigma\right) \\ \Rightarrow Z &= \int \mathcal{D}\sigma\mathcal{D}u\, e^{iS_{\text{eff}}}\,, \end{aligned} \tag{4.7}$$

where the effective action for the Lagrange multiplier fields is given by

$$S_{\text{eff}} = \int d^2x \left[\frac{1}{4\pi g}\sigma - \frac{N}{4}\,\mathrm{Tr}\log(i\partial\!\!\!/) + \frac{N}{2}\,\mathrm{Tr}\log\left(-\partial^2-\sigma-\bar{u}\frac{1}{i\partial\!\!\!/}u\right)\right]. \tag{4.8}$$

Since we are taking the limit $N\to\infty$ with g_0N finite, we see that all terms in the action are of order N. We can evaluate this integral by the method of steepest descent, i.e. by finding the classical value of σ, u that minimizes the exponent, as is done for instance in [84, 85]. This gives the variational equations

$$\begin{aligned} \langle x|\frac{1}{-\partial^2-\sigma(x)-\bar{u}\frac{1}{i\partial\!\!\!/}u}|x\rangle &= \frac{1}{2\pi Ng} \\ \langle x|\frac{\frac{1}{\partial\!\!\!/}u}{-\partial^2-\sigma(x)-\bar{u}\frac{1}{i\partial\!\!\!/}u}|x\rangle &= 0\,. \end{aligned} \tag{4.9}$$

Because the right hand sides are constant, the left hand sides must also be constant. A solution to these equations is given by

$$u(x) = 0 \qquad \sigma(x) = -m^2\,. \tag{4.10}$$

It is easy to see that $\frac{1}{\partial}u(x) = const.$ has as its only solution $u = 0$. This is in contrast to the supersymmetric case [84], where there are three solutions. Now m^2 must satisfy

$$\int d^2k \frac{1}{k^2 + m^2} = \frac{1}{2\pi g_0} . \tag{4.11}$$

Using a simple-momentum cutoff, $\frac{1}{2\pi g_0 N} = \frac{1}{2\pi} \log \frac{\Lambda}{m}$. By renormalizing at a scale M we get

$$\frac{1}{2\pi g_0 N} = \frac{1}{2\pi g N} + \frac{1}{2\pi} \log \frac{\Lambda}{M} . \tag{4.12}$$

Solving for the mass m we get $m = M \exp[-1/gN]$. Since this is a physical mass we expect that it does not depend on the renormalization scale. Using the Callan-Symanzik equation for m,

$$\left(M \frac{\partial}{\partial M} + \beta(g) \frac{\partial}{\partial g} \right) m(g, M) = 0 , \tag{4.13}$$

gives the beta function $\beta(g) = -g^2 N$. The mass is the same in the bosonic, supersymmetric, [81, 83] and heterotic model. This could have been predicted since the first order β function is the same in all models, $\beta_{ij} = \alpha' R_{ij}$. Another way to get the same result is to calculate the effective potential for the σ field and see that the minimum of the potential is not at zero but at $\sigma = Me^{-1/gN}$. One can go further and examine the effective action (4.8). It is easy to evaluate the counterterms needed for one-loop renormalization, as we have already computed the wave function renormalization of the σ field, and doing so one finds

$$\mathcal{L}_{0,\text{eff}} = \frac{1}{4\pi g} \left(1 + gN \log \frac{\Lambda^2}{M^2} \right) \sigma - \frac{N}{4} \operatorname{Tr} \log \partial\!\!\!/ + \frac{N}{2} \operatorname{Tr} \log \left(-\partial^2 - \sigma - \bar{u} \frac{1}{i\partial\!\!\!/} u \right) . \tag{4.14}$$

The bare and the dressed quantities are related by

$$\sigma_0 = Z\sigma \qquad u_0 = Z^{1/2} u \qquad g_0 = Z^{-1} g \qquad Z = 1 + \frac{gN}{2} \log \frac{\Lambda^2}{M^2} . \tag{4.15}$$

Calculating the quadratic terms in the fields u, σ will give us the propagators for these fields. We can easily find

$$S_{\text{eff}} = \frac{N}{2} Tr \frac{1}{-\partial^2 - m^2} \bar{u} \frac{1}{i\partial\!\!\!/ - m} u - \frac{N}{4} \operatorname{Tr} \frac{1}{-\partial^2 - m^2} \sigma \frac{1}{-\partial^2 - m^2} \sigma . \tag{4.16}$$

The next step is to evaluate the propagators. One finds [83, 84]

$$S_u(k) = -\frac{2i}{N} (k\!\!\!/ - 2m) V(k^2) \qquad D_\sigma(k) = \frac{2i}{N} (4m^2 - k^2) V(k^2) , \tag{4.17}$$

where in d dimensions

$$V(k^2) = \frac{(4\pi)^{d/2}}{4\Gamma(2-d/2)} \left(\frac{4m^2-k^2}{4}\right)^{1-d/2} \left({}_2F_1(2-d/2,1/2,3/2;\frac{k^2}{k^2-4m^2})\right)^{-1} . \quad (4.18)$$

In two dimensions this simplifies to

$$V(k^2) = \pi\sqrt{\frac{k^2}{k^2-4m^2}} \left(\operatorname{arctanh}\sqrt{\frac{k^2}{k^2-4m^2}}\right)^{-1} . \quad (4.19)$$

It is easy to see that the u propagator in $d=2$ dimensions has a pole at $k^2 = 4m^2$. This means that there is a particle with this mass. Since the classical equations give $u = -iS\not{\partial}\Psi$, there is a boson-fermion bound state, created by the operator $S\not{\partial}\Psi$. This is in agreement with [83], but there is no supersymmetric corresponding fermion-fermion bound state, since the Gross-Neveu interaction that is responsible for it is absent.

One can also extend the calculation of [84, 86] to show that there is no multi-particle production in the heterotic sigma model. For example, the process $2 \to 4$ particles can be shown to vanish. The reasoning is that the formalism of [86], valid for the bosonic case, can be extended to include superfields.

4.3 Critical exponents in the $1/D$ expansion

4.3.1 General discussion

The method used to determine the critical exponents is the one developed in [80, 87] for the bosonic model and extended to the supersymmetric case in [88, 89]. To this end one writes expressions for the propagators of the fields near the critical point. In keeping with the notation of [80, 87, 90] we assign dimensions to the fields

$$\begin{aligned} \dim[S] = \dim[\Psi] - \frac{1}{2} &= \Delta_S = (d-2+\eta)/2 \\ \dim[\sigma] = \dim[u] + \frac{1}{2} &= \Delta_\sigma = 2-\eta-\chi\,. \end{aligned} \quad (4.20)$$

For small but non-zero x, the two-point functions may be expanded as follows:

$$\begin{aligned} G_{SS}(x) &= \frac{\Gamma_{SS}}{x^{2\Delta_S}}(1+\Gamma'_{SS}x^{2\lambda}) \qquad G_{\Psi\Psi}(z) = \frac{1+\gamma_P}{2}\frac{\Gamma_{\Psi\Psi}\not{x}}{x^{2\Delta_S+2}}(1+\Gamma'_{\Psi\Psi}x^{2\lambda}) \\ G_{\sigma\sigma}(x) &= \frac{\Gamma_{\sigma\sigma}}{x^{2\Delta_\sigma}}(1+\Gamma'_{\sigma\sigma}x^{2\lambda}) \qquad G_{uu}(x) = \frac{1-\gamma_P}{2}\frac{\Gamma_{uu}\not{x}}{x^{2\Delta_\sigma}}(1+\Gamma'_{uu}x^{2\lambda})\,, \end{aligned} \quad (4.21)$$

where

$$\gamma_P = \rho^0 \rho^1 = \begin{pmatrix} 1 & 0 \\ 0 & -1 \end{pmatrix} \tag{4.22}$$

is the chirality matrix in 2 dimensions. We have omitted the $O(N)$ indices because both the propagators and the vertex are proportional to $\delta_{\mu\nu}$. So all Green's functions can be expressed as a scalar function times products of $\delta_{\mu\nu}$, and one does not have to worry about tensor structures of the form $(x-y)^\mu (x-y)^\nu$. Then one can write the Dyson equations in a $1/D$ expansion for the propagators. Graphical expressions of these equations are shown in figures 4.2 through 4.5. The Dyson equations impose consistency conditions on the critical exponents that determine them completely. The graphs that appear in the Dyson equations are the 1PI graphs with the exception of graphs which contain subgraphs that already appear in the Dyson equations at a lower effective loop order: in other words, we exclude diagrams that are already taken into account by expressions for the corrected propagators. The effective loop order is the number of loops minus the number of loops involving only the components of the Φ superfield.

The left hand side of each Dyson equation is a 1PI propagator, which is the inverse of the connected two-point function. These inverse propagators are computed by first passing to Fourier space using

$$\int d^d k \frac{e^{-ik\cdot x}}{k^{2\Delta}} = \frac{\pi^\mu \alpha(\Delta) 2^{2(\mu-\Delta)}}{x^{2(\mu-\Delta)}} \, . \tag{4.23}$$

The inverse propagators are found to be[1]

$$
\begin{aligned}
G^{-1}_{SS}(x) &= \frac{p(\Delta_S)}{\Gamma_{SS} x^{2(2\mu-\Delta_S)}}(1 - q(\Delta_S,\lambda)\Gamma'_{SS} x^{2\lambda}) \\
G^{-1}_{\Psi\Psi}(x) &= \frac{1-\gamma_P}{2}\frac{p(\Delta_S)\not{x}}{\Gamma_{\Psi\Psi} x^{2(2\mu-\Delta_S)}}(1 - s(\Delta_S,\lambda)\Gamma'_{\Psi\Psi} x^{2\lambda}) \\
G^{-1}_{\sigma\sigma}(x) &= \frac{p(\Delta_\sigma)}{\Gamma_{\sigma\sigma} x^{2(2\mu-\Delta_\sigma)}}(1 - q(\Delta_\sigma,\lambda)\Gamma'_{\sigma\sigma} x^{2\lambda}) \\
G^{-1}_{uu}(x) &= \frac{1+\gamma_P}{2}\frac{r(\Delta_\sigma - 1)\not{x}}{\Gamma_{uu} x^{2(2\mu-\Delta_\sigma+1)}}(1 - s(\Delta_\sigma - 1,\lambda)\Gamma'_{uu} x^{2\lambda})\,,
\end{aligned}
\tag{4.24}
$$

where

$$
\mu = d/2 \qquad \Delta_S = \mu - 1 + \eta/2 \qquad \Delta_\sigma = 2 - \eta - \chi\,, \tag{4.25}
$$

and for arbitrary y,

$$
\begin{aligned}
\alpha(y) &= \frac{\Gamma(\mu-y)}{\Gamma(y)} \qquad p(y) = \frac{\alpha(y-\mu)}{\pi^{2\mu}\alpha(y)} \qquad r(y) = \frac{y p(y)}{\mu - y} \\
q(y,\lambda) &= \frac{\alpha(y-\lambda)\alpha(y+\lambda-\mu)}{\alpha(y)\alpha(y-\mu)} \qquad s(y,\lambda) = \frac{y(y-\mu)q(y,\lambda)}{(y-\lambda)(y+\lambda-\mu)}\,.
\end{aligned}
\tag{4.26}
$$

To calculate the beta function, one first evaluates the critical exponents of the model at the fixed point in $d = 2 + \epsilon$ dimensions and then uses the relation

$$
\lambda = -\frac{1}{2}\beta'(g_c)\,, \tag{4.27}
$$

valid at the critical point, to extract $\beta(g)$. This is possible because, in dimensional regularization with minimal subtraction, the only ϵ dependence in $\beta(g)$ is an overall additive term: see [77] for details. Expanding in $1/D$ with $\kappa = gD$ held fixed, one finds

$$
\lambda(\epsilon) = \sum_{i=0}^{\infty}\frac{\lambda_i(\epsilon)}{D^i} \qquad \frac{\beta(g)}{g} = \epsilon - \kappa + \sum_{i=1}^{\infty}\frac{b_i(\kappa)}{D^i} \tag{4.28}
$$

where

$$
\lambda_0(\kappa_c) = \frac{\kappa_c}{2} \qquad b_1(\kappa) = -2\kappa\int_0^\kappa d\xi\frac{\lambda_1(\xi)}{\xi^2} \qquad b_2(\kappa) = -2\kappa\int_0^\kappa d\xi\frac{\lambda_2(\xi) - b_1(\xi)\lambda'_1(\xi)}{\xi^2}\,. \tag{4.29}
$$

[1]Note that $G_{\Psi\Psi}\cdot G^{-1}_{\Psi\Psi}$ does not strictly give the unit matrix but instead $\frac{1+\gamma_p}{2} = \begin{pmatrix} 1 & 0 \\ 0 & 0 \end{pmatrix}$ in two dimensions, which is what we want. Also note that in the Dyson equation for Ψ in the right hand side one encounters u propagators that give the right chiral structure, and vice versa for the Dyson equation of the u field.

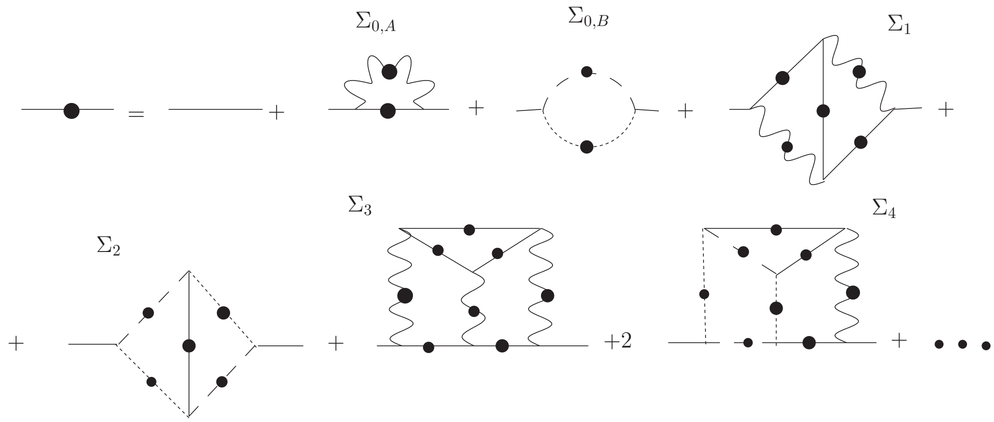

Figure 4.2: The Dyson equations for the S propagator.

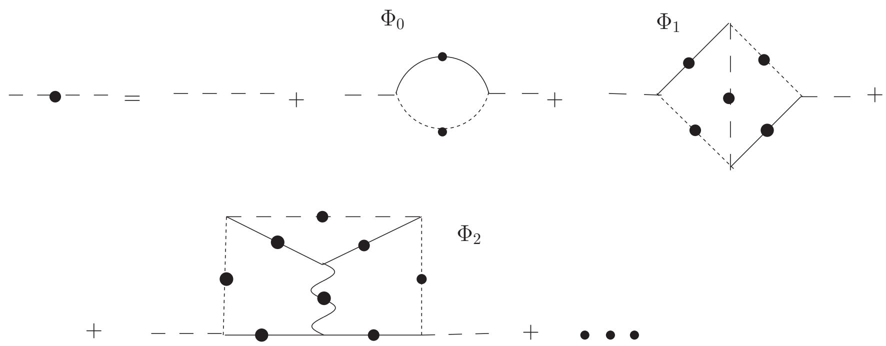

Figure 4.3: The Dyson equations for the Ψ propagator.

Note that the critical exponent λ is a measurable quantity and as such it should not depend on the renormalization scheme used. Passing from the $\lambda_i(\kappa)$ to the $b_i(\kappa)$ does introduce significant scheme dependence.

4.3.2 Critical exponents at order $1/D$

The Dyson equations can be expressed in terms of parameters

$$w = \frac{\Gamma_{SS}^2 \Gamma_{\sigma\sigma}}{(2\pi g)^2} \qquad v = \frac{\Gamma_{SS}\Gamma_{\Psi\Psi}\Gamma_{uu}}{(2\pi g)^2}\,, \tag{4.30}$$

which can be regarded as dressed vertex factors for the two vertices shown in figure 4.1. The leading non-trivial Dyson equations come from the graphs labeled $\Sigma_{0,A}$, $\Sigma_{0,B}$, Φ_0, Π_0, and F_0 in figures 4.2 through 4.5: the tree-level graphs make no contribution to the leading

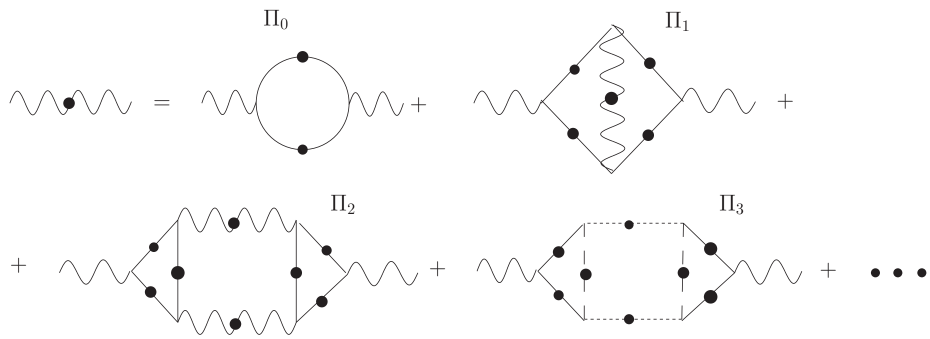

Figure 4.4: The Dyson equations for the σ propagator.

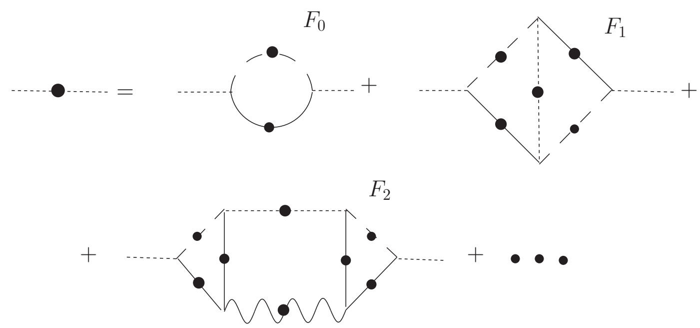

Figure 4.5: The Dyson equations for the u propagator.

scaling behavior. The quantities Γ'_{SS}, $\Gamma'_{\Psi\Psi}$, $\Gamma'_{\sigma\sigma}$, and Γ'_{uu} describe how far one is removed from the fixed point; so in particular one must be able to set them all to zero and get a self-consistent set of equations. Then the dependence of each graph on the position-space separation x is just an overall power of x. Matching these overall powers leads simply to the constraint $\chi = 0$. Matching other factors leads to the equations

$$\begin{aligned} p(\Delta_S) + w + v &= 0 \qquad & r(\Delta_S) + v &= 0 \\ \frac{1}{N} r(\Delta_\sigma - 1) + v &= 0 \qquad & \frac{2}{N} p(\Delta_\sigma) + w &= 0 \,, \end{aligned} \tag{4.31}$$

which determine the quantities Δ_S, Δ_σ, w, and v as functions of μ and N. The system is in fact over-determined if we recall the relations (4.25) and the constraint $\chi = 0$. But we will see in section 4.4.1 that $\chi = 0$ is only a leading order result; thus to solve (4.31) we expand

$$\eta = \sum_{i \geq 0} \frac{\eta_i}{D^i} \qquad \chi = \sum_{i \geq 0} \frac{\chi_i}{D^i} \qquad w = \sum_{i \geq 0} \frac{w_i}{D^i} \qquad v = \sum_{i \geq 0} \frac{v_i}{D^i} \,. \tag{4.32}$$

Then one straightforwardly extracts from (4.31) the coefficients

$$\begin{aligned} \eta_0 &= 0 \qquad \chi_0 = 0 \qquad w_0 = 0 \qquad v_0 = 0 \\ \eta_1 &= -2\frac{\Gamma(2\mu-1)}{(\mu-1)^2\Gamma(1-\mu)\Gamma^2(\mu-1)\Gamma(\mu+1)} \\ w_1 &= \frac{(2-\mu)\Gamma(\mu-1)\Gamma(\mu+1)}{2\pi^{2\mu}}\eta_1 \\ v_1 &= -\frac{(1-\mu)\Gamma(\mu-1)\Gamma(\mu+1)}{2\pi^{2\mu}}\eta_1 \,. \end{aligned} \tag{4.33}$$

Higher order coefficients receive contributions from higher order graphs. Note that $\chi_0 = 0$ could be obtained either from matching overall powers of x or from the equations (4.31).

Now consider non-zero coefficients Γ'_{SS}, $\Gamma'_{\Psi\Psi}$, $\Gamma'_{\sigma\sigma}$, and Γ'_{uu}: this corresponds to moving away from the fixed point. Linearizing the Dyson equations leads to the constraints

$$\begin{aligned} -p(\Delta_S)q(\Delta_S,\lambda)\Gamma'_{SS} + w(\Gamma'_{SS}+\Gamma'_{\sigma\sigma}) + v(\Gamma'_{\Psi\Psi}+\Gamma'_{uu}) &= 0 \\ -r(\Delta_S)s(\Delta_S,\lambda)\Gamma'_{\Psi\Psi} + v(\Gamma'_{SS}+\Gamma'_{uu}) &= 0 \\ -r(\Delta_\sigma-1)s(\Delta_\sigma-1,\lambda)\Gamma'_{uu} + Nv(\Gamma'_{SS}+\Gamma'_{\Psi\Psi}) &= 0 \\ -p(\Delta_\sigma)q(\Delta_\sigma,\lambda)\Gamma'_{\sigma\sigma} + N\Gamma'_{SS}w &= 0\,. \end{aligned} \tag{4.34}$$

Graphically, these equations arise from using the leading power-law expressions (e.g. $\Gamma_{SS}/x^{2\Delta_S}$ rather than $G_{SS}(x)$) for all propagators except one, chosen arbitrarily; and for that one, use the correction term (e.g. $\Gamma_{SS}\Gamma'_{SS}/x^{2\Delta_S-2\lambda}$). The linear equations (4.34) must admit a non-zero solution for Γ'_{SS}, $\Gamma'_{\Psi\Psi}$, $\Gamma'_{\sigma\sigma}$, Γ'_{uu} in order for the correction terms to describe a genuine deformation of the critical point. So the corresponding determinant must vanish, which leads to

$$\begin{aligned} &\left[(w+v)q(\Delta_S,\lambda) + w\left(1-\frac{2}{q(\Delta_\sigma,\lambda)}\right) - \frac{v}{s(\Delta_\sigma-1,\lambda)}\right](1-s(\Delta_\sigma,\lambda)s(\Delta_\sigma-1,\lambda)) \\ &\qquad = v\frac{(1-s(\Delta_\sigma-1,\lambda))^2}{s(\Delta_\sigma-1,\lambda)}\,. \end{aligned} \tag{4.35}$$

Note that setting $v = 0$ gives the equation valid for the bosonic model as expected. To simplify (4.35), one can use (4.33) and note that $w_1 = v_1\frac{2-\mu}{\mu-1}$. So far we have not used any expansion in $1/D$. Using the expansions (4.32) and

$$\lambda = \sum_{i\geq 0}\frac{\lambda_i}{D^i} \tag{4.36}$$

we can determine

$$\lambda_0 = \mu - 1 \qquad \lambda_1 = \frac{1}{2}(2\mu - 1)(\mu - 1)\eta_1 \,. \tag{4.37}$$

Another way to compute the original determinant, is the following: one notes that $r(\Delta_S)s(\Delta_S, \lambda) \sim 1/D^0$, while all other terms scale at least as $1/D^1$. This means that, in expanding the 4×4 determinant of (4.34), the first order contribution comes only from the determinant of the 3×3 matrix

$$AI \equiv \begin{pmatrix} -p(\Delta_S)q(\Delta_S, \lambda) + w & w & v \\ w & -p(\Delta_\sigma)q(\Delta_\sigma, \lambda)/N & 0 \\ v & 0 & -r(\Delta_\sigma - 1)s(\Delta_\sigma - 1, \lambda)/N \end{pmatrix} . \tag{4.38}$$

where in each element of the matrix we only keep the first term in the $1/D$ expansion. This determinant provides the first $1/D$ term of (4.35) and thus reproduces (4.37).

It is interesting to compare with the bosonic case. It is easily seen that $\lambda_1^{\text{het}} = \frac{1}{2}\lambda_1^{\text{bos}}$, even though η_1^{het}, w_1, and v_1 are not so simply related to η_1^{bos} and the corresponding vertex factor for the bosonic case. The relation $\lambda_1^{\text{het}} = \frac{1}{2}\lambda_1^{\text{bos}}$ is expected: we know that $\lambda_1^{\text{sup}} = 0$ in the type II case, and having half the fermions in the heterotic case will cancel only half the bosonic contribution.

4.3.3 A check of the calculation

Following [90], we see that η is the anomalous dimension of the S propagator. So far we have computed it in the $1/D$ expansion using techniques in position space. One can also straightforwardly compute η_1 in momentum space using the expressions for the propagators that we have previously found (4.17). Firstly we note that for small k,

$$\tilde{G}_{SS}(k) \sim k^{-2+\eta} \sim k^{-2+\eta_o}\left(1 + \frac{\eta_1}{N}\log k + \mathcal{O}(1/N^2)\right) , \tag{4.39}$$

with $\tilde{G}_{SS}$ the Fourier transform of the S propagator. But $\tilde{G}_{SS}(k)$ can also be determined from the one-particle irreducible diagrams $\Sigma(k^2)$:

$$\tilde{G}_{SS}^{-1}(k) = k^2 + \Sigma(k^2) - \Sigma(0) \sim k^2(1 - \frac{\eta_1}{N}\log k) , \tag{4.40}$$

since $\eta_0 = 0$. Having calculated the propagators of the lagrange multiplier fields it is straightforward to compute the $\Sigma(k^2)$ from the one-loop diagrams. We find

$$\begin{aligned}\Sigma(k^2) &= \int \frac{d^dp}{(2\pi)^d}\frac{i}{(p-k)^2}D_u(p^2) - \int \frac{d^dp}{(2\pi)^d}\,\mathrm{tr}\,\frac{i}{(\not{k}-\not{p})}S_u(\not{k}) = \frac{2}{N}\int \frac{d^dp}{(2\pi)^d}\frac{\mathrm{tr}(\not{k}\not{p})V(p^2)}{(p+k)^2} \\ &= \frac{2^{d-2}/N\sqrt{\pi}}{{}_2F_1(2-d/2,1/2,3/2,1)\Gamma(2-d/2)\Gamma(\frac{d-1}{2})}\int_0^M dp\int_0^\pi d\theta\frac{p^2k\cos\theta\sin^{d-2}\theta}{p^2+k^2+2pk\cos\theta}\end{aligned} \tag{4.41}$$

where we have put $m^2 = 0$ as usual [89], and M is the cutoff. One notes that, for small k the $k^2\log k$ behavior comes from the small p region [90]. The integral is trivial to do, and for the $k^2\log k$ part it gives

$$\Sigma(k^2) = -\frac{2^{d-1}}{Nd}\frac{1}{{}_2F_1(2-d/2,1/2,3/2,1)\Gamma(2-\frac{d}{2})\Gamma(\frac{d}{2})}k^2\log k\,. \tag{4.42}$$

It is easy to see using $d = 2\mu$ and properties of the Gamma function that this coincides with the expression for η_1 in (4.33). An easier way to do the checking is the following. One can write similar expressions for $\Sigma(k^2)$ for the bosonic and supersymmetric models [80, 89]. Then it is easy to observe that

$$\Sigma_{\mathrm{bos}}(k^2) - \Sigma_{\mathrm{bos}}(0) = -\Sigma_{\mathrm{sup}}(k^2) + 2\Sigma_{\mathrm{het}}(k^2)\,. \tag{4.43}$$

This easily gives[2]

$$2\eta_{\mathrm{het}} = \eta_{\mathrm{bos}} + \eta_{\mathrm{sup}}\,. \tag{4.44}$$

With [80, 89]

$$\eta_{\mathrm{bos}} = \frac{(2-\mu)}{\mu}\eta_{\mathrm{sup}} \qquad \eta_{\mathrm{sup}} = \frac{4}{N}\frac{\Gamma(2\mu-2)}{\Gamma^2(\mu-1)\Gamma(2-\mu)\Gamma(\mu)} \tag{4.45}$$

we find $\eta_{\mathrm{het}} = \frac{1}{\mu}\eta_{\mathrm{sup}}$ which agrees with (4.33).

4.4 Results at order $1/D^2$

Each graph in figures 4.2-4.5 carries an overall factor $1/D^M$ where M is the number loops minus the number of loops containing only S and Ψ. To see this, first note that each

[2] We have used that $\Sigma_{\mathrm{sup}}(0) = 0$ and $\Sigma_{\mathrm{het}}(0) = 0$.

propagator G_{XX} carries a factor Γ_{XX} (where $X = S$, Ψ, σ, or u). Next note that the amplitude for each graph must contain an overall factor which is a product of the factors $w = \Gamma_{SS}^2 \Gamma_{\sigma\sigma}/(2\pi g)^2$ and $v = \Gamma_{SS}\Gamma_{\Psi\Psi}\Gamma_{uu}/(2\pi g)^2$, one for each vertex in the graph. The overall factor $1/D^M$ arises because w and v scale as $1/D$ and because each loop containing only S and Ψ carries a factor of N. The graphs in figures 4.2 and 4.3 are those with $M \leq 2$, and the ones in figures 4.4 and 4.5 are those with $M \leq 1$. Together, these are all the graphs that can contribute to η, w, v, and λ through order $1/D^2$, and they also determine χ through order $1/D$. Because we quote final results in terms of $1/D$, we must keep in mind the relation between expansions in $1/N$ and $1/D$:

$$w = \sum_{i \geq 0} \frac{\tilde{w}_i}{N^i} = \sum_{i \geq 0} \frac{w_i}{D^i} \qquad w_1 = \tilde{w}_1 \quad w_2 = \tilde{w}_2 - 2\tilde{w}_1\,, \tag{4.46}$$

with similar relations for other quantities.

4.4.1 Calculation of η_2

A technical complication arises in the $1/D^2$ corrections to the Dyson equations that was explained and resolved in [80, 87]. The problem is that the higher-loop graphs diverge when $\chi = 0$. In fact, $\chi = 0$ only up to $1/D$ corrections. But it convenient to regularize the "divergence" and extract finite expressions for the two-loop Dyson equations through the following steps:

1. Shift $\chi \to \chi + \Delta$.
2. Expand the amplitudes for individual graphs in powers of Δ.
3. Cancel $1/\Delta$ terms against certain counter-terms in the Lagrangian.
4. Fix χ_1 by setting to zero certain terms in the Dyson equation which depend logarithmically on the position-space separation x and which, if non-zero, would spoil self-consistency.

We will now go through these steps in detail for the Ψ propagator. The reader who wishes to bypass the technical details can skip to (4.56) and (4.57), which are the two-loop Dyson equations with all divergences removed. But the results (4.54) and (4.58) for χ_1 provide important consistency checks.

When $\chi \neq 0$, x dependence cannot be canceled out of the Dyson equations in a simple way: setting $\Gamma'_{SS} = \Gamma'_{\Psi\Psi} = \Gamma'_{\sigma\sigma} = \Gamma'_{uu} = 0$, one obtains for the Ψ propagator's Dyson equation

$$r(\Delta_S) + v(x^2)^\chi + v^2(x^2)^{2\chi}\Phi_1 + Nwv^2(x^2)^{3\chi}\Phi_2 = 0\,. \tag{4.47}$$

Here Φ_1 and Φ_2 are functions of Δ_S, Δ_σ, and μ which diverge when $2\Delta_S + \Delta_\sigma - 2\mu = -\chi = 0$. Although these are in some sense an artifact of a limit ($\chi \to 0$) which one cannot take independently of the large N limit, it is convenient nevertheless to regulate them, as explained above, by shifting

$$\chi \to \chi + \Delta\,. \tag{4.48}$$

The amplitudes $\Phi_{1,2}$ may then be expanded as

$$\Phi_i = \frac{X_i}{\Delta} + \Phi'_i + O(\Delta)\,, \tag{4.49}$$

where both X_i and Φ'_i are functions of Δ_S, Δ_σ, and μ, subject to $2\Delta_S + \Delta_\sigma - 2\mu = 0$. In appendix D we exhibit $\Phi_{1,2}$ in the form (4.49), as well as a number of related quantities that enter into other Dyson equations. To cancel the divergent $1/\Delta$ terms in $\Phi_{1,2}$, one may rescale the lagrange multiplier fields in the original action (4.3). This rescaling amounts to adding counter-terms to the action, and it can be expressed, to the relevant order, as

$$v \to \left(1 + \frac{m_1}{N}\right) v \qquad w \to \left(1 + \frac{m_1}{N}\right) w\,. \tag{4.50}$$

(The factor on v and w is the same because of supersymmetry.) Subjecting (4.47) to the shift (4.48) and the rescaling (4.50), it becomes, keeping terms up to $1/N^2$,

$$\begin{gathered} r(\Delta_S) + (x^2)^\chi\Big(v + v^2\Phi'_1 + Nv^2w\Phi'_2\Big) + \\ (x^2)^\chi\Big(v_1\frac{m_1}{N} + v_1^2(x^2)^\chi\frac{X_1}{\Delta} + Nv_1^2w_1(x^2)^{2\chi}\frac{X_2}{\Delta}\Big) = 0 \end{gathered} \tag{4.51}$$

The last line contains all the divergent pieces. Setting $\chi = 0$ [80] and taking the limit $\Delta \to 0$ determines m_1 as

$$-v_1\frac{m_1}{N} = v_1^2\frac{X_1}{\Delta} + Nv_1^2w_1\frac{X_2}{\Delta}\,. \tag{4.52}$$

Plugging (4.52) back into (4.51), and now considering a finite χ we get

$$r(\Delta_S) + (x^2)^\chi \left(v + v^2\Phi_1' + Nv^2 w\Phi_2'\right) + v_1^2 X_1 \left(\frac{(x^2)^{2\chi} - (x^2)^\chi}{\chi}\right) \\ + N v_1^2 w_1 X_2 \left(\frac{(x^2)^{3\chi} - (x^2)^\chi}{\chi}\right) = 0\,. \tag{4.53}$$

When one expands $\chi = \chi_1/N + O(N^{-2})$, there are terms that behave as $\log x^2$. One gets rid of these if χ_1 obeys

$$\chi_1 = -v_1 X_1 - 2v_1 w_1 X_2\,. \tag{4.54}$$

We could have derived (4.52),(4.54) purely within the $N \to \infty$ limit. In this setup there is no need for Δ and χ is taken to be finite. Note that it behaves as $\chi \sim 1/N$ since $\chi_0 = 0$ (4.33). The Dyson equation after the rescaling (4.50) is (4.51) with Δ replaced with χ. In taking the $N \to \infty$ limit there are terms that diverge linearly with N and terms that behave as $\log x^2$. Respectively these are

$$(x^2)^\chi \big(v_1 \frac{m_1}{N} + v_1^2 \frac{X_1}{\chi} + N v_1^2 w_1 \frac{X_2}{\chi}\big) \\ \log x^2 \big(\chi v_1 (1 + \frac{m_1}{N}) + 2v_1^2 X_1 + 3N v_1^2 w_1 X_2\big)\,. \tag{4.55}$$

Setting these to zero fixes m_1, χ_1 as in (4.52),(4.54), with Δ replaced by χ. We choose to keep the Δ shift, as is common in the literature [80, 87, 91, 6]. If one wishes to translate our results, in the $N \to \infty$ formalism, only a simple substitution of $\Delta \to \chi_1/N$ is needed in the values of the diagrams given in Appendix D. What is left is the finite correction to the leading Dyson equation for the Ψ propagator:

$$r(\Delta_S) + v + v^2\Phi_1' + Nwv^2\Phi_2' = 0\,. \tag{4.56}$$

Following the same procedure for the S, σ, and u Dyson equations, one gets the finite equations

$$p(\Delta_S) + w + v + w^2\Sigma_1' - v^2\Sigma_2' + Nw^3\Sigma_3' - 2Nv^2 w\Sigma_4' = 0 \\ p(\Delta_\sigma) + \frac{N}{2}w + \frac{N}{2}w^2\Pi_1' + \frac{N^2}{2}w^3\Pi_2' - \frac{N^2}{2}wv^2\Pi_3' = 0 \\ r(\Delta_\sigma - 1) + Nv + Nv^2 F_1' + N^2 wv^2 F_2' = 0\,, \tag{4.57}$$

where Σ'_i, Π'_i, and F'_i are the finite parts of Σ_i, Π_i, and F_i, listed in Appendix D. The minus signs in (4.57) come from fermion loops. From each Dyson equation one also gets a new determination of m_1 and χ_1:

$$\begin{aligned}
m_1 &= \frac{1}{\Delta}\frac{w_1^2 S_1 - v_1^2 S_2 + w_1^3 S_3 - 2w_1 v_1^2 S_4}{w_1+v_1} & \chi_1 &= \frac{-w_1^2 S_1 + v_1^2 S_2 - 2w_1^3 S_3 + 4w_1 v_1^2 S_4}{w_1+v_1} \\
m_1 &= -\frac{1}{\Delta}(w_1 P_1 + w_1^2 P_2 - v_1^2 P_3) & \chi_1 &= -w_1 P_1 - 2w_1^2 P_2 + 2v_1^2 P_3 \\
m_1 &= -\frac{1}{\Delta}(v_1 Y_1 + w_1 v_1 Y_2) & \chi_1 &= -v_1 Y_1 - 2w_1 v_1 Y_2\,,
\end{aligned} \tag{4.58}$$

where P_i, S_i, Y_i are the residues of Π_i, Σ_i, and F_i, respectively.

Fortunately, the four seemingly independent determinations of m_1 and χ_1 all agree, as one can check by explicitly evaluating (4.52), (4.54), and (4.58) using expressions from Appendix D with $\Delta_S = \mu - 1$ and $\Delta_\sigma = 2$. This provides a check that the renormalization procedure we have chosen to cancel the divergences of higher-loop graphs is consistent. Other schemes change the values for individual amplitudes, but the critical exponents remain the same [88].

Interestingly, there is yet another consistency check on χ_1. One can show from (4.54) or (4.58) that

$$\chi_1 = \mu(2\mu-3)\eta_1\,. \tag{4.59}$$

This is seen to comply with a scaling law formulated for the bosonic model in [90]:

$$2\lambda = 2\mu - \Delta_\sigma\,. \tag{4.60}$$

That this relation is also valid in our case can be seen by applying the Callan-Symanzik equation near the critical point for $\langle\sigma(p)\sigma(-p)\rangle$ or $\langle\bar u(p)u(-p)\rangle$ propagator.

Now we can solve (4.56)-(4.57) by eliminating w and v:

$$r(\Delta_S) = \frac{1}{N} r(\Delta_\sigma - 1) + \frac{v_1^2}{N^2}(F'_1 - \Phi'_1) + \frac{w_1 v_1^2}{N^2}(F'_2 - \Phi'_2)\,. \tag{4.61}$$

Expanding Δ_S, Δ_σ in (4.61), we can determine $\tilde\eta_2$

$$\begin{aligned}
\frac{\tilde\eta_2}{\eta_1^2} &= \frac{1}{2\mu} + (\mu-1)(2\mu-1)\left(-1 + \pi\cot\mu\pi + H(2\mu-2)\right) \\
&+\frac{\mu}{\mu-2} + \frac{1}{2(\mu-1)} - 1 - \mu(\mu-2)\left(B(2\mu-3) - B(\mu-1) - \frac{1}{\mu-1} + \frac{1}{2\mu-3} - 2\right)
\end{aligned} \tag{4.62}$$

where $H(x) = \psi(x+1) - \psi(1)$ and the $B(x)$ function is defined in the appendix. The first line just comes from the Hatree-Fock diagrams, i.e. by iterating the 1/N Dyson equation to the next order, the second is the contribution of Φ_1, F_1 and the third comes from Φ_2, F_2. We also can determine the values of w_2, v_2 as

$$\begin{aligned}\frac{\tilde{w}_2}{\eta_1 w_1} = & \frac{(2\mu-1)(\mu-1)}{\mu-2}\left(3-\mu+(\mu-2)\pi\cot\mu\pi+(\mu-2)H(2\mu-3)\right) \\ & -\mu\left((7\mu-9)B(\mu-1)+(13-10\mu)B(2)+(3\mu-4)B(2\mu-3)\right) \\ & -\mu+2\mu(\mu-1)-\frac{\mu(\mu-1)}{2\mu-3}\end{aligned} \tag{4.63}$$

$$\frac{\tilde{v}_2}{\eta_1 v_1} = \frac{\tilde{\eta}_2}{\eta_1^2} - \frac{1}{2\mu} - \frac{\mu}{2} + \mu(\mu-2) + 2\mu(\mu-2)\left(B(2)-B(\mu-1)\right). \tag{4.64}$$

In (4.63), the first three terms come from iteration of the first order equations, while in (4.64), the first two terms come from such iteration.

4.4.2 Calculation of λ_2

As in section 4.3.2, the calculation of λ_2 through order $1/D^2$ requires evaluating each graph with one propagator altered from its leading power behavior (e.g. $\Gamma_{SS}/x^{2\Delta_S}$ for an S propagator) to its sub-leading power behavior (e.g. $\Gamma_{SS}\Gamma'_{SS}/x^{2\Delta_S-2\lambda}$). The four Dyson equations lead to four linear equations in the quantities Γ'_{SS}, $\Gamma'_{\Psi\Psi}$, $\Gamma'_{\sigma\sigma}$, and Γ'_{uu}:

$$\begin{aligned}(-p(\Delta_S)q(\Delta_S,\lambda)+w+\Sigma_S)\Gamma'_{SS}+(w+\Sigma_\sigma)\Gamma'_{\sigma\sigma}+(v+\Sigma_u)\Gamma'_{uu}+(v+\Sigma_\Psi)\Gamma'_{\Psi\Psi}&=0\\ (-r(\Delta_S)s(\Delta_S,\lambda)+\Phi_\Psi)\Gamma'_{\Psi\Psi}+(v+\Phi_S)\Gamma'_{SS}+(v+\Phi_u)\Gamma'_{uu}&=0\\ \left(-\frac{p(\Delta_\sigma)q(\Delta_\sigma,\lambda)}{N}+\Pi_\sigma\right)\Gamma'_{\sigma\sigma}+(w+\Pi_S)\Gamma'_{SS}+\Pi_\Psi\Gamma'_{\Psi\Psi}+\Pi_u\Gamma'_{uu}&=0\\ \left(-\frac{1}{N}r(\Delta_\sigma-1)s(\Delta_\sigma-1,\lambda)+F_u\right)\Gamma'_{uu}+(v+F_S)\Gamma'_{SS}+(v+F_\Psi)\Gamma'_{\Psi\Psi}&=0\,,\end{aligned} \tag{4.65}$$

where for example we denote by Σ_Ψ all the diagrams that appear in the S propagator where the Ψ propagator is corrected. As in section 4.4.1, the amplitudes diverge when $2\Delta_S + \Delta_\sigma - 2\mu \to 0$, and the same procedure described there to regulate and subtract the divergences and to remove terms proportional to $\log x^2$ carries over to the present case. The finite parts of all the quantities in (4.65) are given in Appendix E, as well as some further remarks on their evaluation.

The system (4.65) must have a nonzero solution for the Γ's, so the determinant must be zero. This determines λ_2. A way to calculate the determinant to sufficient accuracy is to note that $r(\Delta_S)s(\Delta_S,\lambda) \sim 1/N^0$, and then expand the determinant into three 3×3 determinants, i.e. expanding in the line of Ψ field Dyson equation. All terms have to be expanded up to $1/N^2$ accuracy. One also notes that λ_2 only appears in the expansion of $p(\Delta_S)q(\Delta_S,\lambda)$ at this order. So λ_2 is going to be a linear combination of the various sums of diagrams given in the appendix, factors of w_2 and v_2, and terms that come from iterating the $1/N$ equations. The final result is quite involved and we prefer to give it implicitly as

$$\begin{aligned}\frac{\tilde{\lambda}_2}{\eta_1^2} = &-\frac{1}{2(\mu-1)^2} - \frac{25}{2(\mu-1)} + 25 - \frac{5(\mu+1)}{2(\mu-2)} - \frac{5}{4(2\mu-3)} - \frac{\mu-2}{2} + 50(\mu-1)\\ &+ (\mu-1)\left(-\frac{19}{8}(\mu-2) + \frac{45}{2}(\mu-2)^2 - \frac{3}{2}(2\mu-3)\right) - \frac{\mu^2(2\mu-3)^2}{8(\mu-1)}\\ &+ (\mu-1)^2\left(\frac{21}{4} - \frac{9}{4}(\mu-2) - 75(2\mu-3) - \frac{25}{(\mu-2)} - \frac{10}{(2\mu-3)}\right)\\ &- 2\mu(\mu-1)\tilde{v}_2 - \left(\frac{\mu}{2} + 2\mu(2\mu-3)\right)\tilde{w}_2 - 2\mu(\mu-1)(\mu-2)\frac{F_u+F_S}{\eta_1 v_1}\\ &- \mu(\mu-1)\frac{(2\mu-3)^2}{\mu-2}\frac{\Pi_\sigma}{\eta_1 v_1} - 2\frac{\mu(\mu-1)}{(\mu-2)^2}\frac{\Sigma_S}{\eta_1 v_1} - \mu\left(\frac{\mu-1}{\mu-2} - 2\mu\right)\frac{\Sigma_\sigma}{\eta_1 v_1}\\ &- 3\mu(2\mu-3)(\mu-1)\frac{F_\sigma}{\eta_1 v_1} - \frac{3}{2}\left(\pi\cot\mu\pi + H(2\mu-4)\right).\end{aligned} \tag{4.66}$$

The right hand side is a function of μ which can be obtained explicitly by substituting the expressions (4.33), (4.63), (4.64), (F.1), (F.3), (F.4), (F.7), (F.8), and (F.9) into (4.66).

4.4.3 Calculation of the beta function

As explained in section 4.3.1, we can calculate the beta function once we know λ. Noting that (4.66) gives the $1/N^2$ expansion term and subtracting $2\lambda_1$ we find

$$\lambda_0 = \epsilon/2, \quad \lambda_1(\epsilon) = \frac{\epsilon^2}{4} + \frac{\epsilon^3}{8} - \frac{\epsilon^4}{16} + \mathcal{O}(\epsilon^5) \tag{4.67}$$

$$\lambda_2 = \left(\frac{5}{16} + \frac{9}{4}\zeta(3)\right)\epsilon^4 + \mathcal{O}(\epsilon^5)\,. \tag{4.68}$$

Using (4.29), we compute the beta function for the heterotic string in a constant curvature background:

$$\beta(g) = -Dg^2 - \frac{1}{2}Dg^3 - \frac{g^4 D}{4}\left(1+\frac{D}{2}\right) - \frac{g^5 D^2}{4}\left(\frac{3}{2}-\frac{D}{3}\right) - \frac{3}{2}\zeta(3)g^5D^2 + \mathcal{O}(\frac{1}{D^3})\,. \tag{4.69}$$

It is obvious that there is agreement with the first two loops of the expression (4.1), where we use

$$\beta(g) = M\frac{\partial g}{\partial M} = -\frac{g}{N-1}g^{ij}\beta_{ij} \tag{4.70}$$

and (4.2). We do not know of any calculation of the beta function of the heterotic string in the minimal subtraction scheme that goes beyond two loops. In [92, 93] the beta function was computed using the background field method, and found to be in three loops

$$\beta^{(3)}_{ij} = \frac{\alpha'^3}{8}\left(\frac{3}{2}R_{ikjl}R^{kmnp}R^{l}{}_{mnp} - \frac{1}{2}R_{lm}R_i{}^{lnp}R_j{}^{m}{}_{np} - \frac{1}{2}R_{jl}R^{lmnp}R_{imnp}\right)\,. \tag{4.71}$$

The appearance of the Ricci tensor means that it is not minimal subtraction. Divergences involving the Ricci tensor can only appear through closed loops where at least one propagator starts and ends at the same vertex. Within the minimal subtraction scheme, at more than one loop these terms combined with their counterterms never produce a simple pole [94, 95]. A small check of our result comes from the famous $\zeta(3)$ term, $\frac{\zeta(3)\alpha'^4}{2}R_{mhki}R_{jrt}{}^{m}(R^{k}{}_{qs}{}^{r}R^{tqsh} + R^{k}{}_{qs}{}^{t}R^{hrsq})$. This term is identical in the bosonic [96, 97, 98], supersymmetric [94, 95], and heterotic [99] cases. In an expansion of the Virasoro amplitude, it is associated with the constant term in an expansion in the Mandelstam variables s, t, and u. At loop order $n+1$ in NLσM calculations, it seems likely that the coefficient of $\zeta(n)$ is the same for the bosonic, supersymmetric, and heterotic cases (see [88] for a comparison of the bosonic and supersymmetric cases).

In [100, 99, 101], the absence of a three-loop term of the form α'^3R^3 was noted. The three-point scattering amplitudes suggest that there are also no RF^2 or F^3 in the effective action. One knows that identifying the gauge connection with the spin connection in the heterotic string effective action will give the superstring effective action, where there is no α'^3 term. So if there were any R^3 terms in the heterotic case it would not be possible to cancel them. All this seems in conflict with the (4.69), where the term proportional to g^4 would seem to correspond to an R^3 term in the effective action. But it should be noted that the relation between the effective action and the beta function is [102]

$$2\kappa_D^2\alpha'\frac{\delta S_{\rm eff}}{\delta g_{ij}} = K_{ij}^{kl}\beta_{kl}\,, \tag{4.72}$$

where K_{ij}^{kl} can be computed perturbatively. In the bosonic case, this was done in the minimal subtraction scheme in [102, 103]; in the heterotic case, this was done in a different scheme in [92, 93]; but we do not know of a minimal subtraction calculation of K_{ij}^{kl} in the heterotic case. In the bosonic case, K_{ij}^{kl} receives contributions starting at two loops, and it can be shown that this is compatible with an independent calculation of the effective action using scattering amplitudes. The same thing may happen in the heterotic case: in particular, R^3 terms could indeed be absent from $S_{\rm eff}$, and the g^4 term in (4.69) could come entirely from K_{ij}^{kl}. A similar conclusion is reached in [104, 105] where it is shown that the beta function of the heterotic string in the presence of background gauge fields has a term at three loops that behaves as F^3, even though no corresponding term is present in the the effective action.

Finally, it is possible to make a statement about the three-loop structure of the beta function in the α' expansion. Excluding the Ricci tensor and the Ricci scalar, since the beta function is computed within the minimal subtraction scheme, the terms that are third order in the Riemann tensor and are compatible with the g^4 terms in (4.69) are given by

$$\alpha'^3\left(\frac{1}{8}R_{klmn}R_i{}^{mlr}R_j{}^k{}_{lr} - \frac{1}{16}R_{iklj}R^{kmnr}R^l{}_{mnr}\right)\,. \tag{4.73}$$

4.4.4 Singularities of the critical exponents; central charge of the CFT

Because λ involves products of Γ functions it is natural to investigate the location of its singularities closest to the origin, as in [77]. Because $\lambda_1^{het} = \frac{1}{2}\lambda_1^{bos}$, the location of the pole of λ_1 coincides with the pole in the bosonic case, with half the residue. One also has to note that $\eta_1(\mu)$ behaves as $\eta_1 \sim -\frac{4}{\pi^2}\frac{1}{2\mu-1}$ i.e. it has a simple pole at $\epsilon = -1$. But λ_1's first singularity is at $\epsilon = -3$, since the pole of η_1 is canceled by a similar pole of χ_1. Examining term by term the structure of λ_2 it is easy to see that the singularities of λ_2 come from the η_1^2 factor that multiplies the whole expression (4.66) and from the three-loop diagrams that have the lagrange multiplier field propagator corrected, i.e. $\Pi_{2\sigma}$, Π_{3u}, F_{2u}, and $F_{2\sigma}$. Since

$$R_3(\mu) \sim \frac{-1}{2\mu - 1}, \qquad R_2(\mu) \sim \frac{1}{(2\mu-1)^2} \tag{4.74}$$

and λ_2 has terms that behave as $\sim R_3^2\eta_1^2$ and $R_2\eta_1^2$ times a μ polynomial with no zero at $\mu = 1/2$, we see that it has a fourth order pole. In all, one finds

$$\lambda_1 = -\frac{3/(4\pi^2)}{\epsilon+3} + \mathcal{O}(1) \qquad b_1 \; = -\frac{\log(3+\kappa)}{2\pi^2} + \mathcal{O}(1) \tag{4.75}$$

$$\lambda_2 = \frac{8/\pi^4}{(\epsilon+1)^4} + \mathcal{O}((\epsilon+1)^{-3}) \qquad b_2 \; = -\frac{16/3\pi^4}{(\kappa+1)^3} + \mathcal{O}((\kappa+1)^{-2})\,. \tag{4.76}$$

The $1/(\kappa+1)^2$ term in b_2 comes only from the factors $R_3\eta_1^2$ and from the Hartree-Fock diagrams. The singularities in the heterotic case are at the same locations and of the same order as in the bosonic case.

Because of the sign of b_2, there is clearly a zero of $\beta(g)$ (computed through order $1/D^2$) for negative g, close to $\kappa = -1$. The same caveats discussed in [77] apply: higher order terms in $1/D$ could conceivably cause this zero to disappear or move significantly. In section 4.5 we will comment further on higher-order corrections. For the remainder of this section we will assume that the computation of $\beta(g)$ that we have carried out is precise enough to describe the zero correctly.

The zero of $\beta(g)$ arises through competition between the one-loop term (corresponding to Einstein gravity) and b_2 (corresponding to a combination of all α' corrections to Einstein gravity). Because the geometry has string scale curvatures (more precisely, $L^2 \sim D\alpha'$) there is no reason to think that the worldsheet central charges are particularly close to the flat-space results. Fortunately, one can calculate the central charges using Zamolodchikov's c-theorem:

$$\frac{\partial c}{\partial g} = \frac{3(D+1)}{2g^2}\beta(g)\,. \tag{4.77}$$

The result (4.77) holds for both the holomorphic and the anti-holomorphic sides: c and $\tilde{c}$ differ by a constant. To derive the prefactor on the right hand side of (4.77), one can consider two-point functions of the graviton perturbation $O_{ij} = \frac{1}{2\pi\alpha'}\partial X_i \bar{\partial} X_j + \frac{1}{4\pi}\Psi\partial\Psi$ around flat space, as is done in [77].[3] This prefactor receives higher loop corrections, and knowing K_{ij}^{kl} in higher loops, one can in principal compute them. As in the bosonic and supersymmetric cases, the results suggest that with increasing D the critical point moves closer to $\kappa = -1$: integrating (4.77) leads to

$$\begin{aligned} c &= (D+1) + \frac{3(D+1)}{2}\int_0^{\kappa_c} d\kappa \frac{1}{\kappa}\left(-\kappa + \frac{b_1(\kappa)}{D} + \frac{b_2(\kappa)}{D^2}\right) \approx (D+1)(1-\frac{3}{2}\kappa_c) \\ \tilde{c} &= \frac{3}{2}(D+1) + \frac{3(D+1)}{2}\int_0^{\kappa_c} d\kappa \frac{1}{\kappa}\left(-\kappa + \frac{b_1(\kappa)}{D} + \frac{b_2(\kappa)}{D^2}\right) \approx \frac{3}{2}(D+1)(1-\kappa_c)\,, \end{aligned} \tag{4.79}$$

where we have noted that the central charge of the holomorphic side in flat space is $c = D+1$, while for the anti-holomorphic side it is $\tilde{c} = \frac{3}{2}(D+1)$. The approximate equalities arise from dropping the $b_1(\kappa)$ and $b_2(\kappa)$ terms from the integrand: their only role at this level of approximation is to set κ_c. As κ_c gets closer to -1 (i.e. as D becomes large), the central charges converge to

$$c = \frac{5}{2}(D+1) \qquad \tilde{c} = 3(D+1)\,. \tag{4.80}$$

The result (4.80) for c is the same as in the bosonic case, while for $\tilde{c}$ it is the same as the type II case [77]. As in [77], (4.80) appears to set only an approximate upper bound on the central charges. The dominant error in the calculation 4.79 is from the uncertainty in the prefactor in (4.77). Analogous to the speculations in [77], it is conceivable that the expressions (4.80) might in fact be exact. But this would require a significant conspiracy between the prefactor in (4.77) and the beta function.

The fact that the location of the critical point at finite D is so close to the singularity of λ means that the critical exponent λ evaluated at the critical point is large and positive. This leads to an operator with a large and negative dimension, which appears to violate

[3] Another way to derive (4.77) is to use the relation of the central charge to the spacetime effective action. At least up to two-loop order, the effective action at the fixed point is equal to $-c/2\kappa_D^2\alpha'$ [106, 107, 108]. Also up to two loops, the K_{ij}^{kl} of (4.72) is simply given by a product of Kronecker δ's, as in the bosonic case [103]. Using the fact that in symmetric spaces

$$\beta(g)g_{ij} = -g\beta_{ij} \qquad g^{ij}\frac{\partial}{\partial g^{ij}} = g\frac{\partial}{\partial g}\,, \tag{4.78}$$

one indeed ends up with (4.77).

unitarity. However, one could hope that a consistent GSO projection would project this operator out of the spectrum.

4.5 Discussion

The existence of the AdS_{D+1} critical point depends on competition between one-loop and $1/D^2$ effects. It would therefore be instructive to compute the beta function through order $1/D^3$ and see whether the fixed point persists. Given that the number of diagrams needed for the computation at the next order grows significantly, the shortest path seems to be calculating χ_3 and using (4.60) to deduce λ_3. However, note that for the calculation of χ_3 one needs to derive the residues of diagrams at order $1/D^4$, which include some six-loop diagrams.

There is some reason to think that the singularities of λ at order $1/D^3$ are no worse than at order $1/D^2$: examining the diagrams needed for the Dyson equations of the Lagrange multiplier fields, we see that at order $1/D^3$ these come from either inserting a σ or u propagator in the $1/D^2$ diagrams or inserting a loop of S or Ψ in the middle of the diagram. The computation for the diagrams that come from inserting a σ or u propagator can easily be seen to be reduced to the sum of diagrams similar to Π_2 or Π_3 with one different exponent. A naive calculation does not produce any worse singularities than the ones already contained in Π_2 and Π_3. However, one also has to compute the more difficult diagrams with the additional S or Ψ loop.

It is evident that the methods of [80, 87], has many advantages over calculating Feynman diagrams in momentum space. In the latter approach one encounters difficulties already in calculating second order diagrams, since the propagators of the Lagrange multiplier fields are in general hypergeometric functions. It is noteworthy that even though we start from $d = 2 + \epsilon$ dimensions, one can calculate critical exponents of the $O(N)$ model in any dimension $2 < d < 4$, and there is agreement with the results in three dimensions [109] in the bosonic case.

Perhaps the methods of [80, 87] could be applied to a related quantum field theory:

$$S = \int d^d x \left(\frac{1}{2} \nabla \vec{\Phi} \cdot \nabla \vec{\Phi} + \frac{1}{2} \lambda \sigma \vec{\Phi} \cdot \vec{\Phi} - \frac{\lambda N}{4} \sigma^2 \right) , \tag{4.81}$$

which for $d = 3$ is the proposed dual of an AdS_4 vacuum of a theory with arbitrarily high spin gauge fields [110]. What makes (4.81) susceptible to a position-space treatment analogous to those in [80, 87] is that only cubic vertices are involved. It would be interesting to compute, for example, the four point function of σ to order $1/N^2$ and compare it to the corresponding AdS_4 calculation, as is done for example in [111] at order $1/N$.

Chapter 5

Conclusions

From the early days of both gauge theory and string theory there have been indications of deep connections between the two. In the last decade these indications have been made more concrete with the AdS/CFT correspondence and variants of the initial conjecture. In this thesis we use the AdS/CFT correspondence to study aspects of quark-gluon plasmas of a supersymmetric gauge theory.

Results from the experiments at the Relativistic Heavy Ion Collider suggest that a strongly coupled quark-gluon plasma is formed after collisions of gold nuclei. The initial temperature of the plasma is about 1.5 times larger than the confinement temperature of QCD. The thermal distribution of outgoing particles suggests that the quark-gluon plasma is almost in a state of thermal equilibrium. After the initial formation the QGP expands and cools. Hydrodynamical simulations of the expansion are compatible with a viscosity over entropy ratio lower than 0.2. This means that the QGP must be strongly coupled. These two features of the QGP, strong coupling and time evolution, make standard methods of gauge theories of limited applicability. Perturbation theory cannot attack strong coupling problems and numerical methods on the lattice are limited to static quantities. This leaves room for the use of string theory in order to study some of these processes, such as jet-quenching.

One of the first simplifications done is that we choose to study a supersymmetric theory,

$\mathcal{N} = 4$ Yang-Mills theory, whose description in string theory is known and well studied. Furthermore, when studying jet-quenching, we model the QGP as a static plasma. In string theory, the QGP is modelled by a static black hole in ten dimensional space. The location of its horizon inside AdS space sets the temperature of the theory. This geometry is known as $Schwarzschild - AdS_5 \times S_5$. We will ignore the five dimensions of S_5, as the physics associated with it has, to a large extend, to do with supersymmetry. A moving quark can be thought of as the endpoint of a string dangling from the boundary towards the horizon. This string can source both the graviton and the dilaton in the five dimensional background. Both of these fields propagate to the boundary and leave an "imprint" on the boundary. In the language of gauge theory this can be translated into an expectation value of an operator. For the case of the dilaton, the dual operator is a supersymmetric extension of the trace of the field-strength squared. In chapter 2 we have calculated this expectation value and found that that there is strong directionality. A more complete picture of jet-quenching and the wake has to include the stress energy tensor of the boundary theory.

One should also be cautious in using these tools. First of all we examine a different theory, that is supersymmetric and has all matter fields in the adjoint representation. Moreover it does not exhibit confinement or chiral symmetry breaking. However these phenomena are not present in QCD either above the confinement temperature. On top of that the universality of the viscosity computation gives us hope that we are not far from describing the real physics of jet-quenching. Finally, our results are valid in the large N and large 't Hooft coupling $g_{YM}^2 N$ limit. Most quantities, such as the drag force, the jet-quenching parameter, and the viscosity should get quantum corrections that scale as $\frac{1}{N^2}$ and $(g_{YM}^2 N)^{-3/2}$. Both of these are about 10% and worth computing. It should be noted though that since we do not know how to quantize string theory in a background with a Ramond-Ramond field $\frac{1}{N^2}$ cannot currently be calculated.

In chapter 3 we attack a slightly different question. Classical static black holes are locally stable in asymptotically AdS spaces. When one slightly perturbs the shape of the geometry, all small oscillations will die resulting in a static black hole. The linearized processes governing these phenomena can be described with the help of the master formalism, enabling one to calculate all gravitational quasi-normal modes. Starting from the observation of some low-lying gravitational modes separated from a main series in the case of a global AdS_5 black hole we find some low-lying modes for AdS_4 as well. In order for the perturbation not to deform the boundary one has to use a special boundary condition for the master field, contrary to cases in other dimensions. These low-lying modes are in good agreement with predictions of hydrodynamics of the boundary conformal field theory. Moreover hydrodynamics of the boundary theory suggest that these low-lying modes should be present in all dimensions.

Finally in chapter 4 we calculate some higher order corrections for the supergravity action of the heterotic string. One way, common in the literature is to calculate higher order α' corrections. We take a different path, supposing that the target space of our theory has D dimensions and we expand in $\frac{1}{D}$. Our results are accurate to all orders in α'. One can then easily calculate the beta function and this has a zero close to $gD = 1$. This would suggest a target space with negative curvature, but no matter fields. Conceivably, one could imagine that cubic and higher order corrections in $\frac{1}{D}$ will make this zero disappear or move significantly.

Appendix A

Gauge freedom and boundary conditions

In this section we derive the asymptotic expressions for the metric perturbations δg_{ab} by solving the system of equations (3.7)–(3.13). In doing so, it is important to realize that equations (3.7)–(3.13) don't determine the metric perturbations uniquely. We have seen that the gauge freedom[1]

$$\delta g_{ab} \to \delta g_{ab} + \nabla_a v_b + \nabla_b v_a \tag{A.1}$$

present in any perturbation theory problem in general relativity enables us to set $\delta g_{\rho a} = 0$ (this is what we referred to as axial gauge). However, even after we set $\delta g_{a\rho} = 0$ we still have a residual gauge freedom left, and we would like to understand this residual gauge freedom a bit better before we derive the asymptotic expressions for δg_{ab}.

The first thing to note is that generic gauge transformations of type (A.1) do not preserve the form of the metric (3.7). Instead, generic transformations would just map our initial solution onto something that doesn't transform under the $SO(3)$ isometry group of S^2 in any definite way. We only look at perturbations with the specific $SO(3)$ structure defined in (3.7). Therefore, we need to restrict the class of allowed gauge transformations to the

[1] In this section ∇_a denotes the covariant derivative with respect to the four-dimensional metric (3.1).

ones that preserve this $SO(3)$ structure. Such transformations are of the form

$$v_a(\tau,\rho,\theta,\phi) = \Big(h_\tau(\tau,\rho)\mathbb{S}(\theta,\phi) \quad h_\rho(\tau,\rho)\mathbb{S}(\theta,\phi) \quad h(\tau,\rho)\mathbb{S}_\theta(\theta,\phi) \quad h(\tau,\rho)\mathbb{S}_\phi(\theta,\phi) \Big) \,, \tag{A.2}$$

and they give

$$\begin{gathered} 2\nabla_{(\alpha}v_{\beta)} = 2D_{(\alpha}h_{\beta)}\mathbb{S} \qquad 2\nabla_{(\alpha}v_{i)} = \left[\partial_\alpha h - h_\alpha k_S - \frac{2}{\rho}(\partial_\alpha\rho)h\right]\mathbb{S}_i \\ 2\nabla_{(i}v_{j)} = -2hk_S\mathbb{S}_{ij} + (hk_S + 2\rho f h_\rho)\,\gamma_{ij}\mathbb{S}\,. \end{gathered} \tag{A.3}$$

It is easy to see now that if we start with any scalar perturbation of the form (3.7), we can set $\delta g_{\rho a} = 0$ by solving three first order non-homogeneous differential equations for h_τ, h_ρ, and h. The residual freedom that remains after setting $\delta g_{\rho a} = 0$ is reflected in the choice of the three integration constants (which are functions of τ) that enter in the general solutions of these equations. So in addition to setting $\delta g_{\rho a} = 0$ we also have the freedom to prescribe the time behavior of *three* of the other components of δg_{ab} at a given point. In particular, the gauge freedom allows us to set the large ρ behavior of three such components to have no ρ^2 term in a large ρ series expansion. Requiring all of these components (which are described by the *four* functions $H_T,\ H_L,\ f_\tau,\ f_{\tau\tau}$) to have no ρ^2 terms cannot be accomplished by making a gauge transformation, and is therefore meaningful as a boundary condition on the metric perturbations.

We now turn to the problem of finding the asymptotic expressions for the metric coefficients δg_{ab} in axial gauge. We will set $L = 1$ throughout the entire calculation. With the assumption

$$\begin{aligned} &f_{\rho\rho} = f_\rho = 0 \qquad f_{\tau\tau} = e^{-i\Omega\tau}B(\rho) \qquad f_\tau = e^{-i\Omega\tau}C(\rho) \\ &H_L = e^{-i\Omega\tau}A_L(\rho) \qquad\qquad H_T = e^{-i\Omega\tau}A_T(\rho) \end{aligned} \tag{A.4}$$

we first compute the quantities F and $F_{\alpha\beta}$ that enter in equations (3.11) and (3.12):

$$
\begin{aligned}
F &= \frac{e^{-i\Omega\tau}}{2k_S^2}\left(k_S^2\left[2A_L(\rho)+A_T(\rho)\right]+2\rho f A_T'(\rho)\right)\\
F_{\tau\tau} &= \frac{e^{-i\Omega\tau}}{k_S^2}\left(-2ik_S\rho\Omega C(\rho)+k_S^2 B(\rho)-\rho^2\left[2\Omega^2 A_T(\rho)+ff'A_T'(\rho)\right]\right)\\
F_{\tau\rho} &= \frac{e^{-i\Omega\tau}}{k_S^2 f}\big(k_S f C(\rho)-2i\Omega\rho f\left[A_T(\rho)+\rho A_T'(\rho)\right]+\\
&\qquad\qquad +\rho f k_S C'(\rho)+i\Omega\rho^2 f' A_T(\rho)-k_S\rho f' C(\rho)\big)\\
F_{\rho\rho} &= \frac{e^{-i\Omega\tau}\rho}{k_S^2 f}\left(A_T'(\rho)\left[4f+\rho f'\right]+2\rho f A_T''(\rho)\right)\,,
\end{aligned}
\tag{A.5}
$$

and $F_{\rho\tau} = F_{\tau\rho}$. The plan now is to plug the above expressions into equations (3.11) and (3.12), and find a series solution for the corresponding differential equations. In order to do this though, we need to get hold of the right-hand side of equation (3.12), perhaps in the form of a large ρ series expansion. This can be done by solving the master equation (3.13):

$$
\Phi(\rho) = \varphi^{(0)} + \frac{\varphi^{(1)}}{\rho} + \frac{\varphi^{(2)}}{\rho^2} + \frac{\varphi^{(3)}}{\rho^3} + \cdots\,, \tag{A.6}
$$

where

$$
\begin{aligned}
\varphi^{(2)} &= \left[\frac{9\rho_0^2}{(k_S^2-2)^2}+\frac{k_S^2-\Omega^2}{2}\right]\varphi^{(0)}\\
\varphi^{(3)} &= \left[-\frac{18\rho_0^3}{(k_S^2-2)^3}-\frac{\rho_0(2+k_S^2)}{2(k_S^2-2)}\right]\varphi^{(0)}+\left[\frac{3\rho_0^2}{(k_S-2)^3}+\frac{k_S^2-2-\Omega^2}{6}\right]\varphi^{(1)}
\end{aligned}
\tag{A.7}
$$

and all higher order terms can be expressed in terms of linear combinations of $\varphi^{(0)}$ and $\varphi^{(1)}$. The two constants $\varphi^{(0)}$ and $\varphi^{(1)}$ can thus be interpreted as the two integration constants that appear when we integrate the master equation, which is a second order ODE. The above expansion can then be used to find a series expansion of the right-hand side of equation (3.12). The resulting expressions are long and not that insightful, so we will not reproduce them here; their derivation is nevertheless straightforward.

We now solve for the functions $A_L(\rho)$, $A_T(\rho)$, $B(\rho)$, and $C(\rho)$ that completely determine the metric perturbations via

$$
\begin{gathered}
\delta g_{\rho\rho} = \delta g_{\tau\rho} = \delta g_{\rho i} = 0\\
\delta g_{\tau\tau} = e^{-i\Omega\tau}B(\rho)\,\mathbb{S}(\theta,\phi) \qquad \delta g_{\tau i} = \rho e^{-i\Omega\tau}C(\rho)\,\mathbb{S}_i(\theta,\phi)\\
\delta g_{ij} = 2\rho^2 e^{-i\Omega\tau}\left[A_L(\rho)\,\gamma_{ij}\,\mathbb{S}(\theta,\phi)+A_T(\rho)\,\mathbb{S}_{ij}(\theta,\phi)\right]
\end{gathered}
\tag{A.8}
$$

in four steps:

1. We first solve for $A_T(\rho)$ from the $F_{\rho\rho}$ equation in (3.12) with the LHS given by the corresponding expression in (A.5) and the RHS computed from the series expansion (A.6). We find:

$$A_T(\rho) = A_T^{(0)} + \frac{A_T^{(2)}}{\rho^2} + \left[\frac{k_S^2\rho_0}{2(k_S^2-2)}\left(\varphi^{(1)} + \frac{3\rho_0\varphi^{(0)}}{k_S^2-2}\right) + \right. \\ \left. + \frac{k_S^2(k_S^2-2\Omega^2)}{12}\varphi^{(0)}\right]\frac{1}{\rho^3} + \mathcal{O}\left(\frac{1}{\rho^4}\right) . \tag{A.9}$$

Here, we can think of $A_T^{(0)}$ and $A_T^{(2)}$ as integration constants: we have two integration constants because the differential equation satisfied by $A_T(\rho)$ is second order, as can be easily seen from the $F_{\rho\rho}$ relation in (A.5).

2. Next, we solve for $C(\rho)$ from the $F_{\tau\rho}$ equation in (3.12). Again, the LHS of this equation is given in (A.5), and the RHS can be computed from (A.6). We obtain:

$$C(\rho) = C^{(-1)}\rho + \left[-\frac{ik_S\Omega}{2}\left(\varphi^{(1)} + \frac{3\rho_0\varphi^{(0)}}{k_S^2-2}\right) + \frac{k_S C^{(-1)} + i\Omega(2A_T^{(2)} - A_T^{(0)})}{k_S}\right]\frac{1}{\rho} + \\ + \left[\frac{\rho_0(i\Omega A_T^{(0)} - k_S C^{(-1)})}{k_S} - \frac{ik_S\Omega(k_S^2-2)}{6}\varphi^{(0)}\right]\frac{1}{\rho^2} + \mathcal{O}\left(\frac{1}{\rho^3}\right) , \tag{A.10}$$

where $C^{(-1)}$ is an integration constant—we can see from the $F_{\tau\rho}$ relation in (A.5) that the corresponding differential equation for $C(\rho)$ is a first order ODE, so its solution has to have one integration constant.

3. Similarly, we next solve for $B(\rho)$ from the $F_{\tau\tau}$ equation in (3.12). As can be seen from the $F_{\tau\tau}$ relation in (A.5), this equation doesn't involve any derivatives of $B(\rho)$, so its

solution doesn't involve additional integration constants:

$$B(\rho) = \frac{2(ik_S\Omega C^{(-1)} + \Omega^2 A_T^{(0)} - 2A_T^{(2)})}{k_S^2}\rho^2 + \left[\frac{k_S^2 - 2 + 2\Omega^2}{4(k_S^2-2)}\left(\varphi^{(1)} + \frac{3\rho_0\varphi^{(0)}}{k_S^2-2}\right) + \right.$$
$$\left. + \frac{2\Omega(ik_S C^{(-1)} + \Omega A_T^{(0)}) - 2(1+\Omega^2)A_T^{(2)}}{k_S^2}\right] + \left[\rho_0\left(\varphi^{(1)} + \frac{3\rho_0\varphi^{(0)}}{k_S^2-2}\right) - \right.$$
$$\left. - \frac{2\rho_0\Omega(ik_S C^{(-1)} + \Omega A_T^{(0)})}{k_S^2} + \frac{k_S^2(k_S^2-2)}{6}\varphi^{(0)}\right]\frac{1}{\rho} + \mathcal{O}\left(\frac{1}{\rho^2}\right). \tag{A.11}$$

4. Finally, we solve for $A_L(\rho)$ from the second equation in (3.11) with $\beta = \tau$. Again, this equation doesn't involve any derivatives, so we have no integration constants:

$$A_L(\rho) = \left[\frac{4A_T^{(2)} - k_S^2 A_T^{(0)}}{2k_S^2} - \frac{1}{2}\left(\varphi^{(1)} + \frac{3\rho_0\varphi^{(0)}}{k_S^2-2}\right)\right] +$$
$$+ \left[-\frac{(k_S^2-2)A_T^{(2)}}{2k_S^2} + \frac{k_S^2-2}{8}\left(\varphi^{(1)} + \frac{3\rho_0\varphi^{(0)}}{k_S^2-2}\right)\right]\frac{1}{\rho^2} +$$
$$+ \left[-\frac{\rho_0 A_T^{(2)}}{k_S^2} + \frac{\rho_0}{4}\left(\varphi^{(1)} + \frac{3\rho_0\varphi^{(0)}}{k_S^2-2}\right) + \frac{k_S^2(k_S^2-2)}{24}\varphi^{(0)}\right]\frac{1}{\rho^3} + \mathcal{O}\left(\frac{1}{\rho^4}\right). \tag{A.12}$$

It can be checked that the above series solutions automatically satisfy the other two equations in (3.11) that we have not used. Also, the fact that the integration constants $A_T^{(0)}$, $A_T^{(2)}$, and $C^{(-1)}$ are still undetermined is a consequence of the residual gauge freedom that we discussed at the beginning of this section: these three integration constants allow us to set the values of *three* of the functions $A_L(\rho)$, $A_T(\rho)$, $B(\rho)$, and $C(\rho)$ at a given point to whatever we want.

Requiring that the metric perturbations don't grow like ρ^2 at large ρ and using (A.8)–(A.12), we get $A_T^{(0)} = A_T^{(2)} = C^{(-1)} = 0$, together with

$$\varphi^{(1)} + \frac{3\rho_0\varphi^{(0)}}{k_S^2-2} = 0\,, \tag{A.13}$$

which is the same as (3.21).

We note that the relations (A.13) and $A_T^{(0)} = A_T^{(2)} = C^{(-1)} = 0$ make almost all terms written in the series expansions (A.9)–(A.12) disappear, and we're left just with

$$\begin{aligned}
H_L &= \frac{k_S^2(k_S^2-2)}{24} e^{-i\Omega\tau} \frac{\varphi^{(0)}}{\rho^3} + \mathcal{O}\left(\frac{1}{\rho^4}\right) \\
H_T &= \frac{k_S^2(k_S^2-2\Omega^2)}{12} e^{-i\Omega\tau} \frac{\varphi^{(0)}}{\rho^3} + \mathcal{O}\left(\frac{1}{\rho^4}\right) \\
f_{\tau\tau} &= \frac{k_S^2(k_S^2-2)}{6} e^{-i\Omega\tau} \frac{\varphi^{(0)}}{\rho} + \mathcal{O}\left(\frac{1}{\rho^2}\right) \\
f_{\tau} &= -\frac{ik_S\Omega(k_S^2-2)}{6} e^{-i\Omega\tau} \frac{\varphi^{(0)}}{\rho^2} + \mathcal{O}\left(\frac{1}{\rho^3}\right) ,
\end{aligned} \tag{A.14}$$

which looks incredibly similar to the expressions found in section 3.3.2 of [70] in AdS_5-Schwarzschild. In light of the analysis done in [70], it is worth mentioning that the leading coefficients in (A.14) give, up to a proportionality factor, the expectation value of the stress-energy tensor in the boundary $2+1$-dimensional CFT. Conservation and tracelessness of the stress-energy tensor can then be easily checked using the same approach as in [70].

Appendix B

Anomalies

Since we have coupled only the right moving fermions to gravity it is natural to investigate whether there are anomalies. These are related to a breakdown of general coordinate invariance or local Lorentz invariance. We will investigate only the latter, as is usually done [112]. Indeed when there is a coordinate anomaly one can add a counterterm to the action and convert it to a Lorentz anomaly [113]. It is convenient to use the tetrad formalism. Local Lorentz transformations in this formalism are given by

$$e'_{\mu}{}^{p}(x) = e_{\mu}{}^{q}(x)\Theta^{p}{}_{q}(x)\,. \tag{B.1}$$

The Riemann tensor can be written $R_{\mu\nu}{}^{p}{}_{q}$, with mixed spacetime and tangent space indices, and can be regarded as a two form R_2. We only have to worry about the massless fields of the supergravity sector [112]. The anomaly polynomials for the spinor and the gravitino contain only terms that are proportional to polynomials in $\mathrm{Tr}\, R_2^{\wedge 2m}$. In the AdS space that we are interested in we can calculate

$$R_{\mu\nu}{}^{a}{}_{b}R_{\kappa\lambda}{}^{c}{}_{a} = \frac{1}{L^2}(\delta^{c}{}_{k}R_{\mu\nu\lambda b} + \delta^{c}{}_{\lambda}R_{\mu\nu b\kappa}) \tag{B.2}$$

which when antisymmetrizing to get the wedge product returns zero. So $R_2 \wedge R_2 = 0$ in our case, and we do not have to worry about the gravitational anomalies. Another way to view this is to say that the field strength $H_3 = dB_2$ obeys the modified Bianchi identity

$$dH_3 = \frac{1}{4\pi}(\mathrm{Tr}\, R_2 \wedge R_2 - \mathrm{Tr}\, F_2 \wedge F_2)\,. \tag{B.3}$$

A three form H_3 obeying (B.3) is required for cancelation of perturbative heterotic string worldsheet anomalies, as is briefly reviewed in [114]. Because $\mathrm{Tr}\, R_2 \wedge R_2 = 0$, this is trivially satisfied.

Appendix C

Position space methods for calculating graphs

There are 11 diagrams needed for the calculation of η at $1/D^2$. We designate them by Σ, Π, Φ, F. The way to compute them was developed in [80, 87] for the bosonic graphs and extended to include fermionic graphs in [88, 89]. The main advantage of the method is that there is no need to explicitly evaluate any Feynman diagram. Here we will only give a few key observations that facilitate the evaluation of the diagrams. The first observation is that the chain of two propagators is equal to a propagator times a prefactor. Graphically this is shown in Fig C.1, where $\nu(x_1, x_2, x_3) = \pi^\mu \prod_{i=1}^3 \alpha(x_i)$. The third exponent x_3 is determined by the "uniqueness" [87] requirement $\sum_i x_i = 2\mu$, for the bosonic graphs and $\sum_i x_i = 2\mu - 1$ if there are one or more fermion lines in the graph. An identity exists for a three point vertex, which is similarly related to a "unique" triangle, where now the uniqueness requirement is that $\sum_i x_i = \mu$. If there are one or more fermion lines the uniqueness changes to $\sum_i x_i = \mu + 1$, and the results of [88] are unchanged in our case. There is no similar identity for a four point function, and for the (1,1) supersymmetric model that means that one has to retain the auxiliary field F. In computing the values at order $1/D^2$, χ is set to zero [87]. For a non-zero Δ the diagrams, for example the self energy of Ψ designated A, lose their uniqueness. However one can subtract from A a graph

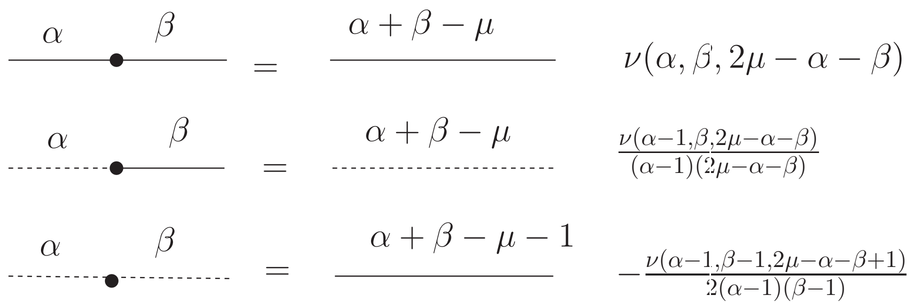

Figure C.1: Products of two propagators are related to a single propagator. So, in a two-loop diagram,(Σ_1 for example) inserting a point in one of the three propagators that connect to one internal vertex can make this vertex unique. The dotted lines denote fermions. Since we are dealing with chiral fermions, taking the trace in the third graph only produces one half the full result. ν is equal to $\nu(x_1, x_2, x_3) = \pi \prod_{i=1}^{3} \alpha(x_i)$.

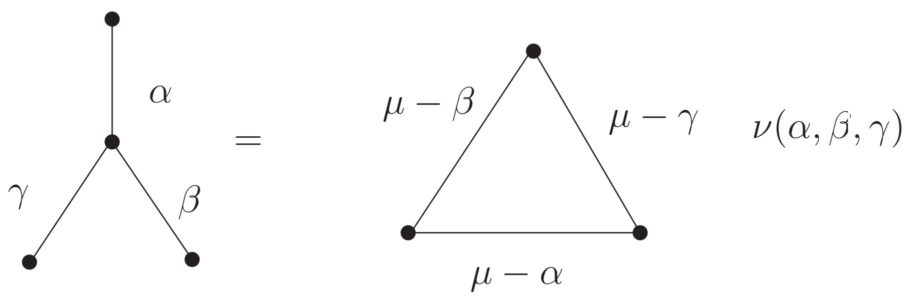

Figure C.2: An identity that allows the integration of a unique vertex. Only bosonic propagators are shown. Similar identities with fermions can which are used in our calculation can be found in [6]

B that has the same divergent substructure as A, but can be calculated for an arbitrary Δ. So one has to compute $(A-B)+B$. Since B can be calculated for arbitrary Δ and contains the divergence, one can evaluate $(A-B)$ at zero Δ when both diagrams become unique. A valuable first step in the calculation is the evaluation of all the self-energy graphs, which we will not include here since it was done in detail in [87, 89]. We just note that the most basic tool is the insertion of a point facilitated by the fact that we can write a propagator as a product of two. Then one can choose one of the exponents in such a way that the vertex that the propagator is attached to, becomes unique.

Appendix D

Calculation of the graphs needed for η_2

We give the results for the various graphs occurring in the $1/D^2$ calculation. We only give the simple pole term and the constant term in an expansion in Δ. The purely bosonic graphs were calculated in [87]. Compared to the calculation of the fermionic graphs in [6], there are differences that have to do with taking the trace of fermion loops, i.e. some factors of two in bosonic diagrams with fermion loops. Otherwise the calculation is almost identical. We find small discrepancies with [6] in some of the diagrams, mostly factors of 2 and some minus signs. The most notable difference is Φ_1, where the residue has a different denominator. We believe that our value is correct, since it leads to the same χ_1 as the evaluations from the other equations (4.58).

$$B(x) = \psi(x) + \psi(\mu - x) \tag{D.1}$$

$$\Sigma_1 = \frac{2\pi^{2\mu}\alpha^2(\Delta_S)\alpha(\Delta_\sigma)}{\Delta\Gamma(\mu)}\left(1 + \frac{\Delta}{2}\left[B(\Delta_\sigma) - B(\Delta_S)\right]\right) \tag{D.2}$$

$$\Sigma_2 = \frac{2\pi^{2\mu}\alpha^2(\Delta_S)\alpha(\Delta_\sigma - 1)}{\Delta\alpha(\Delta_\sigma - 1)\Gamma(\mu)}\left(1 + \frac{\Delta}{2}\left[B(\Delta_\sigma - 1) - B(\Delta_S) + \frac{1}{\Delta_\sigma - 1} - \frac{1}{\Delta_S}\right]\right) \tag{D.3}$$

$$\Sigma_3 = \frac{2\pi^{4\mu}\alpha^3(\Delta_S)\alpha^3(\Delta_\sigma)\alpha(\mu + \Delta_S - \Delta_\sigma)}{\Delta\Gamma(\mu)}\left(\frac{1}{2} + \Delta\left[B(\Delta_\sigma) - B(\Delta_S)\right]\right) \tag{D.4}$$

$$\Sigma_4 = \frac{\pi^{4\mu}\alpha^3(\Delta_S)\alpha^2(\Delta_\sigma - 1)\alpha(\Delta_\sigma)\alpha(\Delta_S + \mu - \Delta_\sigma)}{\Delta\Delta_S(\Delta_S + \mu - \Delta_\sigma)(\Delta_\sigma - 1)^2\Gamma(\mu)} \times \left(1 + \frac{\Delta}{2}\left[B(\Delta_\sigma) + 3B(\Delta_\sigma - 1) - 4B(\Delta_S) + \frac{3}{\Delta_\sigma - 1} - \frac{2}{\Delta_S}\right]\right) \tag{D.5}$$

$$\Pi_1 = \frac{2\pi^{2\mu}\alpha^2(\Delta_S)\alpha(\Delta_\sigma)}{\Delta\Gamma(\mu)}\left(1 + \Delta\left[B(\Delta_\sigma) - B(\Delta_S)\right]\right) \tag{D.6}$$

$$\Pi_2 = \frac{\pi^{4\mu}\alpha^3(\Delta_S)\alpha^3(\Delta_\sigma)\alpha(\Delta_S + \mu - \Delta_\sigma)}{\Delta\Gamma(\mu)}\left(1 + \Delta\left[4B(\Delta_\sigma) - 3B(\Delta_S) - B(\mu + \Delta_S - \Delta_\sigma)\right]\right) \tag{D.7}$$

$$\Pi_3 = \frac{\pi^{4\mu}\alpha^3(\Delta_S)\alpha^2(\Delta_\sigma - 1)\alpha(\Delta_S + \mu - \Delta_\sigma)}{2\Delta\alpha(\mu - \Delta_\sigma)\Delta_S(\Delta_S + \mu - \Delta_\sigma)(\Delta_\sigma - 1)^2\Gamma(\mu)} \times \Bigg(1 + \Delta\Big[2B(\Delta_\sigma) - 3B(\Delta_S) + 2B(\Delta_\sigma - 1) - B(\Delta_S + \mu - \Delta_\sigma) - \frac{1}{\Delta_S} + \frac{2}{\Delta_\sigma - 1} - \frac{1}{\Delta_S - \Delta_\sigma + \mu}\Big]\Bigg) \tag{D.8}$$

$$\Phi_1 = -\frac{\pi^{2\mu}\alpha^2(\Delta_S - 1)\alpha(\Delta_\sigma)}{\Delta\Delta_S(\Delta_S - 1)\Gamma(\mu)}\left(1 + \Delta\left[B(\Delta_\sigma) - B(\Delta_S - 1) - \frac{1}{\Delta_S - 1}\right]\right) \tag{D.9}$$

$$\Phi_2 = -\frac{\pi^{4\mu}\alpha^3(\Delta_S)\alpha^2(\Delta_\sigma - 1)\alpha(\Delta_\sigma)\alpha(\Delta_S + \mu - \Delta_\sigma)}{\Delta\Delta_S(\Delta_S + \mu - \Delta_\sigma)(\Delta_\sigma - 1)^2\Gamma(\mu)} \times \left(1 + \Delta\left[B(\Delta_\sigma) - 2B(\Delta_S) + B(\Delta_\sigma - 1) + \frac{1}{\Delta_\sigma - 1}\right]\right) \tag{D.10}$$

$$F_1 = -\frac{2\pi^{2\mu}\alpha^2(\Delta_S)\alpha(\Delta_\sigma - 1)}{\Delta\Delta_S(\Delta_\sigma - 1)\Gamma(\mu)}\left(1 + \Delta\left[B(\Delta_\sigma - 1) - B(\Delta_S) - \frac{1}{2\Delta_S} + \frac{1}{\Delta_\sigma - 1}\right]\right) \tag{D.11}$$

$$F_2 = -\frac{\pi^{4\mu}\alpha^3(\Delta_S)\alpha(\Delta_\sigma)\alpha^2(\Delta_\sigma - 1)\alpha(\Delta_S + \mu - \Delta_\sigma)}{\Delta\Delta_S(\Delta_S + \mu - \Delta_\sigma)(\Delta_\sigma - 1)^2\Gamma(\mu)} \times \Bigg(1 + \Delta\Big[B(\Delta_\sigma) + 3B(\Delta_\sigma - 1) - B(\Delta_S + \mu - \Delta_\sigma) - 3B(\Delta_S) - \frac{1}{\Delta_S} + \frac{3}{\Delta_\sigma - 1} - \frac{1}{\Delta_S + \mu - \Delta_\sigma}\Big]\Bigg). \tag{D.12}$$

Note that there is a similar three-loop diagram with Π_3 with the role of the Ψ, u propagators interchanged. But it scales as $1/N^3$. A very useful identity for the evaluation of various quantities given in the text is $B(x) = B(\mu - x)$.

Appendix E

Calculation of the graphs needed for λ_2

In this section we give the formal expressions for the sums of the corrected diagrams (E.2)-(E.11), the values of the 43 individual diagrams that contribute (E.12)-(E.30), and finally the explicit form of the sums (F.1)-(F.9). Beforehand one has to define the functions appearing as

$$\begin{aligned} R_1 &= \psi'(\mu-1) - \psi'(\mu) \\ R_2 &= \psi'(2\mu-3) - \psi'(2-\mu) - \psi'(\mu-1) + \psi'(1) \\ R_3 &= \psi(2\mu-3) + \psi(2-\mu) - \psi(\mu-1) - \psi(1)\,, \end{aligned} \tag{E.1}$$

where $\psi(z) = d\log\Gamma(z)/dz$.

$$\begin{aligned} \Sigma_S = 2w^2\Sigma_{1Sa} + w^2\Sigma_{1Sb} - v^2\Sigma_{2S} &+ Nw^3(2\Sigma_{3Sa} + 2\Sigma_{3Sb} + \Sigma_{3Sc}) \\ &- 2Nv^2w(\Sigma_{4Sa} + \Sigma_{4Sb} + \Sigma_{4Sc}) \end{aligned} \tag{E.2}$$

$$\Sigma_\Psi = -2v^2\Sigma_{2\Psi} - 2Nv^2w(\Sigma_{4\Psi a} + \Sigma_{4\Psi b}) \tag{E.3}$$

$$\Sigma_\sigma = 2w^2\Sigma_{1\sigma} + Nw^3(2\Sigma_{3\sigma a} + \Sigma_{3\sigma b}) - 2Nv^2w\Sigma_{4\sigma} \tag{E.4}$$

$$\Sigma_u = -2v^2\Sigma_{2u} - 2Nv^2w(\Sigma_{4ua} + \Sigma_{4ub}) \tag{E.5}$$

$$\Phi_\Psi = v^2\Phi_{1\Psi} + Nv^2w\Phi_{2\Psi} \qquad \Phi_\sigma = Nv^2w\Phi_{2\sigma} \tag{E.6}$$

$$\Phi_S = 2v^2\Phi_{1S} + 2Nv^2w(\Phi_{1Sa} + \Phi_{2Sb}) \qquad \Phi_u = 2v^2\Phi_{1u} + Nv^2w\Phi_{2u} \tag{E.7}$$

$$\Pi_S = 4w^2\Pi_{1S} + Nw^3(4\Pi_{2Sa} + 2\Pi_{2Sb}) - 4Nwv^2\Pi_{3S} \tag{E.8}$$

$$\Pi_\sigma = w^2\Pi_{1\sigma} + 2Nw^3\Pi_{2\sigma} \qquad \Pi_\Psi = -2Nwv^2\Pi_{3\Psi} \qquad \Pi_u = -2Nwv^2\Pi_{3u} \tag{E.9}$$

$$F_\Psi = 2v^2F_{1\Psi} + 2Nv^2w2F_{2\Psi} \qquad F_S = 2v^2F_{1S} + 2Nv^2w(F_{2Sa} + F_{2Sb}) \tag{E.10}$$

$$F_u = v^2F_{1u} + Nv^2wF_{2u} \qquad F_\sigma = Nv^2wF_{2\sigma} \tag{E.11}$$

There are 19 diagrams associated with the S-propagator and eight for the propagator of the other fields. The value of each graph of each graph is given below for completeness. The bosonic ones were calculated in [87], while similar to the fermionic ones were done in [91].

$$\Sigma_{1Sa} = \frac{\pi^{2\mu}}{(\mu-2)\Gamma^2(\mu)} \qquad \Sigma_{1Sb} = \frac{\pi^{2\mu}}{(\mu-2)^2\Gamma^2(\mu)} \tag{E.12}$$

$$\Sigma_{2S} = -\frac{2(\mu+1)\pi^{2\mu}}{\mu(\mu-1)\Gamma^2(\mu)} \qquad \Sigma_{3Sa} = \frac{(\mu^2-3\mu+1)\Gamma(1-\mu)\pi^{4\mu}}{(\mu-2)^3\Gamma(\mu)\Gamma(2\mu-3)} \tag{E.13}$$

$$\Sigma_{3Sb} = \frac{\pi^{4\mu}\Gamma(2-\mu)}{(2-\mu)\Gamma(\mu-1)\Gamma(2\mu-2)}\left(3R_1 + \frac{2\mu-3}{(\mu-2)^2}\right) \tag{E.14}$$

$$\Sigma_{3Sc} = \frac{\pi^{4\mu}\Gamma(4-\mu)}{(\mu-2)^3\Gamma(\mu-1)\Gamma(2\mu-4)} \qquad \Sigma_{4Sa} = \frac{2\pi^{4\mu}\Gamma(1-\mu)}{\Gamma(\mu)\Gamma(2\mu-2)} \tag{E.15}$$

$$\Sigma_{4Sb} = -\frac{\pi^{4\mu}\Gamma(2-\mu)}{\Gamma(\mu)\Gamma(2\mu-2)}\left(3R_1 + \frac{2\mu-3}{(\mu-1)(\mu-2)}\right) \tag{E.16}$$

$$\Sigma_{4Sc} = \frac{2(\mu-3)(2\mu-3)\Gamma(1-\mu)\pi^{4\mu}}{(2-\mu)\Gamma(2\mu-2)\Gamma(\mu)} \qquad \Sigma_{2\Psi} = \frac{\pi^{2\mu}}{(\mu-1)\Gamma^2(\mu)} = -\Phi_{2S} \tag{E.17}$$

$$\Sigma_{4\Psi a} = \frac{\pi^{4\mu}\Gamma(1-\mu)(2\mu^2-5\mu+1)}{2(\mu-2)\Gamma(\mu)\Gamma(2\mu-2)} = -\Phi_{2Sa} \qquad \Sigma_{4\Psi b} = \frac{\pi^{4\mu}3(\mu-3)\Gamma(2-\mu)R_1}{2(2-\mu)\Gamma(\mu)\Gamma(2\mu-2)} = -\Phi_{2Sb} \tag{E.18}$$

$$\Sigma_{1\sigma} = \frac{\pi^{2\mu}(\mu^2-3\mu+1)}{(\mu-2)^2\Gamma^2(\mu)} = \Pi_{1S} \qquad \Sigma_{3\sigma a} = \frac{\pi^{4\mu}(2\mu^2-7\mu+4)\Gamma(1-\mu)}{(\mu-2)^3\Gamma(\mu)\Gamma(2\mu-3)} = \Pi_{2Sa} \tag{E.19}$$

$$\Sigma_{3\sigma b} = \frac{3\pi^{4\mu}\Gamma(3-\mu)R_1}{(2-\mu)^3\Gamma(\mu-1)\Gamma(2\mu-2)} = \Pi_{2Sb} \qquad \Sigma_{4\sigma} = \frac{\pi^{4\mu}(2\mu-5)\Gamma(1-\mu)}{(\mu-2)\Gamma(\mu)\Gamma(2\mu-2)} = \Pi_{3S} \tag{E.20}$$

$$\Sigma_{2u} = \frac{\pi^{2\mu}}{\Gamma^2(\mu)} \qquad \Sigma_{4ua} = \frac{\pi^{4\mu}(4\mu-9)\Gamma(1-\mu)}{2(\mu-2)\Gamma(\mu)\Gamma(2\mu-2)} = -F_{2sa} \tag{E.21}$$

$$\Sigma_{4ub} = \frac{3\pi^{4\mu}\Gamma(2-\mu)R_1}{2(\mu-2)\Gamma(\mu)\Gamma(2\mu-2)} = -F_{2Sb} \tag{E.22}$$

$$\Phi_{1S} = -\frac{\pi^{2\mu}}{(\mu-1)\Gamma^2(\mu)} \qquad \Phi_{1u} = \frac{\pi^{2\mu}\mu}{(1-\mu)\Gamma^2(\mu)} \tag{E.23}$$

$$\Phi_{2u} = \frac{\pi^{4\mu}\Gamma(1-\mu)(4\mu^2-11m+5)}{2(1-\mu)(\mu-2)\Gamma(\mu)\Gamma(2\mu-2)} \qquad \Pi_{1\sigma} = \frac{3\pi^{2\mu}R_1}{(2-\mu)(2\mu-3)\Gamma^2(\mu-1)} \tag{E.24}$$

$$\Pi_{2\sigma} = \frac{\pi^{4\mu}\Gamma(2-\mu)}{2(2-\mu)^3\Gamma(\mu-1)\Gamma(2\mu-1)}\left(6R_1 - R_2 - R_3^2 + \frac{2(\mu-2)}{(\mu-1)(3\mu-2)}(R_3 - \frac{1}{\mu-2})\right) \tag{E.25}$$

$$\Pi_{3u} = -\frac{\Gamma(2-\mu)\pi^{4\mu}}{4(\mu-2)^2\Gamma(\mu)\Gamma(2\mu-2)}\left(6R_1^2 - R_2 - R_3^2 + \frac{2R_3(\mu-2)-2}{(\mu-1)(2\mu-3)}\right) = -F_{2\sigma} \tag{E.26}$$

$$\Pi_{3\Psi} = \frac{3\Gamma(2-\mu)\pi^{4\mu}R_1}{(2\mu-3)\Gamma(\mu)\Gamma(2\mu-1)} = \Phi_{2\sigma} \qquad F_{1\Psi} = \frac{\mu\pi^{2\mu}}{(1-\mu)\Gamma^2(\mu)} \tag{E.27}$$

$$F_{2\Psi} = \frac{\pi^{4\mu}(4\mu^2-11\mu+5)\Gamma(1-\mu)}{2(1-\mu)(\mu-2)\Gamma(\mu)\Gamma(2\mu-2)} \tag{E.28}$$

$$F_{1S} = -\frac{\pi^{2\mu}}{\Gamma^2(\mu)} \qquad F_{1u} = \frac{3(\mu-1)\pi^{2\mu}}{2(\mu-2)\Gamma^2(\mu)} \tag{E.29}$$

$$\begin{aligned} F_{2u} = \frac{\pi^{4\mu}\Gamma(2-\mu)}{4(\mu-1)^2(\mu-2)^2\Gamma(\mu)\Gamma(2\mu-2)}\Bigg((\mu-1)(6R_1 - R_2 - R_3^2) \\ + \frac{2(\mu-2)R_3}{2\mu-3} + \frac{2}{2\mu-3} - \frac{4}{\mu-1}\Bigg). \end{aligned} \tag{E.30}$$

Appendix F

Summing up graphs

In this subsection we give the explicit values for the various sums appearing in the λ_2 calculation. We have omitted the $1/N^2$ factor that multiplies all of the diagrams so that the expression (4.66) for $\tilde{\lambda}_2$, does not contain any factors of N.

$$\begin{aligned}\frac{\Sigma_S}{\eta_1 v_1} = -1 + \frac{\mu+2}{\mu-1} + \frac{2}{(\mu-1)^2} &+ 2\mu(2\mu-5) + 2\mu(2\mu-3)(\mu-3)(2-(\mu-2)^2) \\ &- 4\mu(\mu-2) - 6\mu(\mu-2)R_1\end{aligned} \tag{F.1}$$

$$\Sigma_\Psi = -\eta_1 v_1 \left(\frac{\mu^2(\mu-2)(2\mu-3)}{\mu-1} + 3(\mu-1)(\mu-3)R_1 \right) = \Phi_S \tag{F.2}$$

$$\Sigma_\sigma = -\eta_1 v_1 \left(\frac{\mu(3+\mu(3\mu-7))}{(\mu-1)^2} + 3\mu(\mu-2)R_1 \right) = \frac{\Pi_S}{2} \tag{F.3}$$

$$\Sigma_u = \eta_1 v_1 (\mu(8-4\mu+3(\mu-1)R_1) = F_S \tag{F.4}$$

$$\Phi_\sigma = \eta_1 v_1 \frac{3\mu(\mu-1)(\mu-2)R_1}{2\mu-3} = (\Pi_\Psi)/2 \tag{F.5}$$

$$\frac{\Phi_u}{\eta_1 v_1} = 1 + 6\mu - 4\mu^2 - \frac{1}{\mu-1} = -\frac{F_\Psi}{\eta_1 v_1} \tag{F.6}$$

$$\frac{\Pi_\sigma}{\eta_1 v_1} = \left(\frac{3\mu(\mu-2)}{2(2\mu-3)} R_1 - \frac{\mu}{\mu-1} \left[6R_1 - R_2 - R_3^2 + \frac{2((\mu-2)R_3-1)}{(2\mu-3)(\mu-1)} \right] \right) \tag{F.7}$$

$$\frac{\Pi_u}{\eta_1 v_1} = \frac{\mu(\mu-1)}{\mu-2} \left(6R_1 - R_2 - R_3^2 + 2\frac{(\mu-2)R_3-1}{(2\mu-3)(\mu-1)} \right) = -\frac{2F_\sigma}{\eta_1 v_1} \tag{F.8}$$

$$\frac{F_u}{\eta_1 v_1} = \frac{3}{4}\frac{\mu(\mu-1)}{\mu-2} + \frac{\mu}{4} \left(6R_1 - R_2 + R_3^2 - \frac{4}{(\mu-1)^2} + \frac{2}{(2\mu-3)(\mu-1)} + \frac{2(\mu-2)}{2\mu-3} R_3 \right). \tag{F.9}$$

Bibliography

[1] M. Kaneta and N. Xu, "Centrality dependence of chemical freeze-out in Au + Au collisions at RHIC," `nucl-th/0405068`.

[2] F. Karsch, "Lattice QCD at high temperature and density," *Lect. Notes Phys.* **583** (2002) 209–249, `hep-lat/0106019`.

[3] **PHENIX** Collaboration, K. Adcox *et. al.*, "Formation of dense partonic matter in relativistic nucleus nucleus collisions at RHIC: Experimental evaluation by the PHENIX collaboration," *Nucl. Phys.* **A757** (2005) 184–283, `nucl-ex/0410003`.

[4] M. D. Baker, "The latest Results from PHOBOS: Systematics of Charged Particle Production through $\sqrt{s_{NN}} = 200\,\mathrm{GeV}$," 2001. PowerPoint talk, available at http://www.phobos.bnl.gov/Presentations/paris01/.

[5] B. Muller and J. L. Nagle, "Results from the Relativistic Heavy Ion Collider," `nucl-th/0602029`.

[6] J. A. Gracey, "Probing the supersymmetric O(N) sigma model to $\mathcal{O}(1/N^2)$: Critical exponent η," *Nucl. Phys.* **B348** (1991) 737–756.

[7] S. Gubser, J. Friess, G. Michalogiorgakis, and S. Pufu, "Pitp 2006 notes." Available online in http://www.admin.ias.edu/pitp/2006files/Lecture notes/Gubser Lecture notes REVISED.pdf.

[8] J. J. Friess, S. S. Gubser, and G. Michalogiorgakis, “Dissipation from a heavy quark moving through N = 4 super- Yang-Mills plasma,” *JHEP* **09** (2006) 072, hep-th/0605292.

[9] G. Michalogiorgakis and S. S. Pufu, “Low-lying gravitational modes in the scalar sector of the global AdS(4) black hole,” *JHEP* **02** (2007) 023, hep-th/0612065.

[10] G. Michalogiorgakis and S. S. Gubser, “Heterotic non-linear sigma models with anti-de Sitter target spaces,” *Nucl. Phys.* **B757** (2006) 146–171, hep-th/0605102.

[11] G. 't Hooft, “A planar diagram theory for strong interactions,” *Nucl. Phys.* **B72** (1974) 461.

[12] J. M. Maldacena, “The large N limit of superconformal field theories and supergravity,” *Adv. Theor. Math. Phys.* **2** (1998) 231–252, hep-th/9711200.

[13] S. S. Gubser, I. R. Klebanov, and A. M. Polyakov, “Gauge theory correlators from non-critical string theory,” *Phys. Lett.* **B428** (1998) 105–114, hep-th/9802109.

[14] E. Witten, “Anti-de Sitter space and holography,” *Adv. Theor. Math. Phys.* **2** (1998) 253–291, hep-th/9802150.

[15] O. Aharony, S. S. Gubser, J. M. Maldacena, H. Ooguri, and Y. Oz, “Large N field theories, string theory and gravity,” *Phys. Rept.* **323** (2000) 183–386, hep-th/9905111.

[16] I. R. Klebanov, “TASI lectures: Introduction to the AdS/CFT correspondence,” hep-th/0009139.

[17] E. D'Hoker and D. Z. Freedman, “Supersymmetric gauge theories and the AdS/CFT correspondence,” hep-th/0201253.

[18] A. Strominger and C. Vafa, “Microscopic Origin of the Bekenstein-Hawking Entropy,” *Phys. Lett.* **B379** (1996) 99–104, hep-th/9601029.

[19] S. S. Gubser, I. R. Klebanov, and A. W. Peet, "Entropy and Temperature of Black 3-Branes," *Phys. Rev.* **D54** (1996) 3915–3919, `hep-th/9602135`.

[20] G. Policastro, D. T. Son, and A. O. Starinets, "The shear viscosity of strongly coupled N = 4 supersymmetric Yang-Mills plasma," *Phys. Rev. Lett.* **87** (2001) 081601, `hep-th/0104066`.

[21] P. Kovtun, D. T. Son, and A. O. Starinets, "Viscosity in strongly interacting quantum field theories from black hole physics," *Phys. Rev. Lett.* **94** (2005) 111601, `hep-th/0405231`.

[22] G. Baym, H. Monien, C. J. Pethick, and D. G. Ravenhall, "Transverse interactions and transport in relativistic quark - gluon and electromegnetic plasmas," *Phys. Rev. Lett.* **64** (1990) 1867–1870.

[23] P. Arnold, G. D. Moore, and L. G. Yaffe, "Transport coefficients in high temperature gauge theories. I: Leading-log results," *JHEP* **11** (2000) 001, `hep-ph/0010177`.

[24] S. C. Huot, S. Jeon, and G. D. Moore, "Shear viscosity in weakly coupled N = 4 super Yang-Mills theory compared to QCD," `hep-ph/0608062`.

[25] S. R. Das, G. W. Gibbons, and S. D. Mathur, "Universality of low energy absorption cross sections for black holes," *Phys. Rev. Lett.* **78** (1997) 417–419, `hep-th/9609052`.

[26] A. Buchel, "On universality of stress-energy tensor correlation functions in supergravity," *Phys. Lett.* **B609** (2005) 392–401, `hep-th/0408095`.

[27] **BRAHMS** Collaboration, I. Arsene *et. al.*, "Quark gluon plasma and color glass condensate at RHIC? The perspective from the BRAHMS experiment," *Nucl. Phys.* **A757** (2005) 1–27, `nucl-ex/0410020`.

[28] B. B. Back *et. al.*, "The PHOBOS perspective on discoveries at RHIC," *Nucl. Phys.* **A757** (2005) 28–101, `nucl-ex/0410022`.

[29] **STAR** Collaboration, J. Adams *et. al.*, "Experimental and theoretical challenges in the search for the quark gluon plasma: The STAR collaboration's critical assessment of the evidence from RHIC collisions," *Nucl. Phys.* **A757** (2005) 102–183, `nucl-ex/0501009`.

[30] **BRAHMS** Collaboration, I. G. Bearden *et. al.*, "Nuclear stopping in Au + Au collisions at s(NN)**(1/2) = 200-GeV," *Phys. Rev. Lett.* **93** (2004) 102301, `nucl-ex/0312023`.

[31] W. Zajc, private communication.

[32] C. P. Herzog, "Energy loss of heavy quarks from asymptotically AdS geometries," *JHEP* **09** (2006) 032, `hep-th/0605191`.

[33] C. P. Herzog, A. Karch, P. Kovtun, C. Kozcaz, and L. G. Yaffe, "Energy loss of a heavy quark moving through N = 4 supersymmetric Yang-Mills plasma," `hep-th/0605158`.

[34] S. S. Gubser, "Drag force in AdS/CFT," `hep-th/0605182`.

[35] J. Casalderrey-Solana and D. Teaney, "Heavy quark diffusion in strongly coupled N = 4 Yang Mills," `hep-ph/0605199`.

[36] U. H. Danielsson, E. Keski-Vakkuri, and M. Kruczenski, "Vacua, propagators, and holographic probes in AdS/CFT," *JHEP* **01** (1999) 002, `hep-th/9812007`.

[37] H. Liu, K. Rajagopal, and U. A. Wiedemann, "Calculating the jet quenching parameter from AdS/CFT," `hep-ph/0605178`.

[38] A. Buchel, "On jet quenching parameters in strongly coupled non- conformal gauge theories," *Phys. Rev.* **D74** (2006) 046006, `hep-th/0605178`.

[39] E. Caceres and A. Guijosa, "Drag force in charged N = 4 SYM plasma," *JHEP* **11** (2006) 077, `hep-th/0605235`.

[40] C. G. Callan and A. Guijosa, "Undulating strings and gauge theory waves," *Nucl. Phys.* **B565** (2000) 157–175, `hep-th/9906153`.

[41] E. Witten, "Anti-de Sitter space, thermal phase transition, and confinement in gauge theories," *Adv. Theor. Math. Phys.* **2** (1998) 505–532, `hep-th/9803131`.

[42] C. Csaki, H. Ooguri, Y. Oz, and J. Terning, "Glueball mass spectrum from supergravity," *JHEP* **01** (1999) 017, `hep-th/9806021`.

[43] G. T. Horowitz and V. E. Hubeny, "Quasinormal modes of AdS black holes and the approach to thermal equilibrium," *Phys. Rev.* **D62** (2000) 024027, `hep-th/9909056`.

[44] **STAR** Collaboration, C. Adler *et. al.*, "Disappearance of back-to-back high p(T) hadron correlations in central Au + Au collisions at s(NN)**(1/2) = 200-GeV," *Phys. Rev. Lett.* **90** (2003) 082302, `nucl-ex/0210033`.

[45] **PHENIX** Collaboration, S. S. Adler *et. al.*, "Modifications to di-jet hadron pair correlations in Au + Au collisions at s(NN)**(1/2) = 200-GeV," `nucl-ex/0507004`.

[46] V. Greco, C. M. Ko, and P. Levai, "Parton coalescence and antiproton/pion anomaly at RHIC," *Phys. Rev. Lett.* **90** (2003) 202302, `nucl-th/0301093`.

[47] R. C. Hwa and C. B. Yang, "Recombination of shower partons at high p(T) in heavy-ion collisions," *Phys. Rev.* **C70** (2004) 024905, `nucl-th/0401001`.

[48] A. Majumder, E. Wang, and X.-N. Wang, "Modified dihadron fragmentation functions in hot and nuclear matter," `nucl-th/0412061`.

[49] R. J. Fries, S. A. Bass, and B. Muller, "Correlated emission of hadrons from recombination of correlated partons," *Phys. Rev. Lett.* **94** (2005) 122301, `nucl-th/0407102`.

[50] N. Armesto, C. A. Salgado, and U. A. Wiedemann, "Measuring the collective flow with jets," *Phys. Rev. Lett.* **93** (2004) 242301, `hep-ph/0405301`.

[51] J. Casalderrey-Solana, E. V. Shuryak, and D. Teaney, "Conical flow induced by quenched QCD jets," *J. Phys. Conf. Ser.* **27** (2005) 22–31, `hep-ph/0411315`.

[52] J. Ruppert and B. Muller, "Waking the colored plasma," *Phys. Lett.* **B618** (2005) 123–130, `hep-ph/0503158`.

[53] J. J. Friess, S. S. Gubser, G. Michalogiorgakis, and S. S. Pufu, "The stress tensor of a quark moving through N = 4 thermal plasma," `hep-th/0607022`.

[54] J. S. F. Chan and R. B. Mann, "Scalar wave falloff in asymptotically anti-de Sitter backgrounds," *Phys. Rev.* **D55** (1997) 7546–7562, `gr-qc/9612026`.

[55] V. Cardoso and J. P. S. Lemos, "Quasi-normal modes of Schwarzschild anti-de Sitter black holes: Electromagnetic and gravitational perturbations," *Phys. Rev.* **D64** (2001) 084017, `gr-qc/0105103`.

[56] J. Natario and R. Schiappa, "On the classification of asymptotic quasinormal frequencies for d-dimensional black holes and quantum gravity," *Adv. Theor. Math. Phys.* **8** (2004) 1001–1131, `hep-th/0411267`.

[57] S. Musiri, S. Ness, and G. Siopsis, "Perturbative calculation of quasi-normal modes of AdS Schwarzschild black holes," *Phys. Rev.* **D73** (2006) 064001, `hep-th/0511113`.

[58] V. Cardoso and J. P. S. Lemos, "Quasi-normal modes of toroidal, cylindrical and planar black holes in anti-de Sitter spacetimes," *Class. Quant. Grav.* **18** (2001) 5257–5267, `gr-qc/0107098`.

[59] P. K. Kovtun and A. O. Starinets, "Quasinormal modes and holography," *Phys. Rev.* **D72** (2005) 086009, `hep-th/0506184`.

[60] I. G. Moss and J. P. Norman, "Gravitational quasinormal modes for anti-de Sitter black holes," *Class. Quant. Grav.* **19** (2002) 2323–2332, `gr-qc/0201016`.

[61] H. Kodama and A. Ishibashi, "A master equation for gravitational perturbations of maximally symmetric black holes in higher dimensions," *Prog. Theor. Phys.* **110** (2003) 701–722, `hep-th/0305147`.

[62] T. Regge and J. A. Wheeler *Phys. Rev.* **108** (1957) 1063.

[63] F. J. Zerilli, "Effective potential for even parity Regge-Wheeler gravitational perturbation equations," *Phys. Rev. Lett.* **24** (1970) 737–738.

[64] H. Kodama, A. Ishibashi, and O. Seto, "Brane world cosmology: Gauge-invariant formalism for perturbation," *Phys. Rev.* **D62** (2000) 064022, `hep-th/0004160`.

[65] O. Aharony, S. S. Gubser, J. M. Maldacena, H. Ooguri, and Y. Oz, "Large N field theories, string theory and gravity," *Phys. Rept.* **323** (2000) 183–386, `hep-th/9905111`.

[66] D. T. Son and A. O. Starinets, "Minkowski-space correlators in AdS/CFT correspondence: Recipe and applications," *JHEP* **09** (2002) 042, `hep-th/0205051`.

[67] G. Policastro, D. T. Son, and A. O. Starinets, "From AdS/CFT correspondence to hydrodynamics," *JHEP* **09** (2002) 043, `hep-th/0205052`.

[68] G. Policastro, D. T. Son, and A. O. Starinets, "From AdS/CFT correspondence to hydrodynamics. II: Sound waves," *JHEP* **12** (2002) 054, `hep-th/0210220`.

[69] P. Kovtun and A. Starinets, "Thermal spectral functions of strongly coupled N = 4 supersymmetric Yang-Mills theory," *Phys. Rev. Lett.* **96** (2006) 131601, `hep-th/0602059`.

[70] J. J. Friess, S. S. Gubser, G. Michalogiorgakis, and S. S. Pufu, "Expanding plasmas and quasinormal modes of anti-de Sitter black holes," `hep-th/0611005`.

[71] V. Cardoso, R. Konoplya, and J. P. S. Lemos, "Quasinormal frequencies of Schwarzschild black holes in anti-de Sitter spacetimes: A complete study on the asymptotic behavior," *Phys. Rev.* **D68** (2003) 044024, `gr-qc/0305037`.

[72] R. A. Konoplya, "Gravitational quasinormal radiation of higher-dimensional black holes," *Phys. Rev.* **D68** (2003) 124017, `hep-th/0309030`.

[73] C. P. Herzog, "The hydrodynamics of M-theory," *JHEP* **12** (2002) 026, `hep-th/0210126`.

[74] J. M. Maldacena, "The large N limit of superconformal field theories and supergravity," *Adv. Theor. Math. Phys.* **2** (1998) 231–252, `hep-th/9711200`.

[75] S. S. Gubser, I. R. Klebanov, and A. M. Polyakov, "Gauge theory correlators from non-critical string theory," *Phys. Lett.* **B428** (1998) 105–114, `hep-th/9802109`.

[76] E. Witten, "Anti-de Sitter space and holography," *Adv. Theor. Math. Phys.* **2** (1998) 253–291, `hep-th/9802150`.

[77] J. J. Friess and S. S. Gubser, "Non-linear sigma models with anti-de Sitter target spaces," `hep-th/0512355`.

[78] A. Sen, "The heterotic string in arbitrary background field," *Phys. Rev.* **D32** (1985) 2102.

[79] C. M. Hull and E. Witten, "Supersymmetric sigma models and the heterotic string," *Phys. Lett.* **B160** (1985) 398–402.

[80] A. N. Vasiliev, Y. M. Pismak, and Y. R. Khonkonen, "1/N expansion: Calculation of the exponents η and ν in the order $1/N^2$ for arbitrary number of dimensions," *Theor. Math. Phys.* **47** (1981) 465–475.

[81] A. M. Polyakov, "Interaction of Goldstone particles in two-dimensions. Applications to ferromagnets and massive Yang-Mills fields," *Phys. Lett.* **B59** (1975) 79–81.

[82] E. Witten, "A supersymmetric form of the nonlinear sigma model in two-dimensions," *Phys. Rev.* **D16** (1977) 2991.

[83] O. Alvarez, "Dynamical symmetry breakdown in the supersymmetric nonlinear sigma model," *Phys. Rev.* **D17** (1978) 1123.

[84] P. M. I.Ya. Aref'eva, V.K. Krivoshchekov, "1/N Perturbation theory and quantum conservation laws for the supersymmetric chiral field," *Theor. Math. Phys.* **40** (1980) 565.

[85] D. J. Gross and A. Neveu, "Dynamical symmetry breaking in asymptotically free field theories," *Phys. Rev.* **D10** (1974) 3235.

[86] A. Zamolodchikov and A. Zamolodchikov, "Relativistic S-Matrix in two dimensions having O(N) isotopic Symmetry," *Nucl. Phys.* **B133** (1978) 525. Also JETP 26 (1977) 457.

[87] A. N. Vasiliev, Y. M. Pismak, and Y. R. Khonkonen, "Simple method of calculating the critical indices in the $1/N$ expansion," *Theor. Math. Phys.* **46** (1981) 104–113.

[88] J. A. Gracey, "On the Beta function for sigma models with N=1 supersymmetry," *Phys. Lett.* **B246** (1990) 114–118.

[89] J. A. Gracey, "Critical exponents for the supersymmetric sigma model," *J. Phys.* **A23** (1990) 2183–2194.

[90] S.-k. Ma, "Critical Exponents above T_c to O(1/n)," *Phys. Rev.* **A7** (1973) 2172.

[91] J. A. Gracey, "Probing the supersymmetric O(N) sigma model to $\mathcal{O}(1/N^2)$: Critical exponent ν," *Nucl. Phys.* **B352** (1991) 183–214.

[92] A. P. Foakes, N. Mohammedi, and D. A. Ross, "Three loop beta functions for the superstring and heterotic string," *Nucl. Phys.* **B310** (1988) 335.

[93] A. P. Foakes, N. Mohammedi, and D. A. Ross, "Effective action and beta functions for the heterotic string," *Phys. Lett.* **B206** (1988) 57.

[94] M. T. Grisaru, A. E. M. van de Ven, and D. Zanon, "Four loop divergences for the $\mathcal{N} = 1$ supersymmetric nonlinear sigma models in two-dimensions," *Nucl. Phys.* **B277** (1986) 409.

[95] M. T. Grisaru, A. E. M. van de Ven, and D. Zanon, "Four loop β function for the $\mathcal{N} = 1$ and $\mathcal{N} = 2$ supersymmetric nonlinear sigma model in two-dimensions," *Phys. Lett.* **B173** (1986) 423.

[96] F. Wegner, "Four loop order beta function of nonlinear sigma models in symmetric spaces," *Nucl. Phys.* **B316** (1989) 663–678.

[97] I. Jack, D. R. T. Jones, and N. Mohammedi, "The four loop metric beta function for the bosonic sigma model," *Phys. Lett.* **B220** (1989) 171.

[98] I. Jack, D. R. T. Jones, and N. Mohammedi, "A four loop calculation of the metric beta function for the bosonic sigma model and the string effective action," *Nucl. Phys.* **B322** (1989) 431.

[99] D. J. Gross and J. H. Sloan, "The quartic effective action for the heterotic string," *Nucl. Phys.* **B291** (1987) 41.

[100] R. R. Metsaev and A. A. Tseytlin, "Curvature cubed terms in string theory effective actions," *Phys. Lett.* **B185** (1987) 52.

[101] Y. Cai and C. A. Nunez, "Heterotic string covariant amplitudes and low-energy effective action," *Nucl. Phys.* **B287** (1987) 279.

[102] A. A. Tseytlin, "Vector field effective action in the open superstring theory," *Nucl. Phys.* **B276** (1986) 391.

[103] I. Jack, D. R. T. Jones, and D. A. Ross, "On the relationship between string low-energy effective actions and $O(\alpha'^3)$ sigma model beta functions," *Nucl. Phys.* **B307** (1988) 130.

[104] U. Ellwanger, J. Fuchs, and M. G. Schmidt, "The heterotic sigma model with background gauge fields," *Nucl. Phys.* **B314** (1989) 175.

[105] U. Ellwanger, J. Fuchs, and M. G. Schmidt, "The heterotic sigma model in the presence of background gauge fields: three loop results," *Phys. Lett.* **B203** (1988) 244.

[106] H. Osborn, "String theory effective actions from bosonic sigma models," *Nucl. Phys.* **B308** (1988) 629.

[107] H. Osborn, "General bosonic sigma models and string effective actions," *Ann. Phys.* **200** (1990) 1.

[108] S. P. de Alwis, "Strings in background fields beta functions and vertex operators," *Phys. Rev.* **D34** (1986) 3760.

[109] Y. Okabe and M. Oku, "1/N Expansion up to order 1/N**2. 3. Critical exponents gamma and nu for D = 3," *Prog. Theor. Phys.* **60** (1978) 1287–1297.

[110] I. R. Klebanov and A. M. Polyakov, "AdS dual of the critical O(N) vector model," *Phys. Lett.* **B550** (2002) 213–219, `hep-th/0210114`.

[111] T. Leonhardt, A. Meziane, and W. Ruhl, "On the proposed AdS dual of the critical O(N) sigma model for any dimension $2 < d < 4$," *Phys. Lett.* **B555** (2003) 271–278, `hep-th/0211092`.

[112] M. B. Green and J. H. Schwarz, "Anomaly cancelation in supersymmetric D=10 gauge theory and superstring theory," *Phys. Lett.* **B149** (1984) 117–122.

[113] W. A. Bardeen and B. Zumino, "Consistent and covariant anomalies in gauge and gravitational theories," *Nucl. Phys.* **B244** (1984) 421.

[114] E. Witten, "World-sheet corrections via D-instantons," *JHEP* **02** (2000) 030, `hep-th/9907041`.